Electrospun materials for wound management

by

Zhina Hadisi

B.Sc., University of Tabriz

M.A.Sc., The University of Tehran

A Thesis Submitted in Partial Fulfillment
Of the Requirements for the Degree of
Master of Applied Science
in the Department of Mechanical Engineering

University of Victoria

Supervisory Committee

Electrospun materials for wound management

by

Zhina Hadisi

B.Sc., University of Tabriz

M.A.Sc., The University of Tehran

Supervisory Committee

Dr. Mohsen Akbari, Supervisor
Department of Mechanical Engineering

Prof. Caterina Valeo, Departmental Member
Department of Mechanical Engineering

Prof. David Goodlett, Outside Member
Department of Chemistry

Prof. Xuekui Zhang, Outside Member
Department of Mathematics and Statistics

Abstract

Burn injuries represent a major life-threatening event that impacts the quality of life of patients and place enormous demands on the global health care systems. This study introduces the fabrication and characterization of a novel wound dressing made of core-shell hyaluronic acid -silk fibroin/zinc oxide nanofibers for treatment of burn injuries. The core-shell configuration enables loading zinc oxide (ZO)—an antibacterial agent—in the core of nanofibers, which in return improves the sustained release of the drug and maintains its bioactivity. Successful formation of core-shell nanofibers and loading of zinc oxide are confirmed by transmission electron microscopy (TEM), Fourier-transform infrared spectroscopy (FTIR) and energy dispersive X-ray (EDX), respectively. We examined the antibacterial activity of the dressings with ZO concentrations in the range of 0-5 wt% against *Escherichia coli* (*E. coli*) and *Staphylococcus aureus* (*S. aureus*) and showed that addition of ZO improved the antibacterial property of the dressing in a dose-dependent fashion. However, in vitro cytotoxicity studies showed that high concentration of ZO (>3 wt.%) is toxic to the cells. In vivo studies indicate that the wound dressings loaded with ZO (3 wt.%) substantially improved the wound healing procedure and significantly reduced the inflammatory response at the wound site. Overall, the dressing introduced herein holds great promise for the management of burn injuries.

Keywords: Silk fibroin, core-shell nanofiber, electrospinning, wound healing, burn injury

Table of Contents

List of Figures

List of Tables

List of Acronyms

ZO	Zinc oxide
TEM	Transmission electron microscopy
FTIR	Fourier-transform infrared spectroscopy
EDX	Energy dispersive X-ray
HA	Hyaluronic acid
SF	Silk fibroin
PDGF	platelet-derived growth factor
EGF	epidermal growth factor
TGF- β	transforming growth factor-β
TNF	tumor necrosis factor
IGF	insulin-like growth factor
VEGF	vascular endothelial growth factor
HGF	hepatocyte growth factor
FGF	fibroblast growth factors
ECM	extracellular matrix
MMPs	matrix metalloproteinases
TIMPs	tissue inhibitors of metalloproteinases
PABA	para-aminobenzoic acid
DNA	Deoxyribonucleic Acid
PNIPAm	poly(N-Isopropylacrylamide)
PEGDA	poly(ethylene glycol) diacrylate
ROS	reactive oxygen species
AgNPs	Silver nanoparticles
UV-spec	ultra-violet spectrophotometer
PBS	phosphate-buffered saline
PVP	polyvinylpyrrolidone
PECF	pseudo extracellular fluid
HaCat	Human keratinocytes
DMEM	Dulbecco's Modification of Eagles Medium
FBS	fetal bovine serum
DMSO	Dimethyl sulfoxide
P(VDF-TrFE)	poly (vinylidene fluoride-trifluoroethylene)
NF-κB	Nuclear factor kappa B
ERK	extracellular signal-regulated kinase

H&E	haematoxylin and eosin
MT	Masson's trichrome
BSA	bovine serum albumin
RE	regenerated epidermis
CD68	Cluster of Differentiation 68
RHAMM	Receptor for Hyaluronic Acid Mediated Motility
HPF	high power field
CSA	Colorimetric sensor array
VOC	Volatile organic compounds
eNose	electronic nose
LB	liquid broth media
TSA	tryptic soy agar
MSSA	Methicillin-Sensitive Staphylococcus aureus
MRSA	Methicillin-Resistant Staphylococcus aureus
ppb	parts per billion
AuNPs	11-mercaptoundecanoic acid capped gold nanoparticles
PPE	poly(p-phenyleneethynylene)

Acknowledgments

First and foremost, I would like to thank my supervisor Dr. Mohsen Akbari for his advice and guidance throughout this project and many others undertaken during my time at the Laboratory for Innovations in Micro Engineering (LIME). I will always be thankful for the opportunity he provided me in being part of his amazing lab and team. Next, I would like to thank my fellow lab members without whom this work would not have been possible and my time as a graduate student at the University of Victoria wouldn't have been nearly as fun as it was. Lastly I would like to thank my parents and my husband for always having my back. Without their support I would not be where I am today.

Dedication

I would like to dedicate this thesis to my parents and my husband. I thank you for setting me on this life long journey of learning. Your continued support has been instrumental in my academic achievements to date.

Chapter 1: Introduction

1.1 The structure and function of skin

Skin as the largest organ in the body covers the body's external surface. It consists of three main layers including the epidermis (top layer), dermis (middle layer), and the hypodermis (the bottom or fatty layer), all three of which have different anatomy and function[1]. The structure of skin can be seen from Figure 1. This complex structure accounts as the body's initial barrier against pathogens, UV light, and chemicals, and mechanical injury. It also regulates body's temperature and the amount of water released into the environment[2].

1.1.1 Epidermis function

The epidermis as the top layer of the skin has a varying thickness from 0.1 mm up to 1.5 mm depending on the body site (Figure 1). Keratin, a protein inside skin cells, makes up the skin cells and, along with other proteins, sticks together to form this layer[3].

The function of epidermis listed as below[4]:

- **Acts as a protective barrier:** The epidermis keeps bacteria and germs from entering your body and bloodstream which causing infections. It also protects against different weather conditions such as rainy and sunny days.
- **Makes new skin:** The epidermis continually makes new skin cells. These new cells replace the approximately 40,000 old skin cells that your body sheds every day. It builds new skin every 30 days.
- **Body protection:** Langerhans cells in the epidermis are part of the body's immune system. They help fight off pathogens and organisms that causing infection.

- **Provides skin color:** The epidermis contains melanin, the pigment that gives skin its color. The amount of melanin you have determines the color of your skin, hair and eyes. People who make more melanin have darker skin and may tan more quickly.

1.1.2 Dermis function

Beneath the epidermis, the collagen-rich dermis layer makes up 90% of skin's thickness. The main cell type of the dermis is fibroblast but several types of innate immune cells such as macrophages, mast cells, and innate lymphoid cells are found in this layer. This middle layer of skin contains[5-6]:

- **collagen and elastin:** Collagen is a protein which is responsible for providing mechanical support and withstanding applied external forces. Another protein found in the dermis is elastin that keeps skin flexible.
- **Hair:** The roots of hair follicles attach to the dermis.
- **Oil:** Oil glands in the dermis keeps the skin soft and smooth. Oil also regulates the amount of water. For example, it prevents skin from absorbing too much water when you swim or get caught in a rainstorm.
- **Sweat glands:** they release sweat through skin pores. Sweat helps regulate your body temperature.
- **Blood vessels:** they provide nutrients to the epidermis, keeping the skin layers healthy.

1.1.3 Hypodermis

The lowermost layer of skin, or hypodermis, is the fatty layer (Figure 1). The hypodermis[7-8]:

- **Cushions muscles and bones:** Fat in the hypodermis protects muscles and bones from injuries when you fall or are in an accident.
- **Has connective tissue:** This tissue connects layers of skin to muscles and bones.

- **Helps the nerves and blood vessels:** Nerves and blood vessels in the dermis (middle layer) get larger in the hypodermis. These nerves and blood vessels branch out to connect the hypodermis to the rest of the body.
- **Regulates body temperature:** Fat in the hypodermis keeps you from getting too cold or hot.

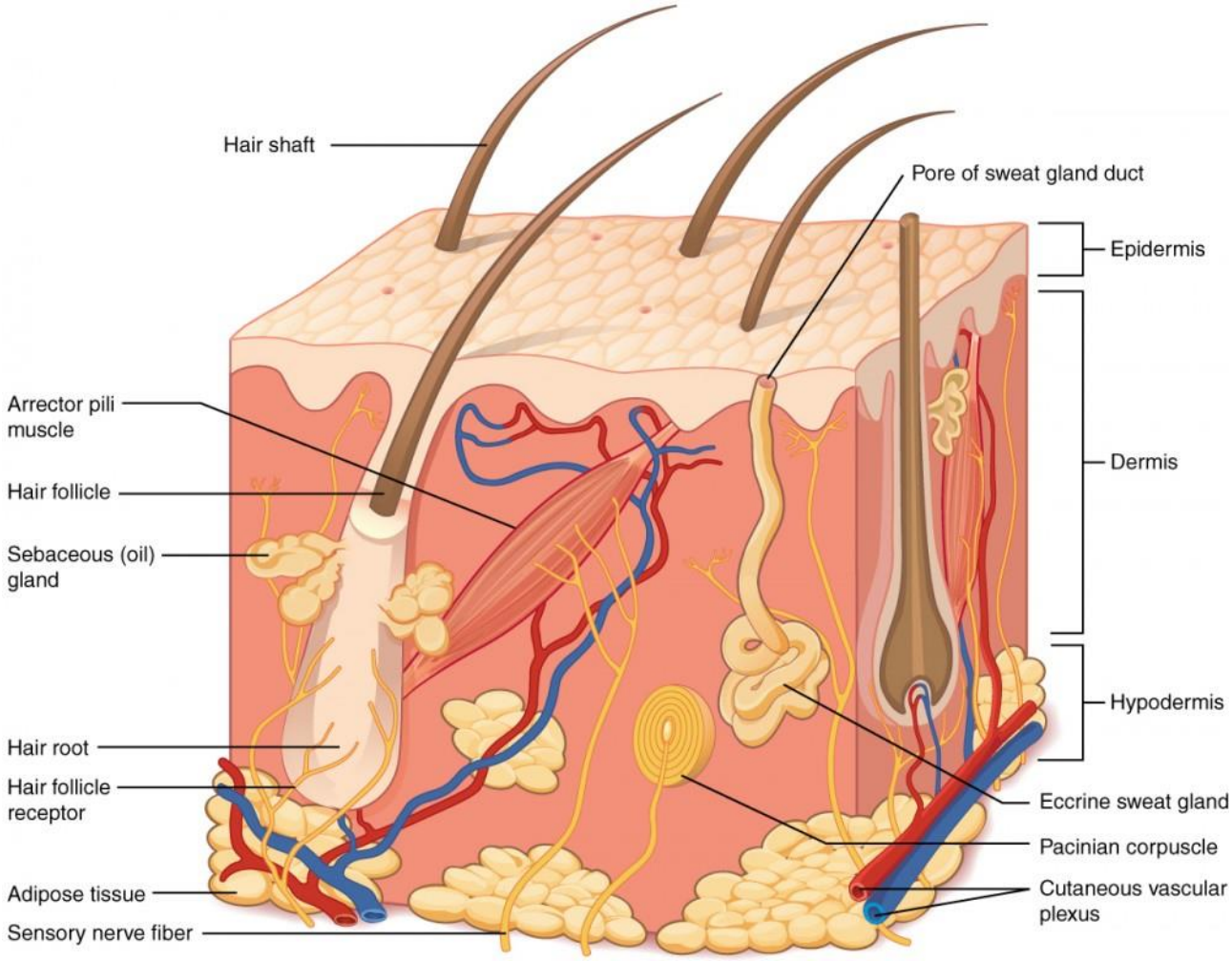

Figure 1: Layers of skin. The skin is composed of three main layers: the epidermis, made of closely packed epithelial cells, and the dermis, made of dense, irregular connective tissue that houses blood vessels, hair follicles, sweat glands, and other structures. Beneath the dermis lies the hypodermis, which is composed mainly of loose connective and fatty tissues [https://courses.lumenlearning.com/suny-ap1/chapter/layers-of-the-skin/].

1.2 Different type of wounds

A wound is defined as any type of damage or breakage on the surface of the skin. The wounds can be due to accidents like burns, paper cuts, skin tears or surgical, any underlying disease, or some other skin conditions that may develop in the wound, for example, eczema or psoriasis [9]. Skin wounds are

the fourth common skin problem in the world. Many people are affected by skin wounds worldwide represent a major challenge to wound care professionals, with the required treatment consuming a large portion of healthcare resources [10]. Over 6.5 million patients in the United States suffered from skin wounds and their treatments cost over US$ 25 billion annually in 2009 [11]. Based on the recent report, Medicare cost projections ranged from $28.1 billion to $96.8 billion for diagnosis, management and treatment of the wounds [12]. Skin wounds classified into two major groups; acute wounds and chronic wounds.

1.2.1 Acute wounds

An acute wound is an injury to the skin that occurs suddenly rather than over time. It heals at the predictable and expected rate of the normal wound healing process. Acute wounds can occur anywhere on the body and vary from superficial scratches to deep wounds damaging blood vessels, nerves and muscles. The healing process of acute wounds is well-organized and predictable in which platelets, keratinocytes, fibroblasts, vascular cells, and immune cells repair the skin tissue and restore its integrity[13].

1.2.2 Chronic wounds

Chronic wounds are defined as injuries that do not heal in less than three months[14]. These lesions represent a major challenge to wound care professionals, with the required treatment consuming a large portion of healthcare resources[10]. Chronic wounds can be categorized into three major groups of diabetic foot ulcers, leg ulcers, pressure sores and some type of burn wounds[10]. With an increase in prevalence of diabetes, ischemic vascular disorders, and obesity, the incidence of chronic wounds is also on the rise[15]. Common features of chronic wounds include persistent infection, increased inflammation, and the formation of antibiotic-resistant biofilm[14, 15-16]. Studies on the cellular and molecular mechanisms of healthy and acute wound healing in animal models have been widely successful and highly researched; however, chronic wound repair requires more comprehensive investigation[10,17-18]. Difficulties in recapitulating the clinical and microbiological complexities of

chronic wounds in animal models remains a challenge, as the pathologies differ among chronic wound types[14]. Though these wounds remain difficult to treat, by understanding the underlying wound pathophysiology and developing advanced management protocols using optimized models, successful healing can become the rule as opposed to the exception.

1.2.2.1 Burn wounds

Burn injuries represent a major life-threatening and life-altering event that significantly affects the quality of life of the patients. A recent report from the World Health Organization (WHO) estimates 180,000 deaths per year as a result of burn injuries with the majority of incidents occurring in low- and middle income countries [19]. The damages caused by burns are painful and can significantly compromise the integrity and protective function of the skin and establish a dangerous avenue for infections leading to the delayed wound healing process[19-21].

1.3 Wound healing and burns

Optimal wound healing involves four continuous and overlapping phases including hemostasis, inflammation, proliferation, and remodeling [22]. Burn wound healing depends on the depth of burns. Burn wounds can be classified based to involvement degree of skin and depth of injury as follows [23]:

- **First-degree burn or epithelial burns** - Skin is erythematic without vesication. First-degree burns are one of the mildest forms of skin injuries, and they usually don't need any medical treatment. However, it can be quite large or painful.
- **Second-degree burns** - Involving epidermis and variable thickness of dermis. This can be divided into:
    - **Second-degree superficial** –where vesication and inflammation is seen in skin as only papillary dermis is involved.
    - **Second-degree deep** -eschar formation is seen as it involves deep reticular dermis.

- **Third-degree burn** - Also known as full thickness burns - eschar formation is present in these burns and widespread thickness with a white, leathery appearance. [24-25].

The schematic of different degree of burns and their features can be seen in Figure 2.

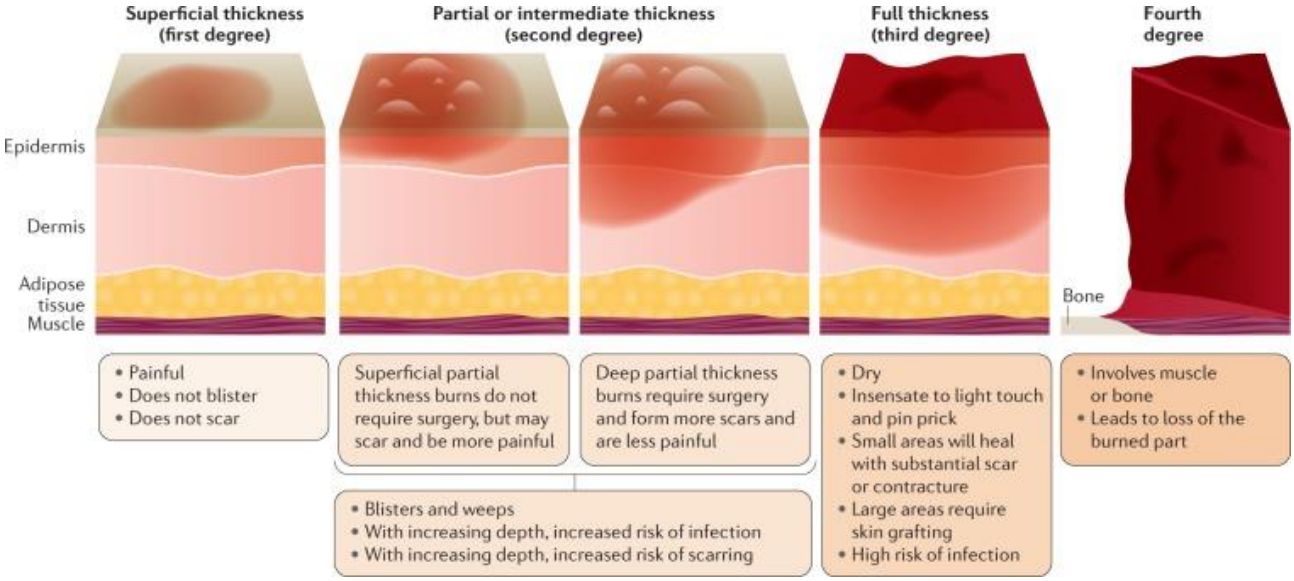

Figure 2: the schematic of different degree of burns and their features26.

In first degree and second-degree superficial burns, primary healing process is by intention. Second-degree superficial burns mainly heal from epithelium of hair follicle remnants, which are located in the superficial dermis. Healing process is taken place within 5-7 days which is almost scar less. In second-degree deep and third-degree burns, healing is by secondary intention including epithelization and contraction. Areas of deep second *degree* and *third-degree burns* may continue to build up *scar* tissue for at least two years [23].

Overall, The natural healing of these wounds involves dynamic and overlapping phases (Fig. 3) that include an inflammatory phase, which is initiated by neutrophils and monocytes homing to the injury site via localized vasodilation.

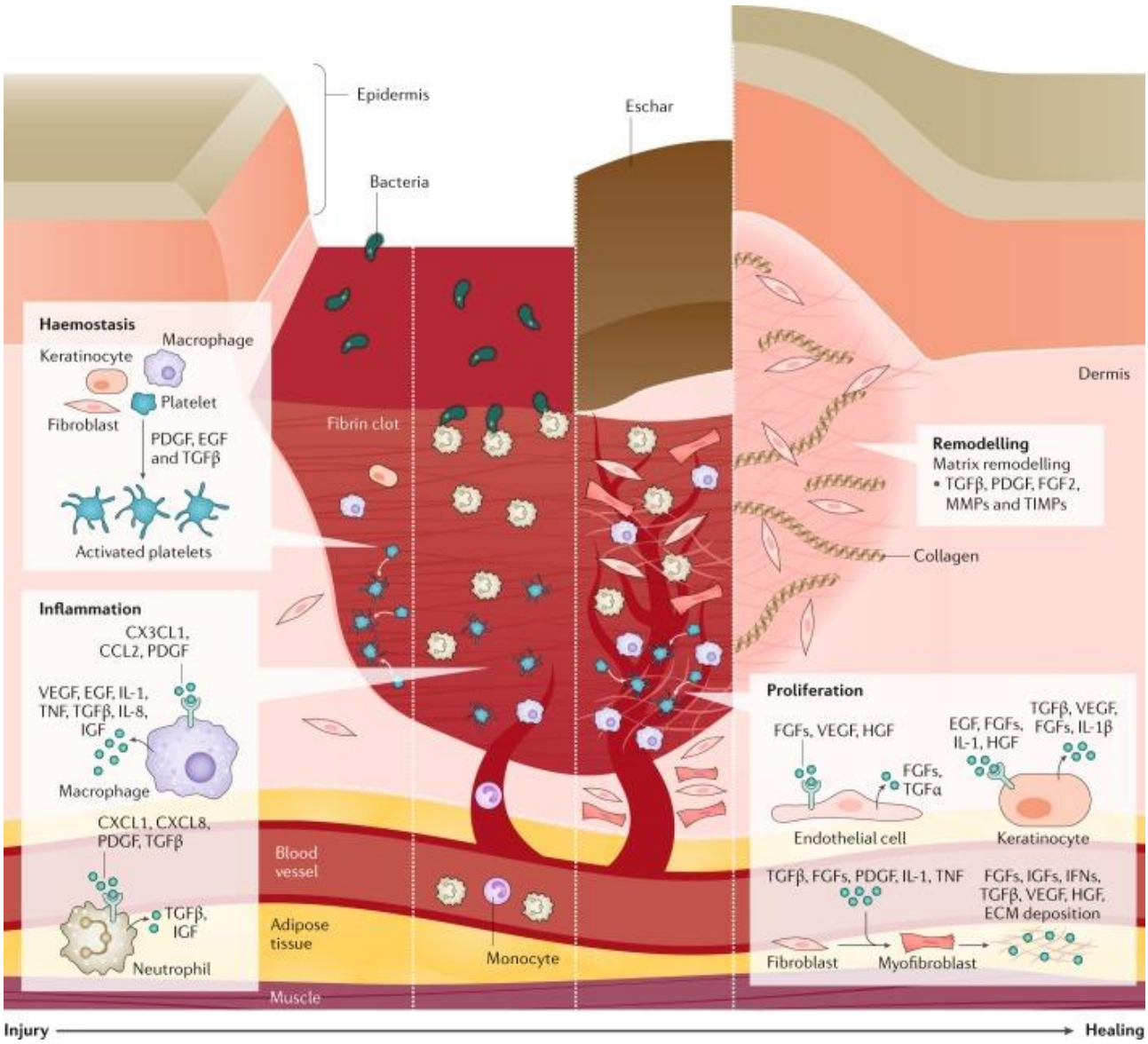

Figure 3: four phases of burn wound healing. Hemostasis occurs immediately after the injury. Inflammation begins within 24 hours of the injury and lasts for weeks to months depending on the severity of injury. The next phase, proliferation, involves the recruitment and activation of fibroblasts and keratinocytes to the wound site. In the final phase, remodeling, granulation tissue matures and the ECM is remodeled under the influence of growth factors, matrix metalloproteinases (MMPs) and tissue inhibitors of metalloproteinases (TIMPs), which leads to increased tensile strength. The length of healing depends on multiple factors including the injury severity, inflammatory cascade activation and nutrition. IFN, interferon 26.

1.4 Wound management

With recent advancements in the biomaterial sciences, many advanced wound dressings have emerged with the ability to treat infections, accelerate wound healing, and reduce or prevent scar formation[27]. Wound infection in burn injuries is a major clinical challenge that can significantly delay the healing process, extend hospitalization, and add to the cost of treatment. In severe cases, infections

can lead to amputation, septic shock, or death[28]. An ideal wound dressing covers the entirety of the wound area to protect the wound from external pathogenic microorganisms, maintains the physiologic wound moisture, is oxygen permeable, and accelerates wound healing[29]. Traditional dressings such as medical gauze or bandages merely provide physical barriers against external pathogens[30], whereas more advanced wound dressings can contain bioactive molecules and drugs to treat infections, reduce excessive inflammation and pain, and promote vascularization, epithelization, and scar formation[30]. Wound dressings can be fabricated from natural or synthetic materials in the form of textiles[31], thin films[32], foams[33], hydrogels[34], electrospun nanofibrous mats[35-36], hydrocolloids[37-38], and bi-layered scaffolds[39]. The materials used for wound dressing materials should be biodegradable, highly biocompatible, and should not adhere to the wound bed to avoid tissue damage and pain upon removal[30]. Additionally, the dressing should be able to maintain the exudate level in the wound area while preventing the exudate in the wound bed from pooling, which can result in moisture-associated wound damage and maceration[40-42]. Drug-loaded dressings should also preserve the bioactivity of the loaded therapeutic agent and release it at a desirable rate[29]. This section is focused on the different agents, including antibiotics, nanoparticles, and natural compounds, that can be incorporated into the dressings to lend antimicrobial properties to a wound dressing.

1.4.1 Antibacterial loaded materials

Infection is a major clinical challenge for patients with burn injuries as it can significantly delay the wound healing process and increase the length of hospitalization [43]. Wound dressings impregnated with antibacterial agents have been extensively used in the literature. Currently, several antibiotic agents such as aminoglycosides[44], glycopeptides[45], tetracyclines[46], and quinolones[47] have been loaded in wound dressings to treat wound infections locally. These active agents aim to disrupt the functions of bacteria or interfere with the bacterial metabolic pathways causing lysis or disturbing growth[48]. Most existing antibacterial agents eradicate bacteria by 1) inhibiting the biosynthesis of cell walls in susceptible microbes, 2) blocking the key metabolic pathways in bacteria required to support growth

and interfering with protein production[49], and 3) inhibiting synthetization of nucleic acid. For example, beta-lactam and glycopeptites interfere with bacterial cell wall synthesis[49-50]. Glycopepetides bind to the amino acids of the cell wall to prevent new units being added to the peptidoglycan and inhibit the function of glycosyltransferase for polymerases amino acid and sugar to peptidoglycan. As a result, bacteria lysis is carried out by heightened internal osmotic pressure, resulting from the shape changes of the bacteria[50]. Secondly, sulfonamide drugs are structural analogs of para-aminobenzoic acid (PABA) and act as competitive antagonists in the microbial cell, blocking synthesis of folic acid and forming reactive and antibacterial pseudometabolite by being incorporated into precursors. Sulfonamides have a wide range of therapeutic applications, as mammalian cells use and adsorb pre-formed folic acid. Sulfonamides present selective bacterial toxicity and show high binding affinity to bacterial enzymes which lead to interference with deoxyribonucleic acid, ribonucleic acid, and protein synthetization[51]. The mechanism of interfering with protein production is adopted by aminoglycosides and tetracyclines antibiotics. These antibiotics bind to 30S ribosome sub-unit, causing misreading of genetic codes and disruption of protein synthesis by obstructing aminoacyl-tRNA access to the ribosome[52-53]. Finally, the mechanism of inhibiting synthetization of nucleic acid prevents bacterial Deoxyribonucleic Acid (DNA) from unwinding and duplicating, and subsequently interferes with nucleic acid synthesis. These types of antibiotics (e.g., quinolone) prevent the production of mRNA by targeting ligase activity of type II topoisomerase, gyrase, and topoisomerase IV. Consequently, cell death occurs as these targets are converted into enzymes that fragment the chromosome[54].

Table 1 summarizes the different studies carried out for fabricating active wound dressings impregnated with antibiotics. Among various antibiotics, tetracycline, gentamicin, ciprofloxacin, and sulfadiazine are the most frequently used antibiotics in active wound dressings[42]. For example, Kamble et al. fabricated an electrospun gelatin wound dressing loaded with ciprofloxacin for inhibiting the growth of Gram-positive (*S. aureus*) and Gram-negative *Pseudomonas aeruginosa* (*P. aeruginosa*) bacteria[35]. The dressing showed 98% higher antibacterial properties at a lower dosage

(0.16 μg/ml of liquid electrospinning solution), compared to the pure drug solution (0.5 μg/ml). In another study, Kurczewska et al. efficiently inhibited *S. epidermidis, S. aureus, S. haemolyticus, S. pneumoniae, S. pyogenes, and E. faecalis* by incorporating an inorganic support (vancomycin-loaded halloysite nanotubes) into an alginate based wound dressing[55]. Other recent progress in this regard includes antibiotic- and growth factor-loading of thermo-responsive poly (N-Isopropylacrylamide) (PNIPAm) -poly(ethylene glycol) diacrylate (PEGDA) microcarriers and incorporating them into alginate based wound dressings to enable on-demand antibiotic release[31]. This system has been shown to be effective in minimizing the growth of Gram-negative (*E. coli*) and Gram-positive bacteria (*S. aureus*). Further, *in vivo* evaluations on diabatic wound models (db/db mice with excised 1.0 cm^2 area of dorsal skin and panniculus carnosus) showed that the engineered active dressing promoted vascularization and consequently improved wound healing outcomes[31].

Altoé et al. conducted a systematic review on animal models used for assessing the effects of antibiotics on the wound healing process[56]. They reported that antibiotics help to reduce the migration of inflammatory cells to the wound area and accelerate the wound healing via enhanced ECM (extracellular matrix) deposition and re-epithelialization; however, their study was limited to non-infected animal wounds. He et al. engineered a hydrogel-based dressing composed of N-carboxyethyl chitosan and benzaldehyde-terminated Pluronic F127/carbon nanotubes for the smart and photothermal stimuli-responsive delivery of an antibiotic (moxifloxacin hydrochloride) to a full-thickness infected skin wound in mice[57]. The results indicated that the antibiotic-impregnated hydrogel increased the wound closure ratio and led to a higher degree of collagen deposition and formation of granulation tissue after 14 days. Roy et al. developed an infected partial thickness burn wound on a porcine model to evaluate the treatment efficiency of a keratin hydrogel dressing impregnated with ciprofloxacin[58]. The researchers found that ciprofloxacin positively impacted the healing rate of wounds infected with *S. aureus* or *MRSA* (*Methicillin-resistant S. aureus*) and reduced the amount of bacterial infection. In another study, wound dressings loaded with gentamicin were tested on the second degree burn wound in guinea pig model. The results indicated that the slow

release of gentamicin from the freeze-dried dressing led to a higher degree of epithelialization and wound contraction, and scar-free tissue reparation [59]; however, recurrent use of antibiotics may lead to bacterial resistance[60]. The development of bacterial resistance is a major clinical challenge in wound management and several studies have shown that the improper use of antibiotics can trigger severe bacterial resistance[61]. A large number of bacteria strains found in wounds have shown resistance to at least one of the widely used antibiotics[62]. The alarming increase in the number of multi-drug resistance bacteria demands new treatment strategies and the development of alternatives to antimicrobial agents.

Table 1: Wound dressings loaded with antibiotic agents.

Antibiotic type	Antibiotic	Dressing type	Materials	Bacteria	Ref.
Aminoglycosides	Streptomycin	Foam	Collagen/Tussah Silk Fibroin	*S. aureus E. coli*	63
	Gentamicin	Hydrogel	Silk Sericin/poly(vinyl alcohol)	*E. coli S. aureus P. aeruginosa*	64
		Electrospun Nanofibrous Scaffolds	Chitosan/Alginate	*S. aureus E. coli*	65
		Membrane	Chitosan/Methoxy polyethylene glycol/polycaprolactone	*S. aureus E. coli*	66
Glycopeptides	Vancomycin	Electrospun Nanofibrous Scaffolds	Gelatin	*E. faecalis S. aureus MRSA*	67
Tetracyclines	**Doxycycline**	Electrospun Nanofibrous Scaffolds	Polylactide	*E. coli*	68
	Tetracycline hydrochloride	Sponge	Fungal Chitosan /*Aloe Vera* extract	*Bacillus subtilis (B. subtilis) S. aureus E. coli Klebsiella pneumonia (K. pneumonia)*	69
		Membrane	Bacterial Cellulose	*E. coli S. aureus B. subtilis*	46
Quinolones	Ciprofloxacin	Electrospun Nanofibrous Scaffolds	Poly(di(ethylene glycol) methyl ether methacrylate) /Poly(l-lactic acid-co-ε-caprolactone)	*E. coli S. aureus*	70
		Polymeric Film	Chitosan/Gelatin/Bone ash	*E. coli B. subtilis*	71

Antibiotic type	Antibiotic	Dressing type	Materials	Bacteria	Ref.
	Levofloxacin	Sponge	Chitosan/Poly(2-hydroxyethyl acrylate)	*Methicillin susceptible Staphylococcus aureus (MSSA) MRSA P. aeruginosa*	[72]
		Electrospun Nanofibrous Scaffolds	Polycaprolactone	*E. coli S. aureus.*	[73]
	Norfloxacin	Sponge	Alginate/Graphene oxide/Polyvinyl alcohol	*E. coli S. aureus*	[74]
	Moxifloxacin	Sponge	Pectin/Carboxymethyl Tamarind Seed	*S. aureus P. aeruginosa*	[75]
Beta-Lactams	Ceftazidime	Electrospun Nanofibrous Scaffolds	Silk Fibroin/Gelatin	*P. aeruginosa*	[76]
	Ampicillin	Sponge	Gelatin/Bacterial cellulose	*E. coli S. aureus*	[77]
		Multilayer Hydrogel	Carboxylated Polyvinyl alcohol/Gelatin/ Hyaluronic Acid	*E. coli S. aureus*	[78]
	Cefazoline	Hydrogel-Textile Patch	Alginate/ Poly(ethylene glycol) diacrylate	*E. coli S. aureus*	[31]
Sulphonamides	**sulfadiazine**	Electrospun Nanofibrous Scaffolds	Zein	*E. coli Bacillus*	[79]
	Sulfanilamide	Fiber	Alginate	*E. coli S. aureus*	[80]

1.4.2 Functionalized materials with nanoparticles (NP)

A promising alternative for treating infected wounds are NP-impregnated dressings. Silver (Ag)[81], iron oxide (Fe_3O_4)[82], titanium dioxide (TiO_2)[83], and zinc oxide (ZO)[84] have been extensively used in wound dressings to prevent bacteria formation in wound beds. These NPs disrupt bacterial activity by 1) inhibiting the synthesis of cell wall/membrane, 2) generating reactive oxygen species (ROS), 3) disrupting energy transduction in membrane through the inhibition of the electron transport chain, 4) causing photocatalysis, inhibiting 5) enzyme and 6) DNA production[85-86]. NPs can be electrostatically adsorbed onto the charged surface groups of lipopolysaccharides in Gram-negative bacteria and peptidoglycan in Gram-positive bacteria[87]. This will lead to the formation of surface pores and increased surface permeability, which consequently causes cell disruption and loss of

intercellular cargo[87]. Furthermore, NPs can penetrate through the bacterial cell membranes and deregulate metabolic pathways or disrupt mitochondria, resulting in the generation of ROS[88]. Nanoparticles can also cause pH changes in the wound bed due to proton efflux, along with unbalanced electrolytes and the formation of oxidative stress by interactions with DNA, lysosomes, ribosomes, and enzymes[89-92]. Silver nanoparticles (AgNPs) are the most frequently used NPs for treating wound infections, owing to their potent antibacterial properties and available diverse surface chemistries[93], and have been used to functionalize wound dressings for the treatment of diabetic ulcers in mouse[94], rat[95], rabbit[96], and porcine models[97]. Several wound dressings containing AgNPs such as Tegaderm Ag, AQUACEL Ag, and Actisorb, have been commercialized to help treat minor skin wounds and infections. A systematic study reported that wound dressings functionalized with NPs demonstrated a potential to treat infected wounds such as burns and gingival ulcers in different laboratory animals [98]. The antimicrobial properties of AgNPs can be tuned by the size, shape, and surface chemistry of the particles, with recent trends oriented toward reducing the MIC (minimum inhibitory concentration) of AgNPs to minimize their associated risks[93]. Other types of NPs, including TiO_2-NPs[99], ZO-NPs[100], and iron-copper NPs[101], have been used for the treatment of infected wounds. Studies showed that the presence of NPs accelerated wound healing by supressing the growth of pathogens and improving collagen deposition and reepithelization in *in vivo* models (Fig. 1B). Table 2 summarizes these examples of wound dressings with incorporated NPs for the treatment of infected wounds[93, 102].

A major challenge associated with the application of NPs in wound dressings is their impact on the functionality of normal cells: the small size of NPs enables them to enter the bodily fluids and penetrate through the membrane of cells in the liver, kidneys, the lungs, and the heart, leading to disruption of normal cell functions and biochemical reactions[93]. It has been reported that AgNPs can cause ROS generation and DNA damage, leading to cytotoxicity, genotoxicity, activated signaling pathways, and induced inflammatory response in cells[103-104]. Another possible side effect associated with the use of AgNPs is the deposition of insoluble silver compounds under the skin, which may

induce skin diseases like argyrosis[105]. Further investigation is required to determine the cytocompatibility of NPs for their application in active wound dressings. The incorporation of natural-based NPs is a burgeoning approach to enhance the antimicrobial activity of wound dressings without inducing cytotoxic effect observed in NPs.

Table 2: Wound dressings functionalized with nanoparticles.

NP type	Dressing type	Materials	Bacteria	Ref.
Silver Nanoparticles (AgNPs)	Electrospun Nanofibrous Scaffolds	Poly(dopamine methacrylamide-co-methyl methacrylate)	*E. coli P. aeruginosa S. aureus*	106
	Membrane (**Pellicle)**	Bacterial cellulose	*E. coli S. aureus*	107
	Hydrogel	Poly (vinyl pyrrolidone)	*E. coli P. aeruginosa S.* aureus *Bacillus cereus* (*B. cereus) MRSA Staphylococcus epidermidis (S. epidermidis) Streptococcus pyogene (*S. *pyogenes) Acinetobacter lwoffii* (*A. lwoffii*)	108
Titanium Dioxide Nanoparticles (TiO_2NPs)	Film	Gellan gum	*E. coli S. aureus*	109
	Film	Bacterial cellulose	*E. coli S. aureus*	110
	Electrospun Nanofibrous Scaffolds	Polyvinyl alcohol/ Pluronic F127	*P. aeruginosa Salmonella Typhi (S. typhi) E. coli*	111
Zinc Oxide Nanoparticles (ZnONPs)	Hydrogel	Polyvinyl alcohol/chitosan	*E. coli S. aureus*	112
	Film	Bacterial cellulose	*E. coli Citrobacter freundii (C. freundii) P. aeruginosa S. aureus*	113
	Electrospun Nanofibrous Scaffolds	Chitosan/Polyvinyl alcohol	*E. coli P. aeruginosa B. subtilis S. aureus*	100
Iron Oxide Nanoparticles (Fe_3O_4NPs)	Membrane	Chitosan/Gelatin	*E. coli S. aureus*	82

In this study we choose ZO-NPs as an antibacterial agent due to the unique properties of ZO. It has been shown that ZO improves epithelialization and enhances the local defense system that reduces bacterial infection and inflammation [114-115]. Furthermore, in a recent in vivo study, Kumar et al.[116]

have reported that chitin hydrogel-based wound dressings impregnated with ZO nanoparticles accelerated the healing process and increased collagen deposition when compared to traditional gauze. In another study, Chhabra et al.[117] showed that the incorporation of ZO into gelatin-based wound dressing could inhibit bacterial growth. They observed faster wound healing compared to the ZO-free wound dressings. This material is now a standard antimicrobial therapy for management of wounds in second- or third-degree burns[118-119].

1.4.3 Natural based component functionalized materials

Wound dressings made of natural-based products have been used for the treatment of wounds for centuries. Several studies have shown that natural-based materials accelerate the wound healing process[120]. Among various biomaterials for wound management, hyaluronic acid (HA) has obtained more attention as it is the major component of the ECM and plays a major role in the wound healing and tissue regeneration process. It has been shown that HA can modulate the three main phases of the wound healing process, including inflammatory responses, migration of cells, and angiogenesis through interactions with specific cell receptors [121]. However, the poor mechanical properties, high swelling ratio, non-controlled drug delivery, and fast degradation rate of HA limit its application in wound dressing applications [122]. Previous studies have shown that the improvement of HA functional properties has been possible by blending HA with other polymers such as chitosan, collagen, polycaprolactone, and gelatin [123]. Recently, polysaccharide blending with other proteins has gained more attention due to its resemblance to ECM composition, biocompatibility, and positive effect on promoting the wound healing process [124-125]. Silk is composed of two main proteins including silk fibroin (SF) and sericin. The sericin protein as a glue wraps around fibroin and can be removed by a thermochemical process. SF is a good candidate to blend with other polymeric phases due to its excellent mechanical properties, biocompatibility, biodegradability, oxygen permeability, and effective wound healing[126].

In this work, we choose HA-SF as basic natural components for making the wound dressing.

1.4.4 Smart dressings

There is a pressing need for developing new technologies for detection and identification of pathogens in medicine. There is a broad involvement of bacterial infections in hospital-acquired infections and many other fields that can resulted in many diseases which are of big concern to the human health [127].

Bacteria is stinky, since they generate Volatile organic compounds (VOCs) to which the mammalian olfactory system is highly responsive. Thus, it can be a key factor for bacterial identification in wounds. As such, a professional microbiologist can identify many bacteria just by smell. For example, Pseudomonas aeruginosa can be identified by sweet grape-like scent [128].

By emerging new techniques in chemical sensing area, wide variety of sensors being available that can sense different analytes with higher sensitivity. Among them, optical-electrical sensors are especially noteworthy [129]. The most popular optical sensors rely on colorimetric or fluorescent changes, resulted by intermolecular interactions between the chromophore or fluorophore with the analytes. Combining techniques based on arrays that use a chemically responsive approach with modern digital imaging, one can provide identifying fingerprints in the response of the sensor arrays with any given analytes [130]. There are two basic criteria for development of colorimetric sensors. First, they should have capacity to interact selectively with analytes. Secondly, they should be able to generate a feedback on that interactions through chromophores or fluorophores by providing a fingerprint pattern.

Chemoresponsive colorant-based sensor arrays made out of dyes and pigments can detect the chemical reactivity of analytes, rather than their physical properties. Thus, this generation of sensors allows high sensitivity even down to parts per billion (ppb). Consequently, colorimetric sensor arrays overcoming the drawbacks of conventional sensor arrays which are only rely on physical absorbtion or nonspecific chemical interactions [131].

1.4.4.1 Colorimetric sensor arrays (CSAs)

The first example of a colorimetric sensor array nose was reported by Suslick, and coworkers, who designed a sensor array using various metalloporphyrins for effective detection of VOCs. Their results showed that metalloporphyrins strongly interacted with analytes which provided strong color change and specific pattern that can be used for identification of analytes [132]. The sensor arrays showed wide range of response to different type of VOCs including alcohols, amines, ethers, aldehydes, ketones, thioethers, phosphines, phosphites, thiols, arenes, and halocarbons, even with sensitivities at ppm level and with high stability in ambient humidity [132].

Next, Rakow et al.[133] was able to develop a colorimetric sensor with more arrays by incorporating other Chemoresponsive dyes such as acid and base indicators, and solvatochromic dyes to a total of 24 sensors . The sensor array was able to fully discriminate among 12 linear, branched or cyclic alkyl amines. As can be seen from Figure 1B, each amine provides a unique color-difference map for easy detection. Similarly, another sensor array was developed by Soga and co-workers for the identification of volatile amines [134]. Developed sensor was able to detect one closely related amine from another based on polarity interactions.

Furthermore, Janzen et al.[135] by extending the colorimetric sensor array to 6×6 arrays by incorporating various new types of dye sensors were able to represent an error-free discrimination among 100 different VOCs by probing a wide range of intermolecular interactions between analytes and sensors, including Lewis acid − base, Brønsted acid − base, metal ion coordination, hydrogen bonding, and dipolar interaction.

1.5 Wound dressings

Wound dressings are materials used to cover and protect wounds. They usually divided into two types including passive dressings (traditional dressings), interactive dressings and bioactive dressings (advanced dressings). Traditional wound dressings are mainly dry gauze and cotton wool without

bioactive components are used in clinics as a typical way to cover the wound. Unfortunately, this methodology does not have positive effects on accelerating the wound healing process. As such, recent efforts have been focused on designing advanced dressings containing stem cells, antibiotics, and bioactive molecules that facilitate wound regeneration[136].

The bioactive dressings are made of polymer materials and biological part processed by high-tech methods, which is a hot spot in the research and development of wound dressings. An ideal wound dressing should absorb wound exudates, provide thermal insulation and mechanical protection to the wound, prevent bacterial colonization, allow gas and nutrient transportation, and reduce the local inflammation response [137]. Different methods are developed to fabricate advanced wound dressings, including the use of textile methods, hydrogel sheets, and electrospinning[138-139].

1.5.1 Electrospinning

Among all type of wound dressings, polymer materials such as nanofibers has gained many attentions due to their light weight and porous structure. Nanofibers are easy to fabricate and can be manufactured in different ways, such as stretching, template synthesis, self-assembly, micro phase separation, and electrospinning. Electrospinning is a simple, cost-effective, and powerful technique for fabricating polymeric nanofibers with different structures, including porous [140], hallow [141], or core-shell fibers [100]. Core-shell electrospun nanofibers compared to the single structure nanofibers have gained more popularity as they enable delivering multiple bioactive molecules with different release kinetics, avoiding any damage of loaded drug from severe environments by incorporation of drug in core, enable sustained release for longer time period along with minimizing the burst release, and superior mechanical properties [142-144].

1.5.2 Incorporation of sensors in nanofiber based dressings

The growing financial burden of wound infections on global health services has initiated technological research in the areas of wound diagnostics and therapeutics using ‘smart’ dressings[27].

Elements such as microelectronic sensors, drug releasing microsystem, microprocessors, and wireless communication radios can be embedded in smart dressings to facilitate advanced wound care[41]. Using these smart dressings, discernable wound parameters include the pH, moisture, temperature, wound oxygen, and uric acid[27]. Smart dressings for the management of infected wounds, which may measure the wound exudate pH and temperature, have gained significant interest[27]. Wound pH is an important indicator of the wound condition and can be correlated with the present bacterial load[145]. The pH of healthy skin is slightly acidic and varies within the range of 4.0–6.0[146]. If the skin barrier is breached during injury, this acidic milieu becomes disturbed when the skin is exposed to internal body fluids with a neutral pH (pH = 7.4)[145]. Infected wounds generally have a pH in the range of 7.15–8.90, and can occasionally rise to pH 9, due in part to the proliferation of present bacteria[147]. A large change in wound pH can therefore provide an early alert of infection, making pH an important parameter in wound healing and characterization. Many sensors with the potential to detect wound pH exist and are commercially available.

In recent years, there have been many efforts to develop pH monitoring dressings for wound monitoring applications. However, only a few number of systems were successful for medical applications because of their complex and time consuming design strategies and discrepancy with aqueous environment. Therefore, there is a huge need for simple, easily prepared, reliable, fibre-based, and affordable systems such as electrospun fiber based sensors to enable wound exudate management and to monitor pH changes in wound surface [148]. Among various nanofiber fabrication methods, electrospinning is one of the most promising methods. In electrospun nanofibers based sensors, the sensor size has been decreased to nano which resulted in increasing the sensitivity and the proportion of atoms distributed on the surface has also been increased accordingly. Furthermore, when fiber diameter shrinks from micro- to nanometer, the specific surface area of the increases accordingly, which provides a large number of areas and channels that enhance the interactions between determinant and nanofibers. Maftoonazad et. Al [149]. fabricated an electrospun nanofiber mat

based on PVA and a natural dye from purple cabbage extract. The mat designed as a pH indicator for values reversibly in the range of 2.0–12.0.

1.6 Conclusion and objectives

Infection is a major clinical challenge for patients with burn injuries as it can significantly delay the wound healing process and increase the length of hospitalization [150]. Wound dressings impregnated with antibacterial nanoparticles made of silver, gold, and ZO have been extensively used in the literature [151-153]. Some investigations have reported the mild hepatotoxic effects of nano silver-loaded wound dressings [154]. In comparison, the unique properties of ZO that improves epithelialization and enhances the local defence system reduces bacterial infection and inflammation [114, 155].

In the present work, we report a novel wound dressing made of HA-SF/ZO composite core-shell nanofibers with antibacterial properties for the treatment of infections in burn injuries (Figure 4). The properties of the fabricated electrospun mats including its structural morphology, hydrophilicity, drug delivery, and antibacterial activity were investigated. Moreover, the effects of ZO concentrations on the proliferation and attachment of dermal fibroblast cells were assessed in vitro and compared with those of electrospun mats without ZO. In particular, we compared the difference in wound contraction as well as the inflammatory response, and formation of new collagen among groups of rats with second-degree burn wounds.

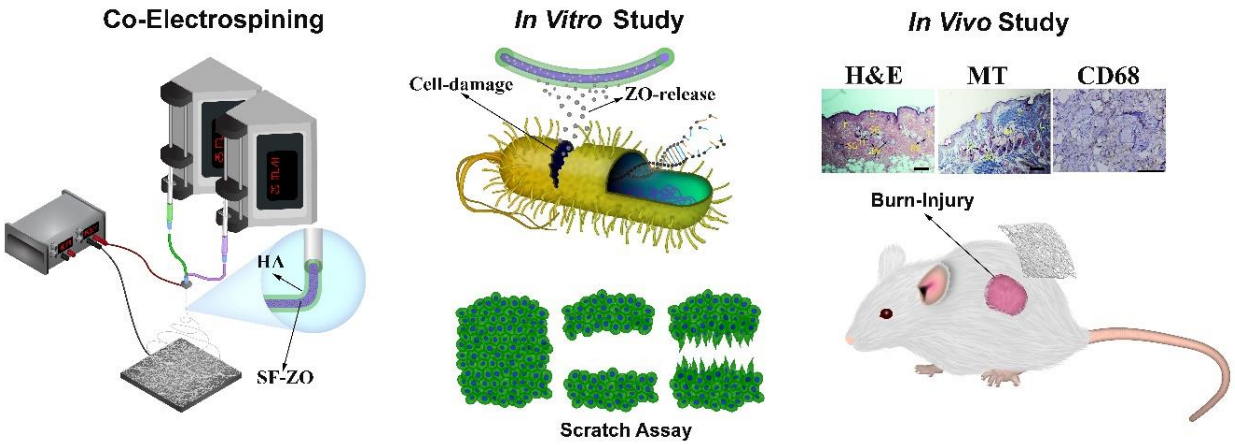

Figure 4: Schematic illustration showing the fabrication of antibacterial HA-SF/ZO nanofibers with core-shell structure and application for burn treatment.

Chapter 2: fabrication and characterization of electrospun wound dressing

Antibacterial dressings are wound covers that alter the wound bed bioburden. Indicated to help reduce the risk of infection in partial- and full-thickness burn wounds. Among the biomaterials used for this purpose, ECM proteins such as hyaluronic acid and silk fibroin have attracted researchers' attention due to their high capability of mimicking the biological properties of ECM, biocompatibility and effective wound healing[156-158].

HA is a natural glycosaminoglycan found in the ECM of most connective tissues (Figure 5). It has numerous functions within the body including wound repair, cell migration, and cell signaling. Due to its versatility, hyaluronic acid has been a major component of biomedical research[159]. The use of HA nanofibers as wound dressing has been well established[160].

Figure 5: HA structure and its biomedical applications[159].

Previous studies have shown that the improvement of HA functional properties has been possible by blending HA with other polymers due to its low mechanical properties and high swelling ratio [123, 161].

Silk is composed of two main proteins including fibroin and sericin. The sericin protein as a glue wraps around fibroin and can be removed by a thermochemical process (Figure 6) [162]. SF has the ultimate mechanical properties (a high ultimate tensile strength of 300–740 MPa) which makes SF as a good candidate to blend with other polymeric phases such as HA [156-158].

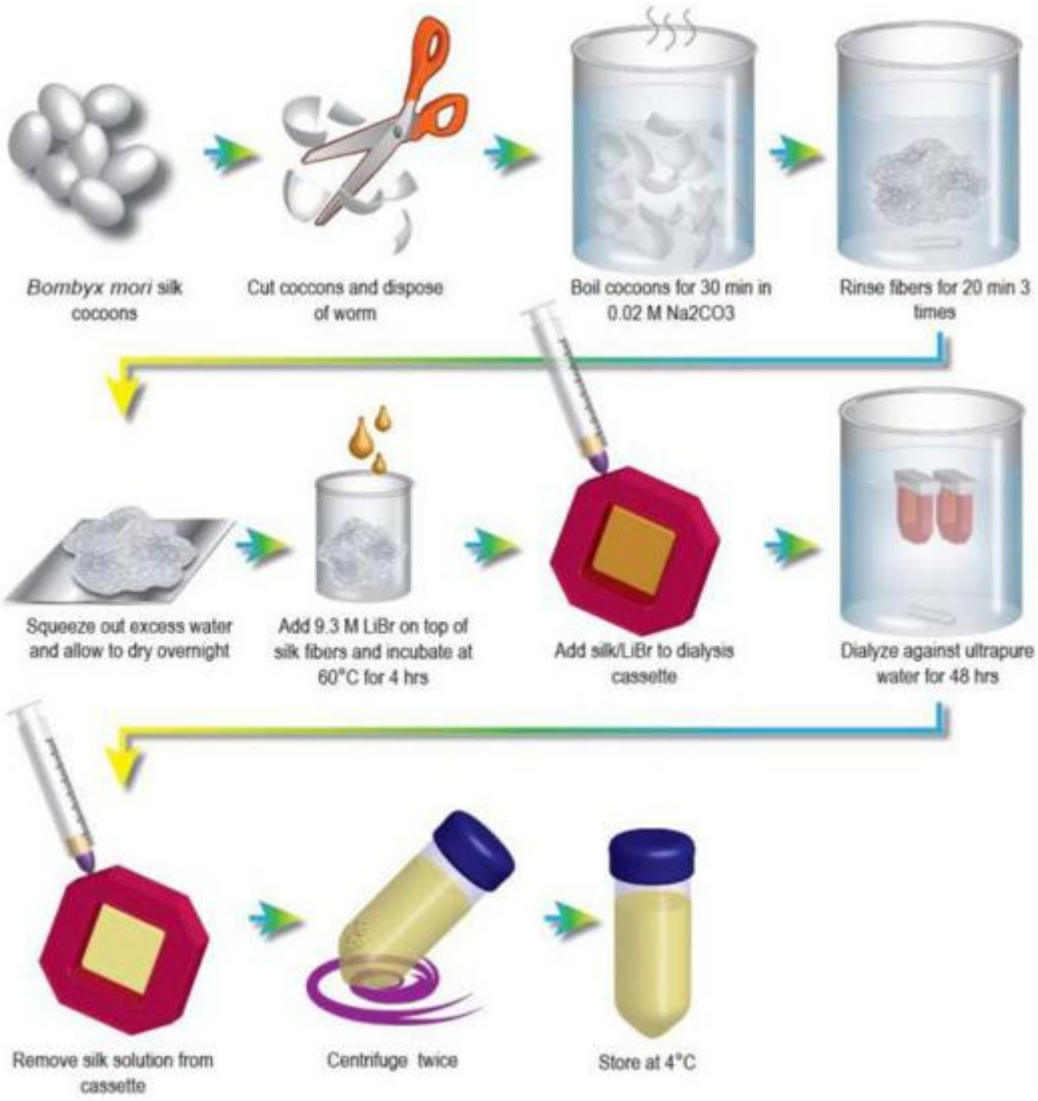

Figure 6: sericin removal procedure[163].

Infection is a major clinical challenge for patients with burn injuries as it can significantly delay the wound healing process and increase the length of hospitalization [150]. Wound dressings impregnated with antibacterial nanoparticles made of silver, gold, and zinc oxide (ZO) have been extensively used in the literature [151-153]. Some investigations have reported the mild hepatotoxic effects of nano silver-loaded wound dressings [154]. In comparison, the unique properties of ZO that improves epithelialization and enhances the local defence system reduces bacterial infection and inflammation [114, 155]. This material is now standard antimicrobial therapy for management of wounds in second or third-degree burns [118-119].

Based on the abovementioned properties, In the present work, we fabricated a novel wound dressing made of HA-SF/ZO composite core-shell nanofibers using coaxial electrospinning method with antibacterial properties for the treatment of infections in second-degree burn injuries.

2.1 Materials and methods

2.1.1 Materials

Silk cocoons from Bombyx mori were obtained from Iranian silk worm research canter. Besides, lithium bromide (LiBr; 746479, Sigma-Aldrich, Saint Louis, USA), sodium carbonate (Na2CO3; 106392, Merck, Germany), cellulose dialysis tube (12 kDa MWCO, Sigma-Aldrich, Saint Louis, USA), formic acid (100264, Merck), absolute ethanol 99.7% (Merck, Germany), glutaraldehyde 25% (820603, Merck, Germany), HA (cosmetic grade, Mw = 2,000,000 Da), sodium hydroxide (NaOH, 97+ ACS grade), ZO nanopowder (<50 nm particle size), and dimethylformamide (DMF, 99.8% ACS) were purchased from Sigma-Aldrich. Ammonium hydroxide (NH4OH, 25% in water) was purchased from Fluka (Switzerland). All reagents used in this work were employed without further purification.

2.1.2 Preparation of electrospun solution

Initially, SF was extracted from Bombyx mori cocoons according to our pervious study [164]. The isolated SF was dissolved in formic acid at 13% (w/v). ZO nanoparticles in three different concentrations (1, 3, and 5% w/v) were added to SF solution. HA solution was prepared by dissolving 1.5% HA in 2:1 solution of NH4OH:DMF [165].

2.1.3 electrospinning of coaxial nanofibers

Coaxial electrospinning procedure was performed at room temperature (Figure 7). SF solution with different concentrations of ZO was used as the core solution and HA solution as the shell solution. The code and composition of each prepared core-shell fibers are summarized in Table 2. For

electrospinning, a 5-mL capacity of syringe loaded with SF-ZO solution was connected to the internal needle with a 0.5-mm diameter, and HA solution was loaded in another 5-mL syringe connected to the external needle with a 0.8-mm diameter. After optimization, coaxial electrospinning was performed at 17 kV (Gamma High Voltage Research, FL, USA) with a constant flow rate of 0.25 mL/h. The distance between collector and needle tip kept at 12 cm.

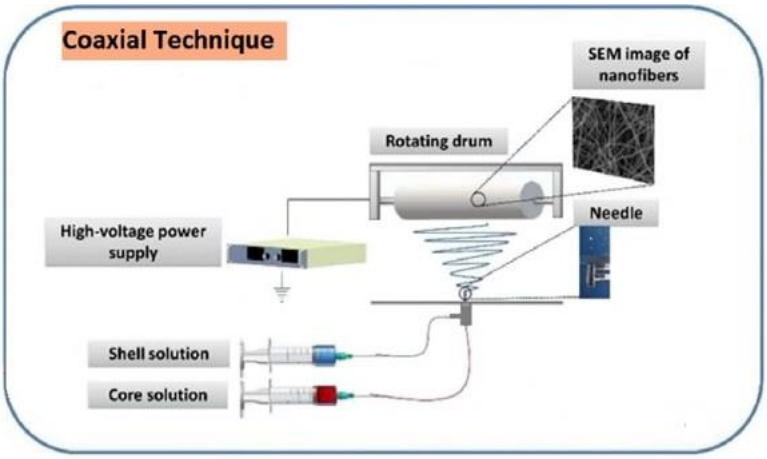

Figure 7: the schematic of coaxial electrospinning technique[160].

2.1.4 characterization of core-shell nanofibers

Morphologies and microstructures of all electrospun mats were analyzed using scanning electron microscopy (SEM; Essen Philips XL 30). SEM images from approximately 50 random fibers were examined to assess the average fiber diameters and distributions using the image analysis software (ImageJ, NIH, USA). The core-shell structures of the electrospun mats were observed using transmission electron microscopy (TEM, FEI TecnaiG2 20 S-Twin. The dispersion of ZO within the SF-HA/5ZO was examinned using EDX elemental mapping. Furthermore, the (FTIR, PerkinElmer–Frontier, USA) was used to study the compositions of the prepared electrospun mats.

Pseudo extracellular fluid (PECF) as simulated wound fluid was used for swelling measurements. PECF was prepared by dissolving 0.68 g of NaCl, 0.22 g of KCl, 2.5 g of $NaHCO_3$, and 0.35 g of NaH_2PO_4 in 100 mL of double distilled water. The pH of PECF was adjusted to 8.5. To determine the equilibrium water uptake, the pre-weighted mats (W_0) were immersed in the PECF

swelling medium (T = 37 ˚C). At predetermined time points, the samples were removed and weighted (W_s). The measurements were carried out for each sample in three replications (n = 3). The amount of water uptake was calculated as follow [166]:

Water Uptake = (W_s-W_0)/W_0Ws-

WoWo×100$\frac{\text{Ws-W0}}{\text{Ws}} \times 100$ (1)

To determine the weight loss of samples including plain HA, plain SF, SF-HA, HA-SF/1ZO, HA-SF/3ZO and HA-SF/5ZO, three disks of each electrospun fibers (diameter=8mm) with the initial weight of (W_0) were immersed into phosphate buffer saline (PBS; pH = 7.4) at 37 ºC with gentle shaking. At each degradation time point, the collected samples freeze dried and weighted (W_d). The percentage mass loss was calculated based on the following equation [166]:

Weight loss (%) = ((W_0-W_d)/W_d)×100Ws-

WoWo×100$\frac{\text{Ws-W0}}{\text{Ws}} \times 100$ (3)

Where W_0 and W_d are initial and final weights of each sample, respectively. Six replicates were used to examine the reproducibility of the results.

2.1.5 In vitro drug release

In vitro ZO release behavior from the HA-SF/ZO electrospun mats was evaluated based on our previous study [167]. Briefly, the samples were immersed in phosphate-buffered saline (PBS) and incubated at 37 °C for 2 weeks. At predetermined time points, 1 mL of the solution containing the ZO was collected from each sample and was replaced by same amount of fresh PBS solution. The amount of released ZO was determined using an ultra-violet spectrophotometer (UV-spec) at its characteristic wavelength of 370 nm [168]. Six replicates were used to examine the reproducibility of the results.

2.1.6 Statistical analysis

The quantitative data were expressed as means ± standard deviations using an ANOVA Calculator: One-Way Analysis of Variance Calculator. P* < 0.05 was considered statistically significant.

2.2 Results and discussion

2.2.1 Morphological study

SEM was used to evaluate the morphologies of the electrospun fibers and determining fiber diameters. The morphology of the HA-SF coaxial nanofibers containing different concentrations of ZO with diameter distribution histograms can be observed in Figure 8a-d. From the SEM images, it was observed that all composite fibers had uniform, circular cross section, porous, and bead-free structures. The mean fiber diameters were determined as 155±11 nm in HA-SF, 164±15 nm in HA-SF/1ZO, 178±17 nm in HA-SF/3ZO, and 189±15 nm in HA-SF/5ZO. Accordingly, the fiber diameter distributions were slightly wider in HA-SF/ZO fibers when compared with that of the ZO-free HA-SF fibers. In fact, it was found that increasing the ZO content resulted in an increase in fiber diameter as a result of higher viscosity. Similar observations were also reported by other studies that the incorporation of agents and particles into electrospun solutions affected the fiber diameters of the electrospun mats through changes in solutions' rheological properties [169-170]. This theory was confirmed by Liao et al. [171], who showed that the concentration of ZO particularly affected the fiber diameter of electrospun ZO-polyvinylpyrrolidone (PVP) nanofibers. They found that the polymer solution containing higher concentration of ZO induce the formation of thicker ZO-PVP composite fibers due to the increase of polymer viscosity. The presence of ZO nanoparticles within composite core-shell fibers was further confirmed by energy dispersive X-ray (EDX) mappings, as shown in (Fig. S1b). Accordingly, EDX elemental mapping showed the homogenous distribution of ZO within HA-SF/5ZO nanofibers. Furthermore, the EDX elemental spectrum (Fig. S1c) of the selected area in the SEM image found signals related to the Zn that further confirm the successful doping of ZO nanoparticles within electrospun fibers.

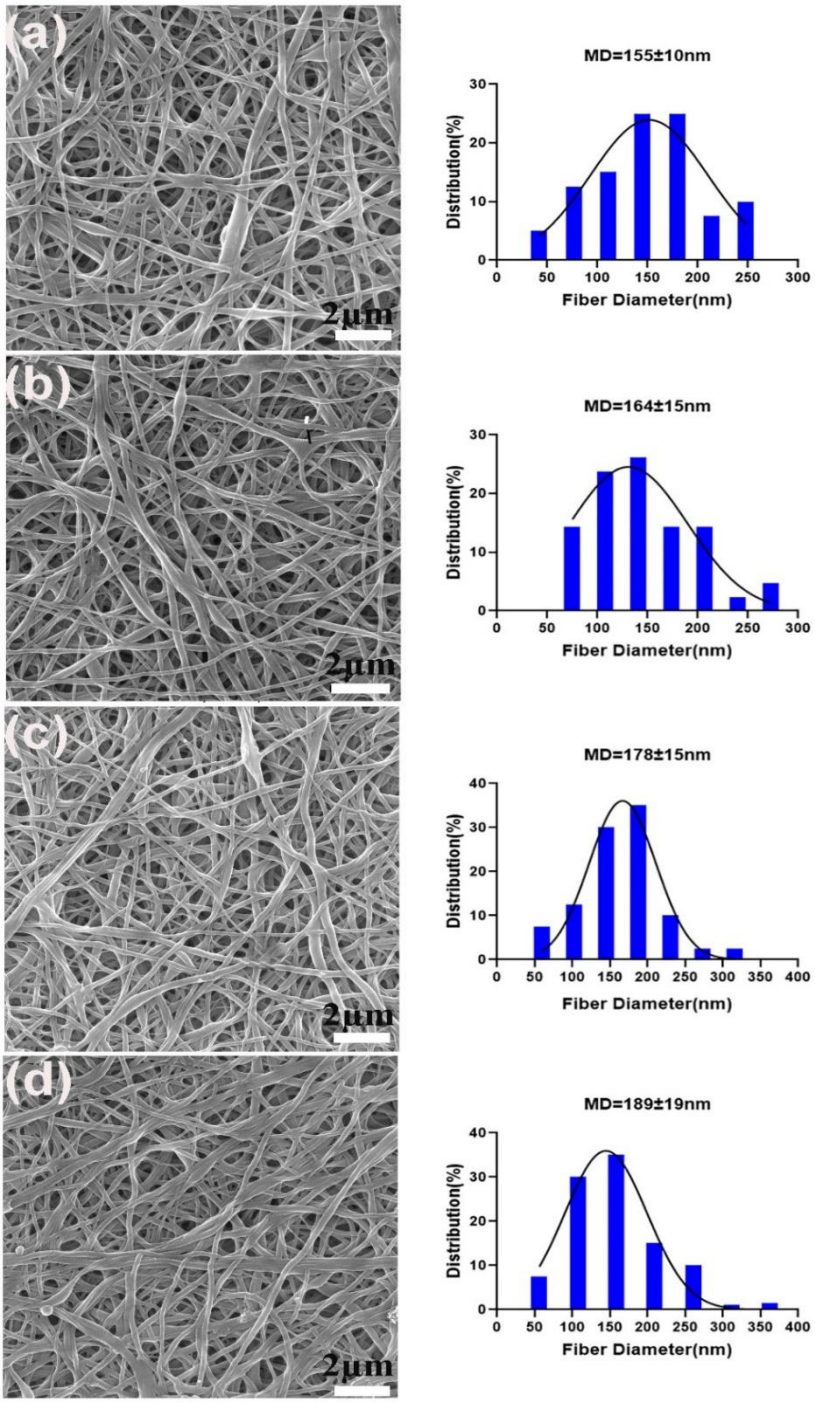

Figure 8: The SEM images and histograms showing the diameter distribution of the fibres formed; (a) HA-SF, (b) HA-SF/1ZO, (c) HA-SF/3ZO, and (d) HA-SF/5ZO (scale bar = 2μm). MD: Mean diameter (nm)

The structure of coaxially electrospun HA-SF fiber was further characterized by TEM to ascertain the fine ultrastructural features of the core-shell structure. The results are shown in Figure 9a. The HA-SF electrospun fiber had an obvious core–shell structure. The dark zone in the TEM image indicated the core layer of 56.42±8 nm in diameter and the brighter region was the shell layer with diameter of 149±5nm. Such core-shell structure was achieved by the quick stretching of

nanofibers followed by rapid evaporation of the organic solvent from the fibers during the electrospinning process.

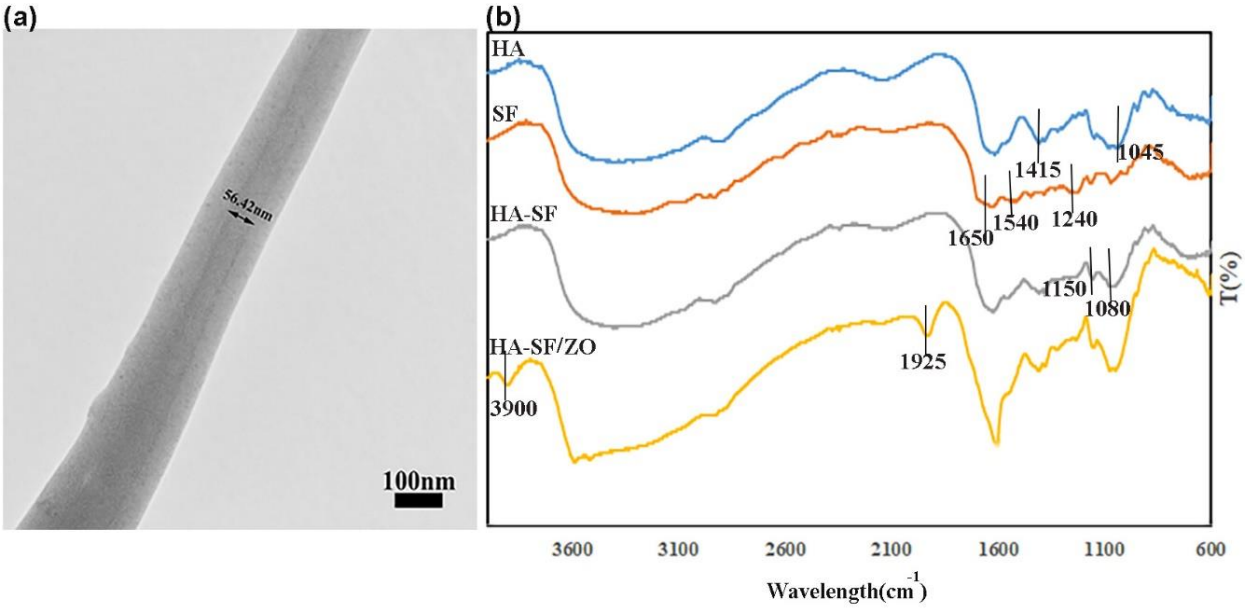

Figure 9: (a) The TEM image of the HA-SF nanofiber with distinguished core-shell structure, (b) the FTIR spectra of HA, SF, HA-SF, and ZO-loaded HA-SF nanofibers.

2.2.2 FTIR

FTIR analysis was performed to further study of structural changes and chemical composition of HA-SF/xZO fibers during electrospinning. Figure 9b shows the FTIR spectra of neat SF, HA nanofibers, SF-HA, and SF-HA/ZO composite fibers. Referring to neat SF, the characteristic peaks were observed at 1,650, 1,540, and 1,240 cm^{-1}, representing amide I (C = O stretching), amide II (N-H bending), and amide III (C-N stretching), respectively [172]. The IR spectra for HA consists of two main peaks at 1415 and 1045 cm^{-1}, which represented the carboxylate symmetric stretching and C−O−C stretching vibration of HA skeleton [173]. In addition, the peak at 1255 cm^{-1} assigned to the stretching region of group protonated COOH [174]. After compositing, SF-HA the characteristic peaks of HA overlapped with the peaks of SF and new peaks appeared at 1150 and 1080 cm^{-1} that indicated the amide and ester linkage. This link was formed between HA and SF due to the reaction between hydroxyl groups of HA with amine groups of SF, which most often formed by the condensation of an alcohol and an acid, with elimination of water. The ester linkage contains the functional group

C=O joined via carbon to another oxygen atom [175]. Furthermore, the appearance of new peaks located at 3900 and 1925 cm−1 could be observed in the HA-SF/ZO composite fibers, but not in the other components, which represented the successful incorporation of ZO into HA-SF core-shell nanofibers.

2.2.3 Wettability

Wettability and water uptake capacity is one of most important factor for evaluating the rate of fluid absorption of wound dressings particularly for exudates wounds. Wound dressings with ability of fluid absorption, facilitate wound healing rate during the rehydrating necrotic tissue, absorbing wound exudates, and nutrient and waste transporting [176]. An ideal wound dressing should possess optimal swelling capacity since high swelling ratio can result in disturbing the wound dressing function due to the blocking the porosity, less oxygen diffusion to the wound site and less adhesion to wound in order to deliver therapeutic agents, while low swelling capacity would impair wound healing procedure [177-178]. The water-absorption capacities of the HA and HA-SF/ZO electrospun mats after 24 h of immersion in PECF (simulated wound fluid) is presented in Figure 10a. As expected, the HA electrospun mats have showed highest swelling ratio (151.49±4.42%) due to the high density of hydrophilic groups and its amorphous nature [179]. However, the water uptake percentage decreased for the HA-SF/ZO core-shell nanofibers to around 85.43±1.56 % in HA-SF, 85.23± 0.79 % in HA-SF/1ZO, 87.29± 0.91 % in HA-SF/3ZO, and 87.53± 1.45% in HA-SF/5ZO. The ZO contents did not significantly affect the wettability of the scaffolds ($p>0.05$). This reduction in water uptake in HA-SF/ZO core-shell fibers compared to the plain HA can be explained by the existence of SF that contains high density of hydrophobic domains, i.e., protein crystals with high degree of crystallinity[180]. These results suggest that incorporation of SF into HA with a core-shell structure can improve the stability of HA by reducing the swelling ratio. Similar results were reported by Hu et al.[181] that blending HA hydrogel with SF improved the stability of HA by reducing the swelling capacity of hydrogel.

Contact angle is another method to measure the wettability of a surface of wound dressings, which has a key role in controlling water loss in an open and wet wounds and also in supporting cell adhesion[182-183]. Figure 10b represents the water contact angle of prepared nanofibers. The HA nanofiber showed the lowest water contact angle (66.88±0.8°) while those of the core-shell HA-SF/ZO fibers were around 77.45±0.5°. The contact angle of HA-SF/ZO core-shell nanofibers are pretty close to the contact angle of tissue culture plates (75.6°). This result indicated that the fabricated nanofibers could potentially support cell adhesion. In fact, the optimum water contact angle value for fibroblast attachment was determined in the range between 65°-75° [184].

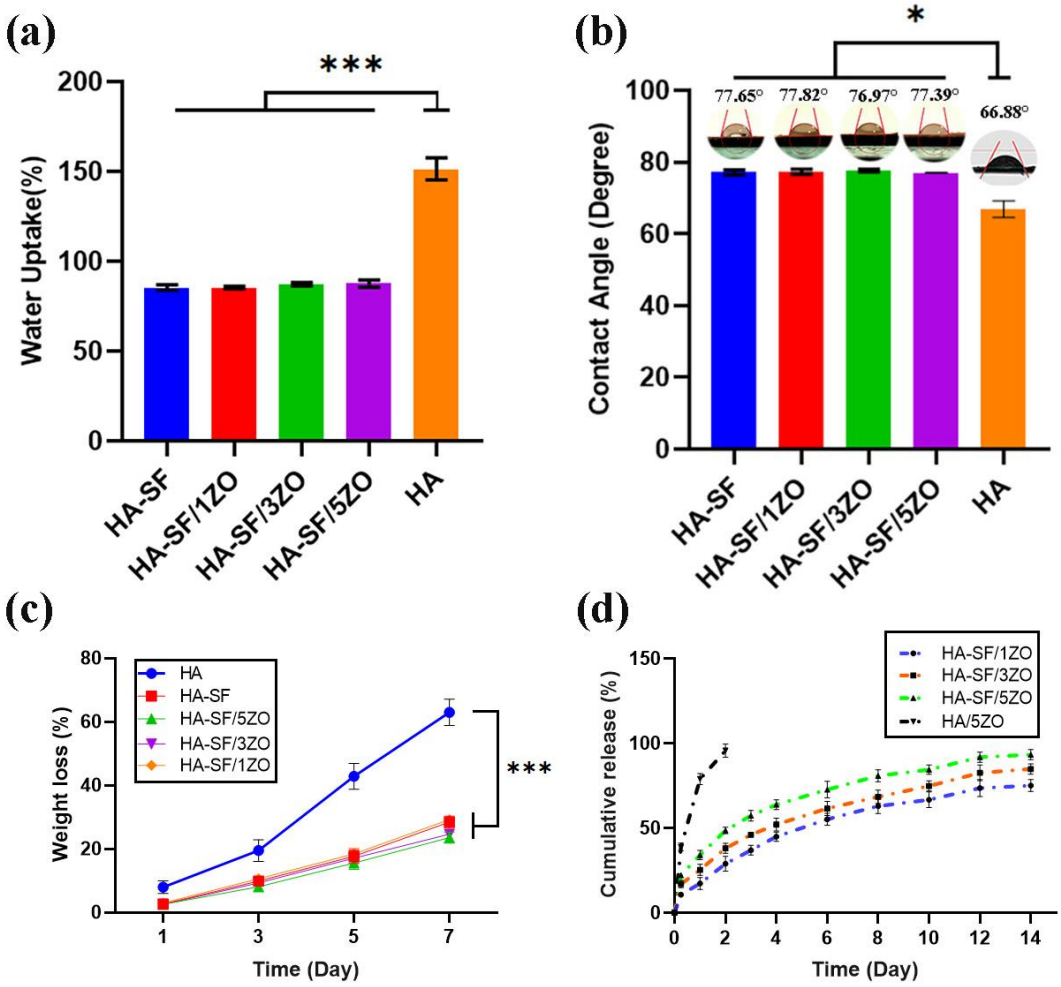

Figure 10: Water uptake, weight loss percentage and drug release profile of electrospun fibers. (a) water uptake percentage after 24 h soaking in PECEF, (b) statistic of water contact angle with shapes of a water droplet on corresponding nanofibers, (c) weight loss profile of samples over 1 week in PBS and (d) ZO release from different electrospun fibers (p<0.05, p**<0.01, p***<0.001). Six replicates were used to examine the reproducibility of the results using ANOVA.*

2.2.4 Degradation study

The degradation rate of drug loaded wound dressings have a direct effect on the stability of loaded drugs, drug release profile, toxicity and mechanical stability [185]. One strategy to control the release rate of drugs from wound dressings is by controlling the degradation rate of material. Fast degradation rate of wound dressings can result in the burst release of drugs and can lead to high cell cytoxicity [186]. Furthermore, the progress of wound healing process depends on the epithelization rate which is synchronized with polymer degradation rate resulting in completion of healing process in a given time frame [187].

Weight loss profile for HA and HA-SF/ZO electrospun dressings has been evaluated through degradation tests in PECEF to assess hydrolytic degradation. Fig. 10c shows the weight loss (%) of samples during 1-week incubation in PECEF. It can be observed that, mass loss is the highest for HA in which 63.2±5% of the studied electrospun mat degraded after 1 week. Such value decreased to 28.99±2.35 % in HA-SF, 29.20± 1.69 % in HA-SF/1ZO, 24.65± 1.76 % in HA-SF/3ZO, and 23.57 ±2.55% in HA-SF/5ZO. This behavior could be explained by reducing the water uptake capacity of HA-SF/ZO mats due to the presence of hydrophobic SF as a core that inhibit further penetration of PBS to the wound dressing which leads to bond cleavage reduction and consequently reduce the hydrolysis process. This finding was consistent with the results obtained by Raia et al.[188]. This indicated that incorporation of SF to HA hydrogel slowed down its degradation rate significantly.

2.2.5 In vitro release study

The continuous and controlled release of antibacterial drugs from wound dressings are an important factor to prohibit bacterial infection [189] . The total ZO release data for HA/5ZO and HA-SF/1-5ZO is presented in Figure 10d. Among all of samples, HA/5ZO displayed a characteristic one-stage release, which high portion of ZO released at a short time period (22 h). This high rate of release in short time in HA/5ZO sample can be attributed to the fast degradation rate, low crystallinity and hydrophilic nature of HA. As showed in Fig. 4d, the core-shell nanofibers displayed biphasic release behavior

with a small initial burst release followed by a sustained release. Initially, the burst release of ZO around 11–22% during the first 6 h occurred through the release of the ZO, which was physically adsorbed or weakly bounded to the polymer nanofibers [190]. Subsequently, the rate of ZO release was slowed over the period of 14 days due to the diffusion mechanism and slow degradation rate of the SF nanofibers [191]. These results indicated that the bacterial infection might be controlled for over 14 days by using our ZO-incorporated core-shell nanofibrous structures. This core-shell structure wound dressings will decrease the frequency of dressing changes in comparison with the traditional cream-based treatment, which requires daily attention [192-193].

2.2.6 Tensile test

Wound dressings should be robust enough to facilitate handling and sterilization before use and withstand the skin tensions post-application. In addition, nanofibrous scaffolds need to be mechanically supportive for cell growth and remodelling [194]. The tensile test results for pure electrospun SF, HA, and core-shell nanofibers are summarized in Table 3. According to Table 3, the elastic modulus for HA-SF/1ZO (6.79±0.21MPa), HA-SF/3ZO (7.12±0.17MPa), HA-SF/5ZO (7.68±0.22 MPa) were significantly lower than that of pure SF (8.87±0.13) and higher than that of pure HA (4.27±0.19). A similar trend also was also observed for ultimate tensile strengths. by contrast, the breaking at strain for HA-SF/ZO (39.03±0.23%), HA-SF/3ZO (40.12±0.18%), HA-SF/5ZO (32.78±0.12%) were higher than that of pure SF (10.12±0.18). These results can be assigned to this fact that SF is very brittle biomaterial with high tensile strength due to the secondary structures of crystalline β-sheets [195]. Furthermore, Enhanced flexibility and elongation at break of SF upon blending with other polymers has been reported before, which related to the formation of flexible intermolecular interactions by hydrogen bonding and decreasing the crystalline regions when blended with SF [196-197]. Altogether, these results suggested that the HA-SF/x(ZO) core-shell fibers were mechanically appropriate for skin tissue engineering and wound dressings application as the tensile

strengths ranging from 0.8 to 30 MPa were reported to be sufficient for applications in skin tissue engineering [198-199].

Table 3: the mechanical properties of electrospun nanofibers

Sample code	Tensile modulus (MPa)	Ultimate tensile (MPa)	Breaking strain (%)
SF	8.87±0.13	36.38±2.21	10.12±0.18
HA	4.27±0.19	19.50±1.18	27.01±0.21
HA-SF/1ZO	6.79±0.21	22.75±2.33	39.03±0.23
HA-SF/3ZO	7.12±0.17	26.65±2.94	40.12±0.18
HA-SF/5ZO	7.68±0.22	28.76±2.18	32.78±0.12

Table 4: the code and composition of electrospun nanofibers

Code	SF (%Wt.)	HA (%Wt.)	ZO (%Wt.)
HA-SF	13%	1.5%	0
HA-SF/1ZO	13%	1.5%	1
HA-SF/3ZO	13%	1.5%	3
HA-SF/5ZO	13%	1.5%	5

Chapter 3: In vitro cell and bacterial study

Biocompatibility of fabricated wound dressings is crucial given its intended purpose for the treatment of burns. Depending on the degree of the burn some or all of the layers of the skin and underlying tissue can be damaged and exposed. In order to test the biocompatibility and healing properties of our nanofibers components, different in vitro cellular tests were conducted.

3.1 In vitro cell culture study

Human keratinocytes (HaCat cells, Addexbio, San Diego, CA, USA) were cultured in Dulbecco's Modification of Eagles Medium (DMEM; Gibco, Scotland) containing 10% fetal bovine serum (FBS; Gibco, Scotland), 100 μg/mL penicillin (Sigma–Aldrich, Saint Louis, USA), and 100 μg/mL streptomycin (Sigma–Aldrich, Saint Louis, USA) in a humidified atmosphere of 5% CO2 at 37 °C. The culture medium was refreshed every 2 days.

3.1.1 SEM imaging of cultured cells

Triplicate specimens (n=3) of the electrospun scaffolds were cut into round disc with 10-mm diameter and sterilized under UV radiation. To evaluate cell adhesion on the scaffolds, 2×10^4 cells per well were seeded on the surface of each nanofibrous mat and cultured for 3 days in 48-well plate. The cells were fixed with 4% (v/v) glutaraldehyde solution in PBS at 4 °C for 30 min. Finally, they were dehydrated in a series of ethanol/distilled water solution (10% ethanol increment; each step 10 min). The morphology of the attached cells on dried electrospun scaffolds was observed under SEM and images were taken [200].

3.1.2 Cell viability and proliferation assay

After HaCat cells were cultured for 3 days on the prepared nanofibers, cell-seeded constructs were stained with 4-μM calcein AM (Invitrogen, San Diego, CA) and 4-μM of propidium iodide (Invitrogen, San Diego, CA) for 30 min. The live cells were shown in green (ex/em ~495 nm/~515

nm). The dead cells were stained red (ex/em ~540 nm/~615 nm) [201]. The relative viability of the cultured HaCat cells was determined using the indirect 3-(4,5-dimethylthiazol-2-yl)-2,5diphenyltetrazolium-bromide (MTT, Sigma Aldrich, USA) assay based on an extraction method following our previously developed protocol [202]. In brief, we first incubated the electrospun scaffolds in cell media for 7 days to extract any possible cytotoxic content that may have been released from the scaffolds into the media. At each time point, the supernatant of each sample was collected, added to a well with HaCat cells, and incubated for 24 hr before performing the MTT assay. Later, the cell medium was removed from each well and 100 µL of MTT agent (0.5 mg/mL in PBS) was added into each well and kept in the incubator for 4 h. After 4 h, 100 µL of Dimethyl sulfoxide (DMSO) was added to the well until formazan crystals were completely dissolved. In the end, the absorbance was read at 545 nm by using plate reader (Stat Fax-2100, Miami, FL, USA). We normalized the results with the readings from cells with control group which was the cultured cells in well plate without nanofiber samples.

3.1.3 Immunostaining assay

To further evaluation the effect of ZO concentration on the morphology of attached cells on core-shell nanofibers after 3 days of submerged culture, the cells were immunostained with E-Cadherin and imaged. Briefly, the supernatant was removed and cells were fixed with 3.7% formaldehyde solution for 15 minutes. Next, samples were incubated with blocking buffer (5% bovine serum albumin and 0.3% Triton X100 in PBS) for 60 min at room temperature. After washing the samples with PBS, they were incubated with E-Cadherin antibody dilution buffer (Rabbit mAb Alexa Fluor® 488 Conjugate, Cell Signaling Technology, CA) at 4 °C overnight. Subsequently, the wells were incubated with DAPI solution (5 µg/mL) for 15 min at room temperature. The cells were then washed with PBS and imaged using fluorescent microscopy.

3.1.4 Scratch wound healing assay

HaCat cells with concentration of 1×10^5 cells/mL were seeded and cultured in the wells of a 6-well plate and culture plates were incubated at 37 °C for 24 h to produce confluent monolayers. Then, the gap with 1-mm width was created onto the monolayer of cells using a p200 pipette tip, and debris was removed by washing the cells twice with warm PBS. The electrospun mats were placed in cell strainer in order to direct release into the cell media. Next, 2 mL of fresh complete medium was added to each well. To determine the rate of cell migration for each treated nanofibers, the samples were continually imaged at 0, 12, 24, and 48 h. Images of the scratched regions were taken by an optical microscope (Olympus). Scratch contraction percentage was calculated from the distance between cell boundaries before the treatment with the samples and after treatment at different time points using the Image J software (NIH, USA). For each well, five images were taken after random selection [203].

3.1.5 Antibacterial study

The antibacterial activities of electrospun mats were evaluated against model microbial species including gram-negative (*E. coli*, ATCC 9637) and Gram-positive (*S. aureus*, ATCC 12600) through the disc diffusion method. Briefly, about 100 µL aliquot of bacteria solution containing 1×10^8 bacteria cells/mL reconstituted in nutrient broth and previously sub-cultured was spread onto an agar petri dish. Electrospun mats with 6-mm diameter were placed on the surfaces of the Petri dishes and incubated at 37 °C for 24 h. Gentamicin discs were chosen as positive control. Finally, the diameters of the inhibition zones were measured using ImageJ. Furthermore, the antibacterial activities of all samples were evaluated through the colony-forming unit (CFU) test [204]. Briefly, the fresh colonies of two bacteria strains were suspended into nutrient broth medium and incubated for 24 h at 37 °C. Afterward, the prepared solutions were diluted to the concentration of 10^7-10^8 cells/mL (OD = 0.08-0.1 at 625 nm). Then, the prepared samples were kept into bacterial solutions and incubated in a shaker incubator at 37 °C with a shaking speed of 100 rpm for 24 h. The bacterial suspension without any nanofibers was considered as a negative control. After that, 10 µL of bacterial medium treated

with different samples was removed and spread onto an agar plate, incubated at 37 °C for another 24 h. Finally, the number of viable bacterial cells were counted using ImageJ.

3.2 Results and discussion

3.2.1 Cell assays

The biocompatibility is another factor that should be considered during the selection of biomaterials for fabrication of wound dressings, since biocompatible wound dressings can enhance cell migration, promote angiogenesis and connective tissue regeneration [30]. We evaluated the cytotoxicity of HA-SF electrospun mats containing different amounts of ZO (0, 1, 3, and 5% Wt.) on HaCat cells *in vitro*. Cells were grown with the electrospun mats for 7 days and their metabolic activity was measured on days 3 and 7 post-culture. Pristine HA-SF electrospun mats exhibited no cytotoxicity to cells during the studied periods (Figure 11d). We noticed a ZO dose-dependent cytotoxicity to HaCat cells for nanofibers containing ZO. The samples showed good cell proliferation after 7 days in culture for up to 3% ZO doping. HA-SF nanofibers with 3% ZO significantly improved cell proliferation in comparison to the other groups. However, HA-SF/5ZO mats showed significant decline ($p<0.05$) in cell viability. It is noteworthy that the cell viability exposed to HA-SF/5ZO extracts declined by increasing culture time from 3 days (90.41 ± 1.69 %) to 7 days (85.64 ± 1.84 %) as a result of more release of ZO.

Moreover, the distributions and viabilities in terms of cell death of 3-day cultured HaCat cells on the HA-SF nanofibers containing different concentrations of ZO were evaluated using SEM as well as confocal microscopy after live/dead cell staining (Figure 11a-b). More live cells and cell spreading were observed in the HA-SF/3ZO group (Figure 11a and b). The cells connected with each other and covered most of the HA-SF/3ZO surface. In comparison, the HA-SF nanofibers with 5 wt.% ZO showed lower cell density and more dead cells. These results indicated that ZO had a stimulating impact on HaCat cell proliferation and attachment. These findings might be related to the positive role of zinc on metabolic processing, ECM regulation, stimulation the proliferation of

epidermal cells (keratinocytes and fibroblasts), increase of collagen synthesis, wound healing modulation, and stabilizing cellular membranes [205-207]. However, the samples indicated a decreased potency to support cell adhesion and proliferation when ZO amount was over 5 wt.%. Similar results were also reported by other studies that higher ZO amount in scaffolds had detrimental impacts on the cell attachment and proliferation. Cell apoptosis was reported for 3.5 wt.% ZO-doped scaffolds [208-209].

Additionally, fluorescent immunostaining was carried out to investigate the effect of ZO concentration on the morphology of HaCat cells. As shown in Figure 11C, HaCat cells attached and spread on all electrospun mats. However, HA-SF nanofibers with 1% and 3% ZO significantly improved cell spreading since cells displayed healthy spindle-like or star-like shape with more filopodial structures. In comparison, cells cultured on HA-SF/5ZO showed a rounded morphology with less filopodial structures. Similar finding was also reported by a previous study, which showed that low concentration of ZO nanoparticles (2 wt.%) within poly (vinylidene fluoride-trifluoroethylene) (P(VDF-TrFE)) electrospun fibers resulted in improving cell spreading and cell elongation, while higher concentration of ZO over 4 wt.% demonstrated less cell adhesion and spreading [210].

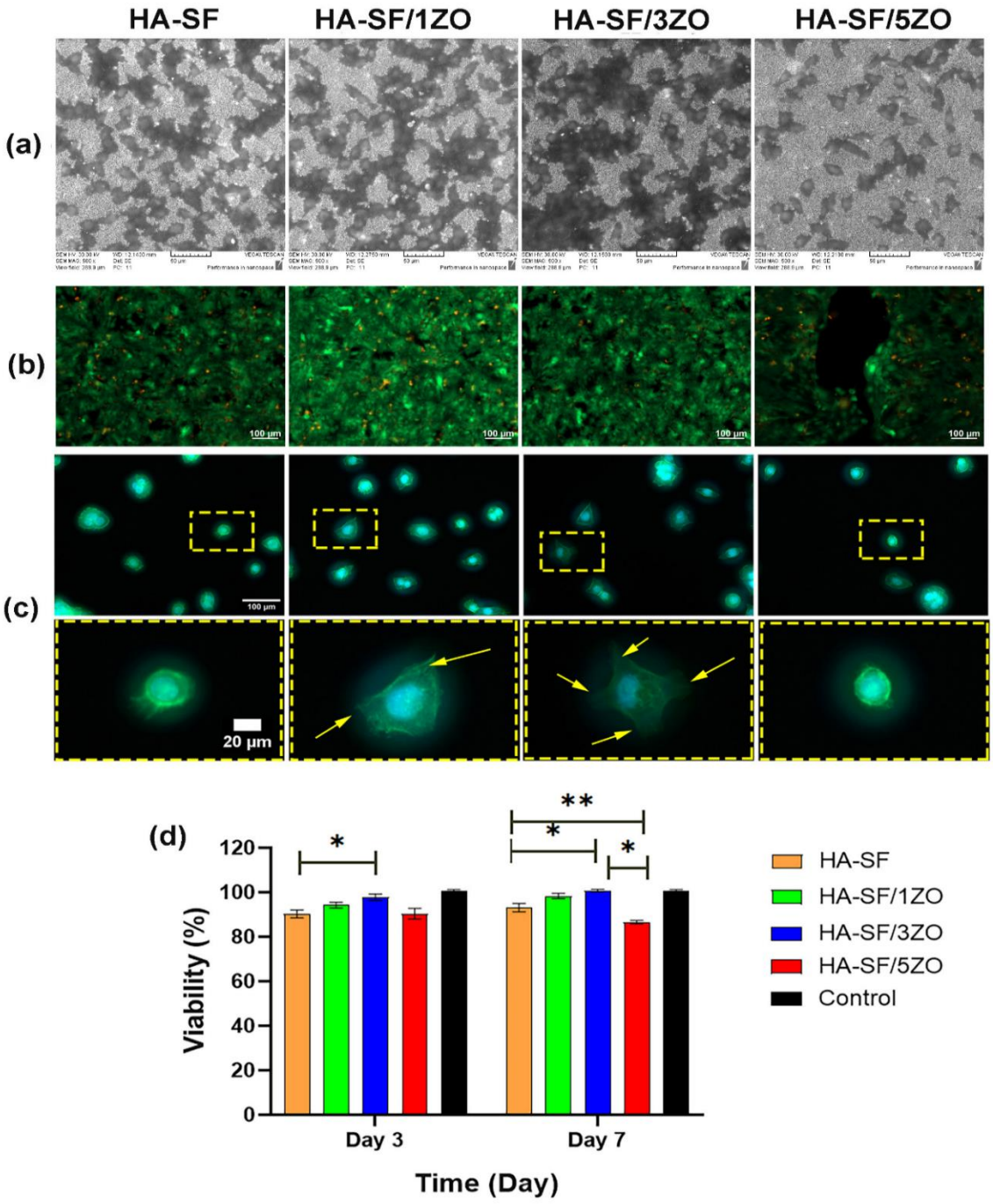

Figure 11: The cell results. (a) SEM images of culture cells for 3 days, (scale bar = 50 µm). (b) Live and dead staining of cultured HaCat cells on nanofibers containing different amount of ZO for 3 days. (c) (c) Fluorescent immunostaining of cells adhering to the mat surfaces after 3 days of culturing (yellow arrows showing the filopodial structures) (d) Indirect MTT assay of different mats over 7 days of culturing (p<0.05, p**<0.01). Eight replicates were used to examine the reproducibility of the MTT results using ANOVA.*

3.2.2 Scratch assay

To evaluate the effects of each wound dressings on keratinocyte migrations, the *in vitro* wound healing assay was conducted. The distance gaps were similar across all the samples during the first

hours (Figure 12). After 24 h, the treatment with HA-SF/3ZO significantly enhanced the migration of HaCat cells towards the open area when compared to the other groups, which about more than 70% of scratched area were closed. The entire gap was covered for the HA-SF/3ZO treated group after 48 h. However, efficient migration was not observed for HA-SF/5ZO group (65.07±1.47%), which could be contributed to the cytotoxicity of this sample. From these findings, we concluded that the wound dressings containing 3%wt. of ZO had a positive effect on keratinocyte migration and wound healing. This study could not provide the detailed insight in to how ZO stimulates keratinocyte migration and their proliferation. However, there are some other studies, which support our observations. Barui et al. [211] reported that ZO promoted the migration of HUVECs cells and accelerated the closing rate in scratch assay. Another study showed that zinc activates the MAPK signalling pathway in HaCat cells, which promoted wound healing [212]. Besides positive effect of ZO in HA-SF/3ZO samples on HaCat migration and wound healing, many studies have shown that HA as a main component of the ECM of basal keratinocytes in epidermis involves in the proliferation and migration of keratinocytes in the wound healing process [213-214]. For example, Choi et al. showed that HA improved the HaCat migration during wound healing process by activation of Extracellular Signal-Regulated Kinase (ERK) and nuclear factor kappa B (NF-Kb) signaling pathways[215].

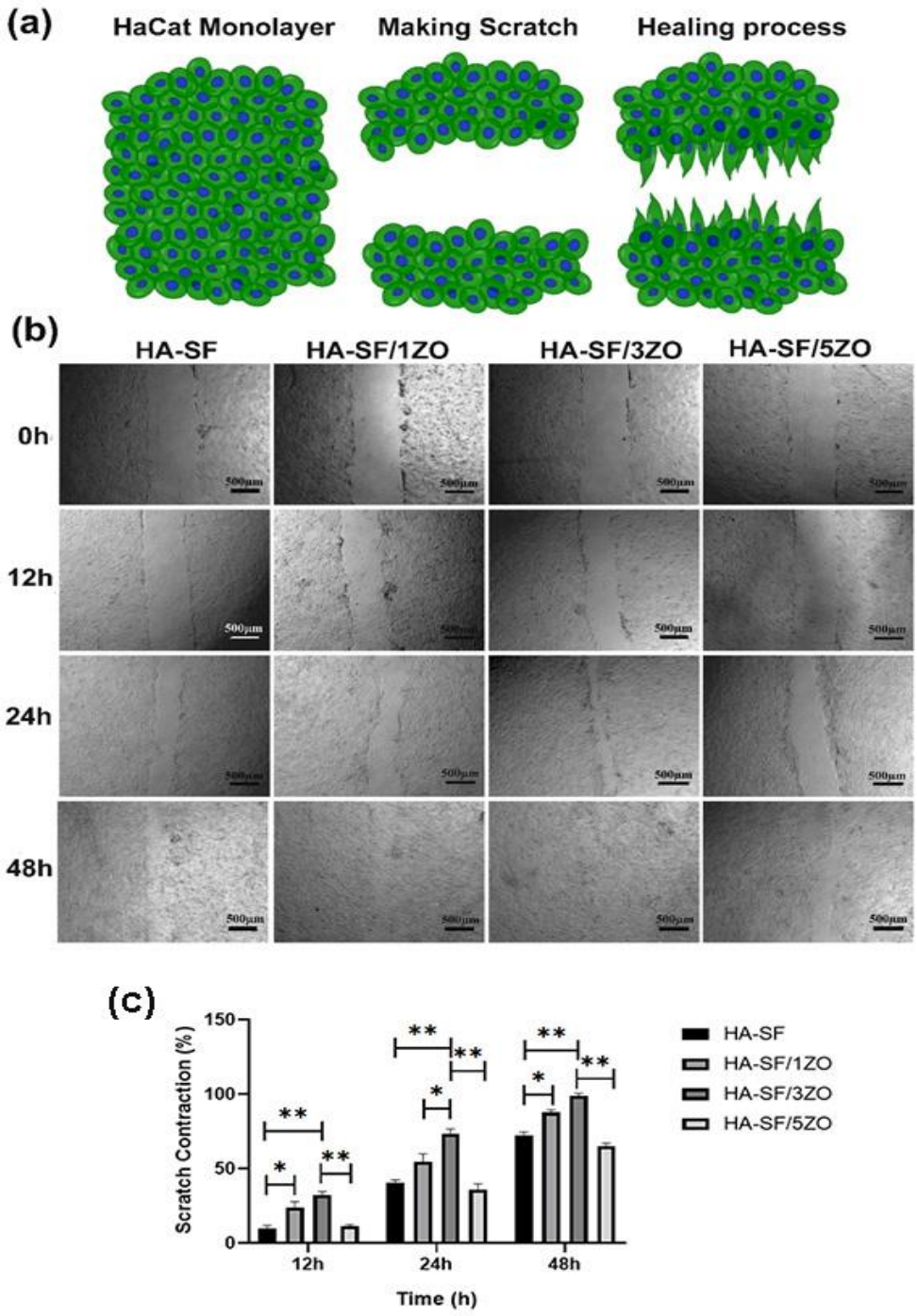

Figure 12: In vitro wound healing scratch assay. (a) Schematic illustration of scratch assay, (b) micrographs of the extent of closure for the evaluation of cell migration over 48 hours and (c) wound contraction rate as a function of time (p<0.05, p**<0.01). Six replicates were used to examine the reproducibility of the results using ANOVA*

3.2.3 Antibacterial study

The antibacterial activity of wound dressings has a key role for wound care , since they accelerate wound healing rate by reducing wound bacterial colonization and infection[42]. The antibacterial

performances of all samples are shown in Figure 13. The inhibitory activities of nanofiber mats on the growth of both bacteria were determined through the disc diffusion and CFU tests. The ZO-loaded nanofibers showed zones of inhibition against both bacterial strains. However, no antibacterial performance was observed for pristine SF-HA nanofibers (Figure 13a). After the incorporation of ZO particles into SF-HA mats, the mean diameters of inhibition zones for *E. coli* increased to 1.21±0.10 mm in HA-SF/1ZO, 2.68±0.11 mm in HA-SF/3ZO, and 2.93±0.12 mm in HA-SF/5ZO after 24 hours' incubation. A same inhibition pattern was observed for *S. aureus* bacterium. The diameters of the inhibition rings were enlarged with increasing the amount of ZO, starting at 1.83±0.09 mm in HA-SF/1ZO, 2.98±0.11 mm in HA-SF/3ZO, and reaching 3.37±0.12 mm in HA-SF/1ZO. Figur 13b presents the antibacterial activities of all samples through the CFU assay after 24 h of incubation with the bacteria. More colonies of *E. coli* and *S. aureus* were formed (Figure 13b) in the bacterial medium agar Petri dish consisting of pristine HA-SF fibers. However, the formations of number of *E. coli* colonies after adding the different concentrations of ZO (1, 3, and 5%Wt) in HA-SF composite nanofibers were reduced to 267±7, 79±3, and 28±2, respectively. The numbers of formed *S. aureus* colonies were 116±3 in HA-SF/1ZO, 42±2 in HA-SF/3ZO, and in 6±1 HA-SF/5ZO. These results suggested that HA-SF/xZO fibers have proper antibacterial activity.

According to the previous studies two possible mechanisms for the antibacterial activities of ZO-loaded composite fibers can be assigned (Figure 14) : (i) induction of oxidative stress in bacteria due to the production of ROS species like H_2O_2, O^{2-},OH^-; and: (ii) direct or electrostatic contact of Zn^{2+} ions with the cell surfaces, which result in damaging the bacterial cell membranes [216-218]. Furthermore, the results showed that the antibacterial activity of ZO-loaded nanocomposite fibers was greater against *S. aureus* compared to *E. coli*. This observation might be due to that the structure and the chemical compositions of the cell walls between *E. coli* and *S. aureus* are different. *E. coli* cell wall consists of lipid A, lipopolysaccharide and peptidoglycan, while *S. aureus* cell wall comprises of only a simple peptidoglycan layer [219-220]. Similar finding was reported by Becheri et al. [221] that , ZO nanoparticles showed greater antibacterial activity on gram-positive (*S. aureus*) than the

gram-negative (*E. coli*) bacteria. They suggested that the outer layer of gram positive *S. aureus* may facilitate ZO adhesion onto the cell wall whereas the surface of gram-negative bacteria may repeal this adhesion.

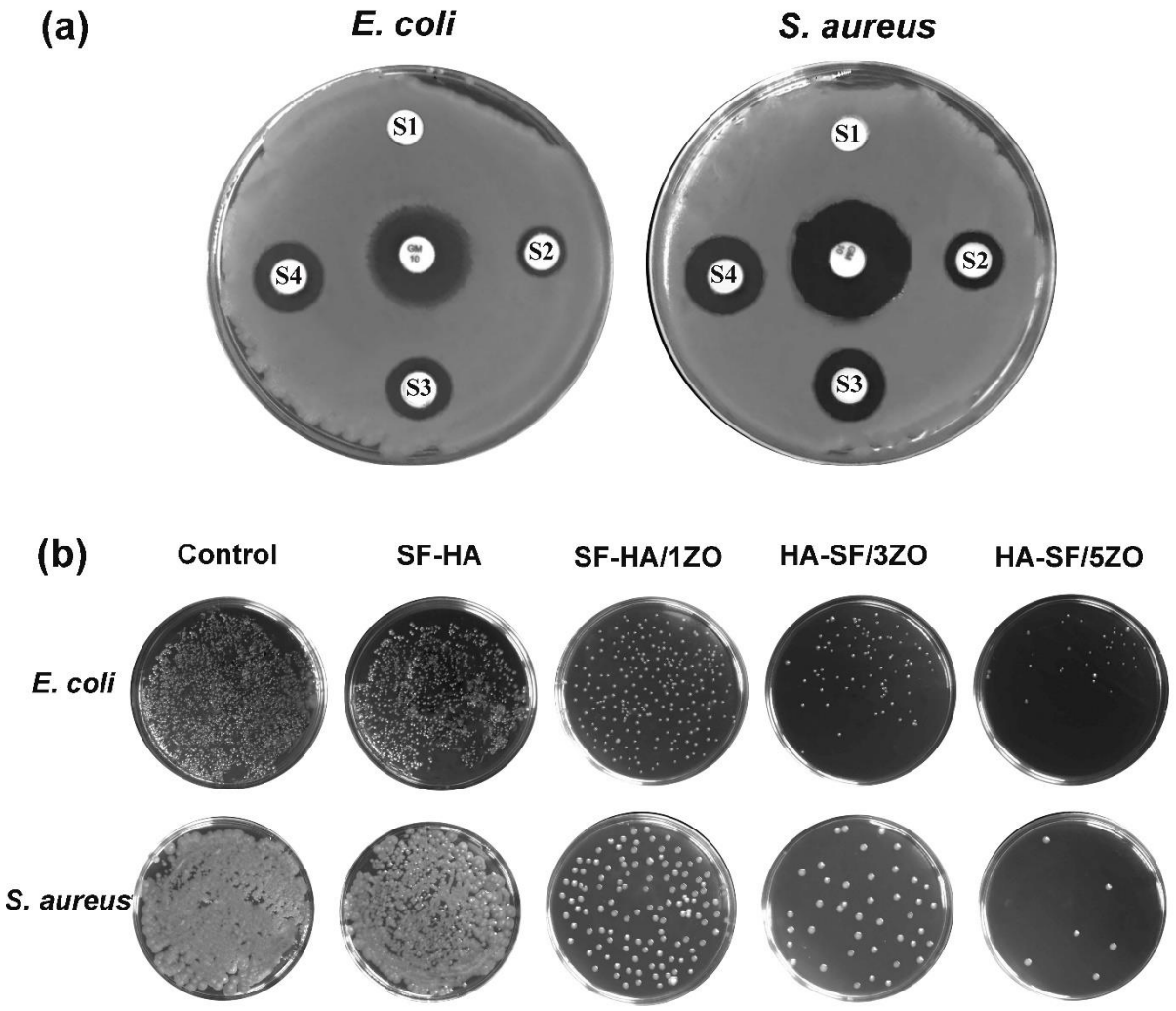

Figure 13: The evaluations of antibacterial activities of different samples against E. coli and S. aureus bacteria (a) disk diffusion method (b) CFU test (S1: HA-SF, S2: HA-SF/1ZO, S3: HA-SF/3ZO, S4: HA-SF/5ZO). Six replicates were used to examine the reproducibility of the results using ANOVA.

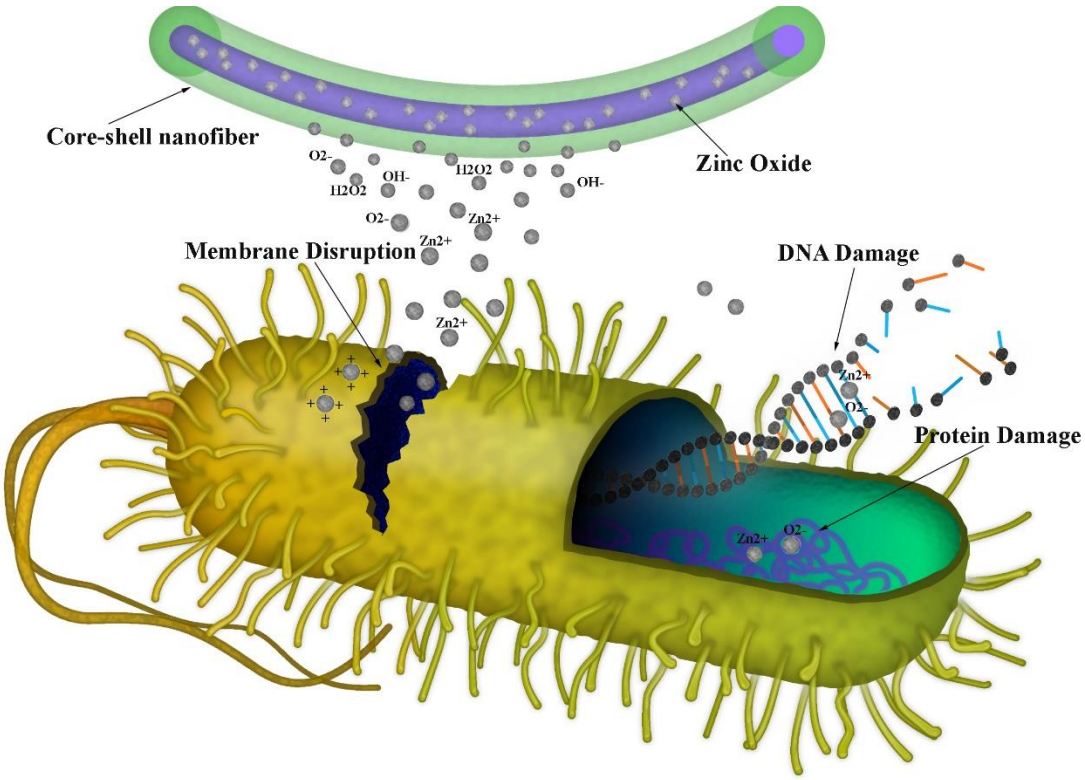

Figure 14: Schematic illustration of antibacterial mechanism of released ZO from HA-SF/ZO nanofibers.

Chapter 4: Animal study

Animal models of wound healing are usually conducted when computer based models or in vitro assays are not enough or when the physiological responses to the wound need to be analyzed. Furthermore, these preclinical investigations facilitate the evaluation and performance of the tested wound dressing in the presence of exudates, blood, inflammatory cells, skin cells, etc., which can have a direct impact on the activity of the skin substitute or wound dressing. Furthermore, to study the effect of the designed wound dressing on the wound, animal studies are crucial to the investigation of the safety of the product [222].

In this work, for in vivo experiments, the HA-SF/3ZO composite nanofiber was selected because of its good performance including high biocompatibility, antibacterial performance, and faster in vitro wound healing activity. Its wound healing efficiency was compared with the ZO-free HA-SF nanofibers and gauze (control) groups.

4.1 In vivo study

Sprague Dawley rats (350-400 g, 6-8 weeks old) were obtained from Pasteur Institute and acclimatized for one week before experimentation. Animal experiments were performed following the policies and procedures of the Institutional Animal Care and Use Committee at Faculty of Veterinary Medicine University of Tehran. The all rats were intraperitoneal anesthetized by injection of a mixture of ketamine (80 mg/kg) and xylazine (1.2 mg/kg), and then the dorsal surface of animals was shaved by clippers and dried. A second-degree burn was induced by applying an 85 °C hot plate (0.5 cm in diameter) for 10s. the wound lesions were photographed by a camera [223]. Afterwards, the rats were randomly divided in three groups (five rats/group) as follows: burns with gauze treatment, burns treated with ZO-free HA-SF wound dressing, and burns treated with HA-SF/ZO (3%) wound dressing. After 7 days, the wound dressings were removed and the amounts of wound closure was calculated as follows [224]:

Wound closure (%)= $((A_0-A_t)/A_0)\times 100\frac{A0-At}{A0} \times 1000$ (3)

where A_0 and A_t are the initial wound area and the wound area at time t, respectively.

Afterwards, the rats were euthanized using lethal dose of ketamine/xylazine (3X anaesthesia dose). The tissues of the treated wounds were harvested for further pathological investigations.

4.1.1 Histological and immunohistochemical staining

The wound tissue sections were collected on day 7. The tissues were fixed in formalin (10%) and were subsequently embedded in paraffin. The tissue blocks were cut into 4-µm sections. The obtained sections were deparaffinisedin xylene and stained with haematoxylin and eosin (H & E). The collagen formation was evaluated by Masson's trichrome (MT) staining. These sections were observed under a light microscope (Olympus BX51) [225].

To identify the anti-inflammatory responses of the prepared wound dressings and macrophage contents within the wound area, the tissue sections were stained with CD68 according to previously developed protocols [226-227]. Briefly, tissue sections were fixed in 4% paraformaldehyde for 30 min. Afterward, the sections were blocked for non-specific protein binding with 5% bovine serum albumin (BSA) in PBS for 10 min. Then the sections were incubated with the primary monoclonal mouse anti-mice CD68 antibodies (1:100 dilutions; Serotec, Raleigh, NC) at 4 ºC in a moist chamber overnight. The sections were washed three times with 0.1% Tween (in PBS). The slides were then incubated with the secondary Dylight 488-conjugated goat anti-rat IgG antibody (1:300 in 1% BSA/PBS) in a moist dark chamber at room temperature for 1 h. The slides were washed with 0.1% Tween in PBS three times prior to the staining of nuclei with 4',6-diamidino-2-phenylindole (DAPI, 1:100) in a moist dark chamber at room temperature for 5 min. Finally, the slides were mounted in fluorescence mounting medium (Vectashield) for observations under a microscope.

4.2 Results and discussion

4.2.1 Wound closure

The wound healing efficacy of HA-SF/3ZO composite nanofiber was compared to the ZO-free HA-SF nanofibers and gauze (control) groups. Both nanofiber mats adhered well to the surface of the wound area and could be easily detached without causing any damage to the wound site. In the wound healing process, it is important that the wound dress is able to integrate well with the wound site for management of exudatives as well as the drug release to accelerate the process of wound healing [228]. Figure 15 depicts the images of the burn wounds after 0 and 7 days of dressing. At day 7, HA-SF and HA-SF/3ZO mats led to 33.13±2.31% and 55.02±1.35% wound closure, respectively. These values were significantly higher than the 21.69±1.25% wound closure observed in the gauze-treated groups ($p^*<0.05$). The obtained data revealed that the wound treated with HA-SF/3ZO wound dressings healed and contracted faster in comparison to the other groups. This higher percentage of wound contraction in the HA-SF/3ZO group might be assigned to the presence of ZO. Many investigations have also shown that ZO has a positive effect on stimulation and migration of epithelial cells and keratinocytes, accelerating the wound closure [117, 211].

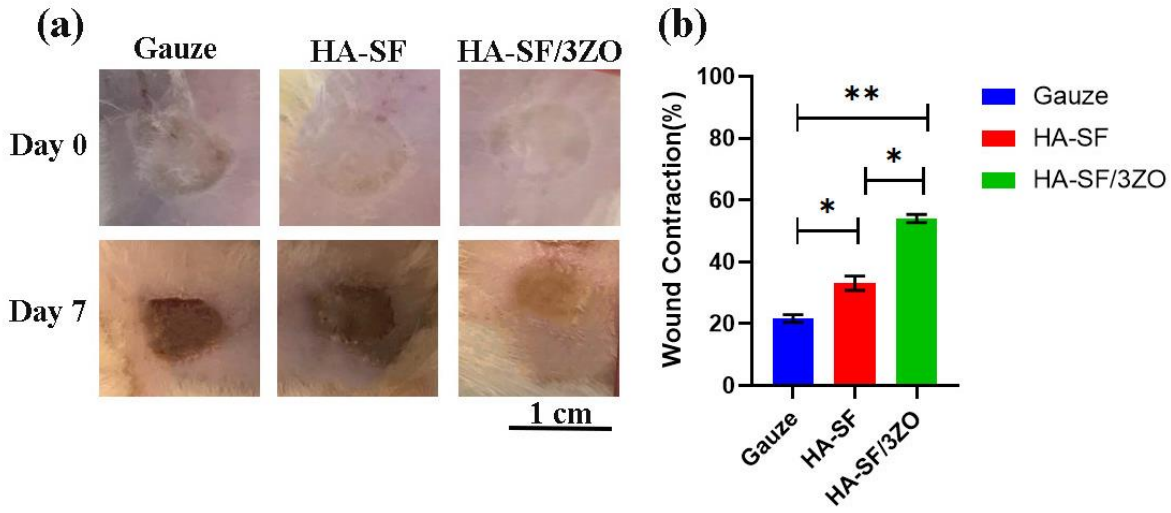

Figure 15: The wound closure results. (a) The pictures of wound contraction rates on days 0 and 7 of control, HA-SF-, and HA-SF-3ZO-treated groups. (b) Graphical representation of percentages of wound contractions on various days (p<0.05 and p**<0.01). 4-5 replicates were used to examine the reproducibility of the results.*

4.2.2 Histopathological analysis

Histopatholgical staining was used to investigate the effects of prepared wound dressings on second-degree burn wound injuries. After 7 days of burn treatment, the mice were sacrificed to collect their skin tissues, which treated with different groups. From H&E and MT stainning (Figure 16 a,b) we observed the regenerated epidermis (RE) at 7 days post wounding in all groups. However, the thickness of RE was greater for HA-SF/3ZO groups when compared with other groups. The wounds treated with HA-SF/3ZO showed bigger healing zone and higher level of collagen formation with minimum inflammatory cell infiltration than the other treatment groups. However, the gauze and HA-SF treated groups still had inflammatory cell infiltration. In addition, the granulation tissue also observed in the wound dressing treatment groups, whereas the content was much bigger in the HA-SF/3ZO treated group. Many new blood vessels could be seen in HA-SF/3ZO groups, which were vital for continuation of the healing process. Another noticable difference in HA-SF/3ZO treated groups after 7 day post treatment was that the number of hair follicle cells and sebaceous glands were much greater than other groups.

The deposited collagen and cellular products at the site of wound were distinguished by using MT staining, and the images are shown in Figure (16b). Expansions of collagen deposition were

noticable in the HA-SF/3ZO treated group. This is the sign of early organization of wound in comparison to other groups. The existance of a cluster of newly formed collagen fibers was remarkable in the newly formed granulation tissue of HA-SF/3ZO wound dressings on day 7 after treatment, while loose collagen fibers with lower density were detected in the gauze treated groups. In HA-SF/3ZO group we observed the assemblages of collagen fibers.The dark and light blue coloured clusters indicated the stiff and loose collagen fibers, respectively. The MT results showed that the thickness of newly formed epidermis in HA-SF/3ZO treated groups are much greater than other groups.

The HA-SF/3ZO wound dressing material advanced the early stage of wound healing process and subsequently remodeling of burned skin during 7 days of treatment. This results can be attributed mainly to the presence of ZO and HA, respectively. Many *in vivo* studies have showed that topical zinc oxide treatments has significant impact on reducing wound debris, accelerate wound healing process and advanced epithelization [205]. It has been shown that zinc plays a key role in modulating every stage of the wound healing process; ranging from cell migration and proliferation , oxidative stress, coagulation, inflammation and immune defense, tissue re-epithelialization, angiogenesis and ECM production [115]. In addition, Lansdown et al. [205] have reported that matrix metalloproteinases (MMPs), as zinc-dependent protein, play a key role in wound healing. The inhibition of MMP activity as a result of Zinc-deficiency significantly delays wound healing.

The HA also considered as one of the main players in the wound healing process. It has been proven to regulate with specific HA receptors, inflammatory responses, synthesis of collagen, cellular migration/prolifration, and angiogenesis, which are the main phases of wound healing [229]. Some series of HA receptors occur on cell surfaces which has critical role at each stage of wound healing; most importantly including CD44 and RHAMM [230]. Interaction of HA with CD44 receptor have been implicated in a series of regulating the inflammatory responses, providing angiogenesis and neovascularization, cell prolifration and reepithelialization [231]. Furthermore, the HA receptor

RHAMM regulates cell migration, activation of cytoskeletal proteins and protein kinases, reduced inflammation and fibrogenesis in wound [232-233].

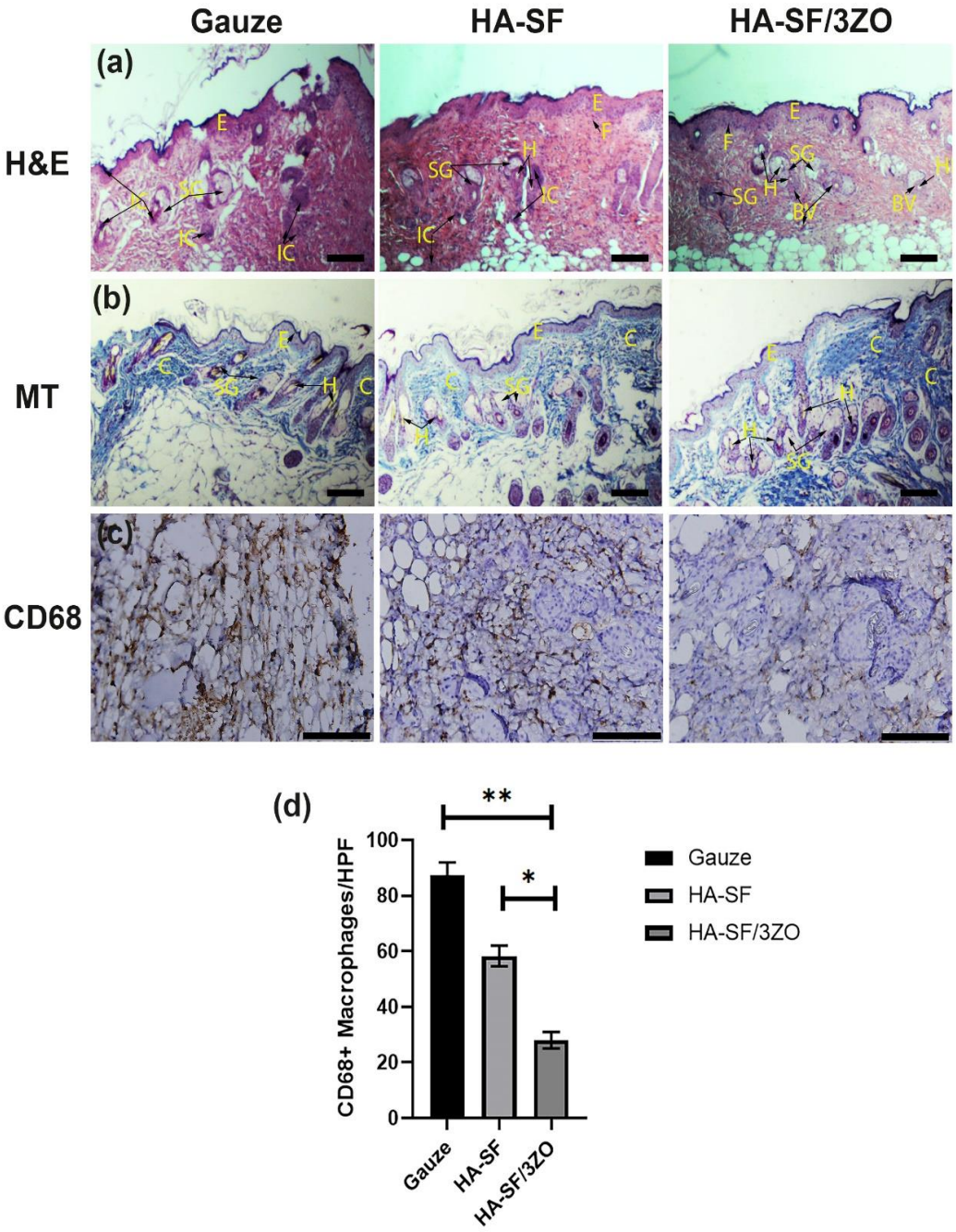

Figure 16: The histopathological results including the bright field microscopic images of (a) H&E, (b) MT, and (c) CD68 immunohistochemically stained wound sections. (d) The number of CD68 macrophages per high power field (HPF) after 7-day post injury with three type of treatments (H: hair follicles; BV: blood vessels; F: fibroblast; C: collagen deposition; IC: inflammatory cells; SG: sebaceous glands; CF: collagen fibers; SG: sweat glands; E: epidermis, scale bars = 100 µm). 4-5 replicates were used to examine the reproducibility of the results.

4.2.3 Immunohistochemically staining

Figure (16. c, d) depicts immunohistochemical CD68-stained wound sections with quantitative analysis of CD68+ cells (/high power fields) after 7 days of treatment with gauze, HA-SF, and HA-SF-3ZO. CD68 is monocyte/macrophage stainning marker to investigate inflammatory stage in wound[124]. Qantitative results revealed that number of macrophages was more in both gauzes (87.33±4.64 cells/high power field, HPF) and SF-HA-treated (58.33±3.68 cells/HPF) groups in comparison to SF-HA/3ZO treated animals (28±2.9 cells/HPF) at 7 days post-injury (Figure 16d). The results indicated that the burn wound treated with HA-SF/3ZO nanofiber significantly decreased the number of macrophages and inflammation due to the presence of ZO. The ZO as an anti-inflammatory agent by decreasing the malondialdehyde level and blocking the pro-inflammatory cytokines including Interleukin-1 (IL-1), Interleukin-1Beta (IL-1β), and Tumor necrosis factor-Alpha (TNF-α) decreases the inflammatory response in burned wound [234-235]. In addition, other reports further revealed that ZO mediated the toll like receptor (TLR/NF-κB) inflammatory signaling pathway, which is associated with decreased inflammation [155].

Chapter 5: Colorimetric sensor arrays (CSAs)

5.1 Introduction

The detection and identification of bacteria within the infected wounds are pressing problems in medicine. A patient may present to the physician symptoms consistent with a bacterial infection, but the physician may be unable to address the infection with the appropriate antibiotic until the identity or antibiotic susceptibility of the bacteria has been determined; as a consequence, the proper treatment of infected wounds remains challenging. Hospitals have used cultured samples from the wounds as the standard for identifying bacterial infections for more than a century. While there have been some improvements in automating the process, the overall method has remained largely constant. Overall, Existing methods for identification of pathogenic bacteria are severely limited by the necessity of long culturing times, the need for highly trained laboratory personnel, and the requirement of expensive and high-maintenance equipment. Bacterial infections really stink that could be the key to a fast diagnosis. they produce volatile organic compounds (VOCs) to which the mammalian olfactory system is highly responsive. Consequently, an experienced microbiologist can readily identify many bacteria by smell. Toward this goal, we have developed a 6×5 simple colorimetric sensing array (CSA) for the detection of VOCs and discrimination among complex mixtures. To develop this sensor dressing array, we used a cross-responsive colorimetric sensor array to monitor the complex composite of volatile compounds produced by different bacterial strains grown in replicate on agar petri dishes and pig skins. The sensor arrays consist of chemically responsive dyes, including metalloporphyrins, pH indicators, metal salts, and solvatochromic dyes spotted on polyvinylidene fluoride (PVDF) membrane, that change color when exposed to a broad range of volatile analytes. Given the wide range of VOCs produced by bacteria, the chemical diversity of the sensor elements present in our array is critical to its capability to respond to broad classes of individual analytes and its ability to distinguish among complex mixtures.

The performance of developed CSAs has been evaluated with different pathogens including bacteria and fungi grown on agar plates and pig skins. The preliminary tests have revealed that arrays of color changing dyes produce unique signatures associated with each pathogen which can be used to diagnose their presence on both TSA plates and pig skins. Furthermore, the stability test reveals that there is no change in the color response of CSAs stored at -4, 25, 37 °C and 100% humidity for more than two weeks.

Meitham Amereh carried out the classification studies using an independent technique (k-nearest neighbors (k-NN) algorithm). The k-nearest neighbors (k-NN) algorithm classifies the results with 94.4% accuracy.

The overarching goal of this research proposal is to perform a feasibility study on developing a colorimetric sensor dressing array which can detect infection and identify wide range of bacteria based on volatile metabolites produced by bacteria in the infected wounds.

5.2 clinical problem

Skin infections are common and can be caused by infiltration of bacteria, fungi or viruses. around 2% of the people will experience a chronic wound infection during their lifetime. These type of wounds mainly affect older patients [236]. Three percent of the population aged over 65 years have open wounds in the United States. The US government estimates that the elderly population will be over 55 million by 2020, indicating that chronic wounds in this population will continue to be an increasingly persistent problem [12]. These type of wounds represent a major challenge to wound care professionals, with the required treatment consuming a large portion of healthcare resources [10]. Based on the recent report, Medicare cost projections ranged from $28.1 billion to $96.8 billion for diagnosis, management and treatment of infected wounds [12].

Infection diagnosis can be a very difficult since different kinds of wounds can show different clinical presentations which mostly dependent on wound location, onset, and type of bacteria. it is further complicated by the existence of biofilms for which no diagnostic method is currently available

[237]. There are several methods for detecting any pathogens in the infected wounds. Performing a swab culture is the most common one. However, a swab culture is not considered as effective as other methods because it is not very accurate. The gold standard method for detection the infection in wound is tissue biopsy. However, tissue biopsy is not commonly done due to its invasiveness, requirement of specific skill sets, painfulness and expensiveness.

Overall, Existing methods for identification of pathogenic bacteria are severely limited by the necessity of long culturing times, the need for highly qualified laboratory staff, and the requirement of expensive and high-maintenance equipment [238-239].

There is a pressing need to develop effective methodologies that enable fast, sensitive, portable, and affordable detection of pathogens in infected wounds. Toward this goal, we have developed a simple colorimetric sensing array (CSA) for the detection of VOCs and discrimination among complex mixtures. To develop this sensor dressing array, we used 30 different cross-responsive colorimetric sensor array to monitor the complex composite of volatile compounds produced by different pathogens.

5.2.1 current methods of infection detection

A patient may present symptoms associated with bacterial infection to a physician. but the physician may not be able to provide a proper antibiotic treatment until the bacteria type is identified or the antibiotic susceptibility of the bacteria has been specified. as a result, sepsis remains one of the major causes of death even among regions of the first world [240].

There are couple methods for identification of bacteria within infected wounds as follow:

1) **Swab culture**: this method helps to determine whether a wound has become infected, which type(s) of bacteria are causing the infection. In this method, A sterile swab may be used to collect cells or pus from a superficial wound site. this method is not considered as effective as other methods since it can mostly identify the presented contaminants, slough and eschar on the surface of the wound [241]. Additionally, this swabbing process in hospitals can take 3-5

days. First, the collected swabs are usually incubated for 24 to 48 hours, till a carbon dioxide sensor detects the presence of bacteria. After that, doctors still need to identify the type and strain of bacteria in the sample, a process that takes up to the another 1-2 days [128].

2) **Tissue biopsy culture**: this method is gold standard for identification of bacteria. In this method, tissue sample in wounded area obtained by punch biopsy or with a scalpel using aseptic technique in the appropriate health care setting. Despite its precision in detection of infection, tissue biopsy is not commonly done due to its invasiveness, requirement of specific skill sets, painfulness and expensiveness [241].
3) **Molecular testing**: Clinical molecular microbiological methods are commonly being used for identification of the microbiota of chronic infections, including wounds, as part of standard patient care. This method is more sensitive than culturing, which results in markedly different results being reported to clinicians. However, the using of molecular test has been limited due to the requirement for highly trained personnel, the need for expensive and high-maintenance equipment, and expensiveness [242].

Current methods for determining the type and strain of pathogenic bacteria are intensively restricted by the necessity of long time period culturing, the requirement for highly trained personnel, the need for expensive and high-maintenance equipment and also ineffectiveness resulted by antibiotic resistance [128].

5.2.2 our solution

There is a pressing need for developing new technologies for detection and identification of pathogens in medicine. There is a broad involvement of bacterial infections in hospital-acquired infections and many other fields that can resulted in many diseases which are of big concern to the human health [127].

Bacteria is stinky, since they generate VOCs to which the mammalian olfactory system is highly responsive. Thus, it can be a key factor for bacterial identification. As such, a professional

microbiologist can identify many bacteria just by smell. For example, Pseudomonas aeruginosa can be identified by sweet grape-like scent [128].

By emerging new techniques in chemical sensing area, wide variety of sensors being available that can sense different analytes with higher sensitivity. Among them, optical-electrical sensors are especially noteworthy [129]. The most popular optical sensors rely on colorimetric or fluorescent changes, resulted by intermolecular interactions between the chromophore or fluorophore with the analytes. Combining techniques based on arrays that use a chemically responsive approach with modern digital imaging, one can provide identifying fingerprints in the response of the sensor arrays with any given analytes [130]. There are two basic criteria for development of colorimetric sensors. First, they should have capacity to interact selectively with analytes. Secondly, they should be able to generate a feedback on that interactions through chromophores or fluorophores by providing a fingerprint pattern.

Chemoresponsive colorant-based sensor arrays made out of dyes and pigments can detect the chemical reactivity of analytes, rather than their physical properties. Thus, this generation of sensors allows high sensitivity even down to parts per billion (ppb). Consequently, colorimetric sensor arrays overcoming the drawbacks of conventional sensor arrays which are only rely on physical absorbtion or nonspecific chemical interactions [131].

Toward that end, we have used 30 different cross-responsive colorimetric dyes, including metalloporphyrins, pH indicators, metal salts, and solvatochromic dyes, that change color when exposed to a broad range of volatile analytes generated by bacteria. We believe that our technology has a great potential for overcoming the abovementioned issues associated with current methods of detection. For example, this CSA technology enable fast (less than 10 hours), sensitive (down to 12 CFU/wound), portable, and affordable detection of pathogens in infected wounds.

5.3 previous works

The first example of a colorimetric sensor array nose was reported by Suslick, and coworkers, who designed a sensor array using various metalloporphyrins for effective detection of VOCs. Their results showed that metalloporphyrins strongly interacted with analytes which provided strong color change and specific pattern that can be used for identification of analytes [132]. The sensor arrays showed wide range of response to different type of VOCs including alcohols, amines, ethers, aldehydes, ketones, thioethers, phosphines, phosphites, thiols, arenes, and halocarbons, even with sensitivities at ppm level and with high stability in ambient humidity [132].

Next, Rakow et al.[133] was able to develop a colorimetric sensor with more arrays by incorporating other Chemoresponsive dyes such as acid and base indicators, and solvatochromic dyes to a total of 24 sensors (Figure 17). The sensor array was able to fully discriminate among 12 linear, branched or cyclic alkyl amines. As can be seen from Figure 1B, each amine provides a unique color-difference map for easy detection. Similarly, another sensor array was developed by Soga and co-workers for the identification of volatile amines [134]. Developed sensor was able to detect one closely related amine from another based on polarity interactions.

Furthermore, Janzen et al.[135] by extending the colorimetric sensor array to 6×6 arrays by incorporating various new types of dye sensors were able to represent an error-free discrimination among 100 different VOCs by probing a wide range of intermolecular interactions between analytes and sensors, including Lewis acid − base, Brønsted acid − base, metal ion coordination, hydrogen bonding, and dipolar interaction.

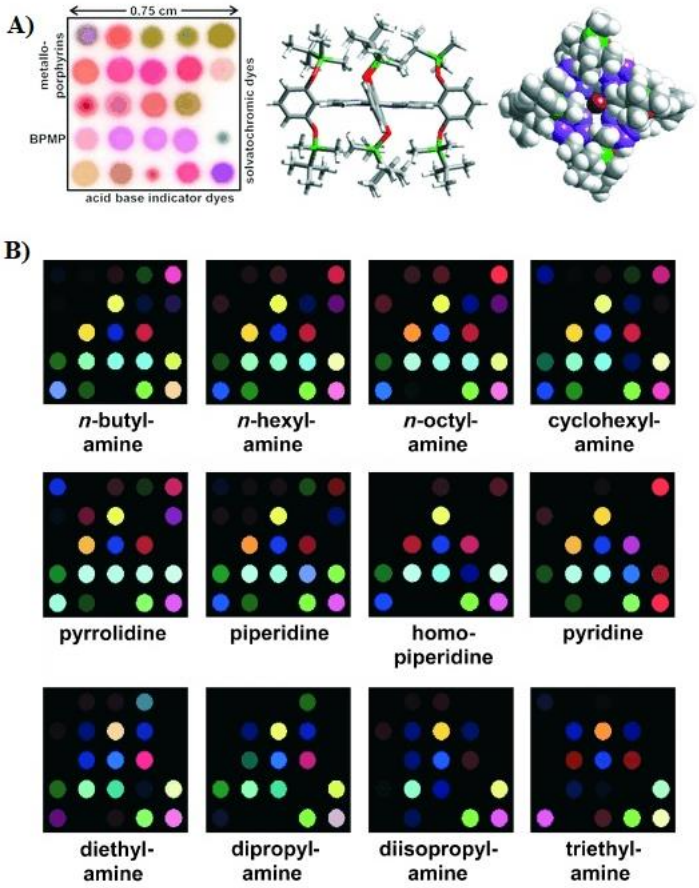

Figure 17: A) Colorimetric sensor array and the structure of the bis-pocket Zn porphyrin 5,10,15,20-tetrakis(2',6'-bis(tert-butyldimethylsilyloxyl)phenyl)porphyrinatozinc(II), shown in framework side view (center) and space-filled top view (right). BPMP=bis- family of 12 amines 133.

CSAs have shown great successful applications for identifying the microbial species, especially bacteria. Carey et al. [128] was able to successfully developed a 6 × 6 array to Identify the strains of human pathogenic bacteria grown on agar plates relies on specific VOCs produced from each pathogen. They were able to identify 10 strains of bacteria including Enterococcus *faecalis* and *Staphylococcus aureus* as well as their antibiotic-resistant with 98.8% accuracy in less than 10 hours, which represents a significant improvement over existence methods in terms of speed, ease of use, and cost.

5.4 Theory

The CSAs typically made out of different colored dyes arranged a two-dimensional grid, which change color upon interaction with various analytes. The pattern of color changes can be used to analyze and identify the substance in question. Pattern recognition is based on the combined response from numerous sensors [243].

Based on the types of intermolecular interactions which resulting in color change, one may divide cross-reactive, Chemoresponsive dyes into five classes as follow [131]:

(i) Brønsted acidic or basic dyes (e.g., various pH indicators). Brønsted -Lowry acids are compounds that can donate protons; bases are proton acceptors. The colors of these type of dyes are totally pH-dependent. For example, their UV − vis absorption spectra change through protonation or deprotonation as the pH changes [244].

(ii) Lewis acid/base dyes (e.g., metal complexes). Most of the strongly odiferous compounds are Lewis bases: amines, carboxylic acids, sulfides, and phosphines. Among them, metalloporphyrins are considered as a most common choice for the sensing of metal-ligating volatiles because of the open coordination sites and the large color changes from both wavelength and intensity shifts of strong $\pi - \pi^*$ ligand binding. Furthermore, Lewis acid/base dyes are used for anion/cation detection, which are often dominated by electrostatic forces or hydrogen bonding [245-246]. Representative examples of porphyrins, porphyrinoids, and other types of Lewis acid/base dyes that have been used as optical sensors are shown in Figure 18.

(iv) colorants with large permanent dipoles (i.e., zwitterionic vapochromic or solvatochromic dyes) for detection of local polarity or hydrogen bonding[247].

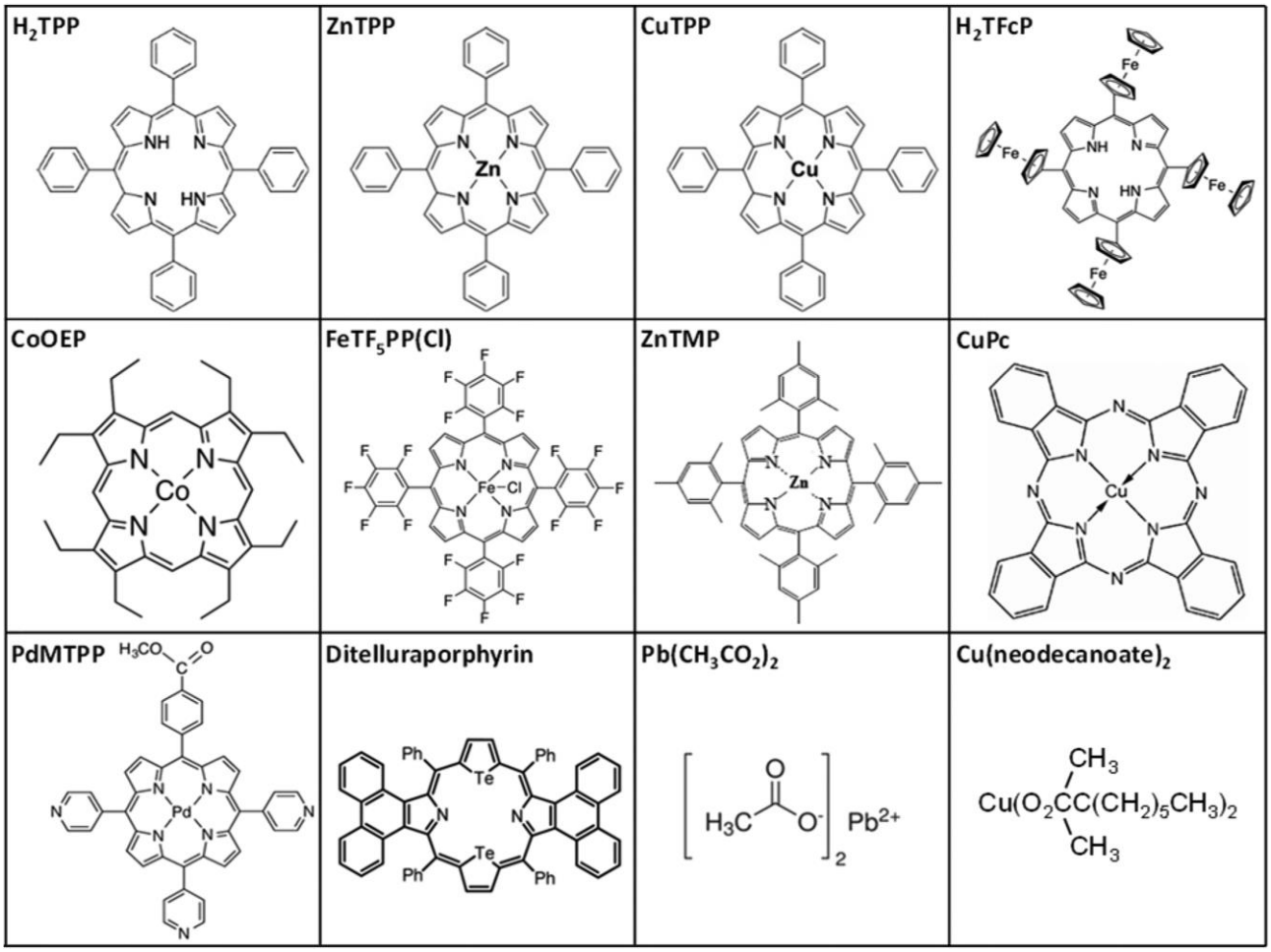

Figure 18: the structures of representative Chemoresponsive dyes, including porphyrins or porphyrinoids, and others containing Lewis acid metal ions.

(v) chromogenic aggregative materials (e.g., plasmonic nanoparticles and nanoscale transition metal sulfides). The color change in this class of dyes are induced by particle aggregation. The first version of chromogenic aggregative indicators, e.g., simple precipitation of metal salts or formation of metal nanoclusters upon reactions with sulfides, indeed derives from classical qualitative spot tests [248].

5.5 Experimental

Taking into consideration the high moisture content of the wound in this study, 18 hydrophobic indicators were screened out and purchased from Sigma-Aldrich. Furthermore, the analytically pure liquids, namely chloroform, ethanol, and methanol, purchased from Sigma-Aldrich. Table 5 summarizes the list of the dyes and the solvents that used for developing the CSAs.

Table 5: The list of dyes used in the colorimetric sensor array for bacterial identification

The dyes list	Abbreviation	Solvent	Type of dye	Response/ Detection
Brilliant yellow	BY	Methanol	Brønsted acidity/basicity dye	• amines • fatty acids
Phenol red	PR	Methanol	Brønsted acidity/basicity dye	• amines • fatty acids
Bromothymol blue	BB	Methanol	Brønsted acidity/basicity dye	• free fatty acids • bromothymol blue turns yellow in the presence of carbon dioxide and turns back to blue in the presence of oxygen. • ammonia
Comassie blue	CB	Methanol	NA	NA
Richards Dye	Ri	Methanol	Solvatochromic dye	• detect large permanent dipoles to sense local polarity (e.g. alcohols) • amines
Bromophenol red	BR	Methanol	Brønsted acidity/basicity dye	• amines • fatty acids
alpha-naphtholphthalein	NP	Methanol	Brønsted acidity/basicity dye	NA
5,10,15,20-Tetraphenyl-21H,23H-porphine iron(III) chloride	TTP- iron(III)	Chloroform	Lewis acid/base dye (metalloporphyrins)	• detect metal-ligating vapors such as SO2 • ammonia
5,10,15,20-Tetraphenyl-21H,23H-porphine cobalt(II)	TTP-cobalt(II)	Chloroform	Lewis acid/base dye (metalloporphyrins)	detect metal-ligating vapors such as: • nitrogen oxide (NO) • ammonia • alcoholic vapors • high affinity to NO • excellent sensitivity and fair selectivity toward 50 ppm of CO, 5000 ppm of CO2, 4.8 ppm of H2S, and 1 ppm of NH3
5,10,15,20-Tetraphenyl-21H,23H-porphine copper(II)	TTP-copper(II)	Chloroform	Lewis acid/base dye (metalloporphyrins)	• nitrogen oxide (NO) • ammonia

The dyes list	Abbreviation	Solvent	Type of dye	Response/ Detection
5,10,15,20-Tetraphenyl-21H,23H-porphine zinc	TTP-zinc	Chloroform	Lewis acid/base dye (metalloporphyrins)	• ammonia • 2,4,6-trinitrotoluene (TNT) • ethanol • triethylamine • and toluene
2,3,7,8,12,13,17,18-Octaethyl-21H,23H-porphine zinc(II)	TTP-zinc(II)	Chloroform	Lewis acid/base dye (metalloporphyrins)	• ammonia • 2,4,6-trinitrotoluene (TNT)
Hemin	He	NaOH (1.4M)	Fluorescent dye	NA
Nile red	NR	methanol	Solvatochromic dye	• dimethylamine • ethanol • benzene • acetic acid
Bromocresol green	BG	ethanol	Brønsted acid/base dye	responds through visible colour change to basic volatile spoilage compounds, such as: • trimethylamine (TMA) • ammonia (NH_3) • dimethylamine (DMA) collectively known as Total Volatile Basic Nitrogen (TVB-N)
Cresol red	CR	Mixture of NaOH and ethanol	Solvatochromic dyes	• Formaldehyde • Organophosphates • aldehydes
Nitrazine yellow	NY	methanol	Brønsted acid/base dye	• Ammonia

some of the above mentioned dyes such as BY, PR, Ri, BB, BR and NP showing different color changes in different pHs. In this regard, for making ACID/BASE solutions out of them we used following solutions:

1) NaOH 0.1 Molar
2) HCl 0.5 Molar

5.6 Fabrication of CSAs

There are two common methods for developing CSAs. First method is stamping, which all chemical dyes loaded into a Teflon ink well. Next, Sensor arrays will be printed using an array of floating slotted pins by dipping into the ink well and transferring to the substrate [249]. In the other method, the CSAs can be printed by inkjet printing. In this method, Inks will be filtered through a syringe filter prior to use. Next, Arrays will be printed by inkjet printer with specific spacing between sensors[134].

In this study, we have started developing 6×5 CSAs manually by delivering 0.5µl of each dye on a hydrophobic polyvinylidene fluoride (PVDF). Meanwhile, we are making a new stamping machine to be able to produce large quantities of CSAs. Figure 19 shows the schematic of our stamping machine. This manufacturing system can print on PVDF ranging in size from an 8 x 10 cm sheet to a 26 cm by 6 m long roll. The PVDF roll is set on a rod and fed through a set of rollers (1). G-code tells the rollers how far to run the PVDF, causing it to stop right after the stamp head. The stamp head, made of 30 small channels that hold various dyes with marker tips interfacing between the channels and PVDF, moves down to stamp the CSA in the desired pattern (2). Dyes are loaded by pipetting ~ 0.5 ml of liquid in each channel. The pressure of the marker tips against the PVDF is controlled through a Z axis induction sensor. The stamp head moves across the PVDF stamping each row then the roller moves the PVDF forward so a new row can be stamped. Once the stamped sensors reach the end of the build plate, the second roller picks up the PVDF and rolls it back up to be stored and cut (3). The whole system is controlled through a touch screen UI running Octoprint software.

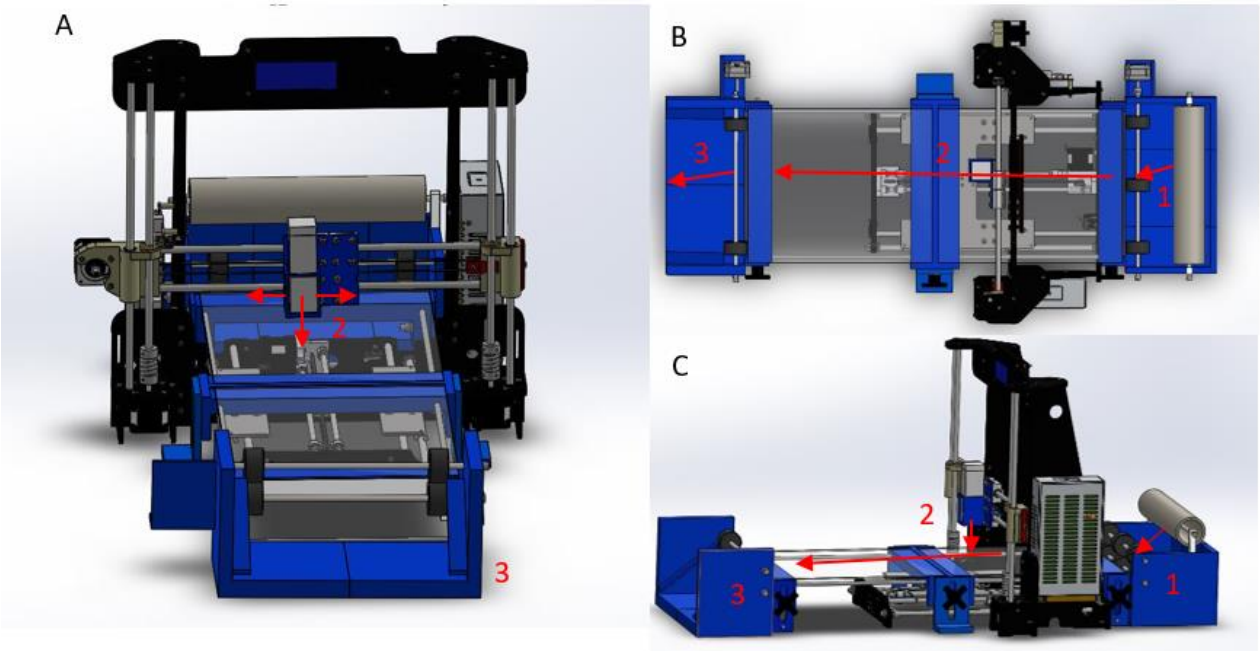

Figure 19: the schematic of stamping machine. A) Front, B) Top and C) Side view

5.6.1 Image processing

The analysis of digital images in analytical chemistry increased by more than 87% between 2005 and 2015, as the detection of analytes improved with an increase in the availability of imaging devices [250]. particularly, the determining of analytes using red, green, and blue colors (RGB) has led to state of the art of CSAs referred to as opto-electronic noses, which provide discriminatory power between analytes by using arrays of color-changing sensors when interacting with the test substance, similar to the sense of smell [251].

In this study, we have developed a code for getting color difference maps from each CSAs exposed to different pathogens. Accordingly, at specific times the CSA was pictured using a smart phone camera for monitoring the color change in response to different pathogens. A portable LED light box was used to ensure consistent lighting conditions for all photos. Afterwards, the color difference maps were generated by subtracting the average RGB value at the center of each spot after pathogen exposure from the RGB values of the baseline image spots, and taking the absolute value of the result:|ΔR|, |ΔG|, |ΔB| using our written code.

For easier visualization, the range of values obtained were expanded to 0-255 to cover the complete 8-bit RGB range.

Figure 20 shows the images of one of CSAs before and after exposure along with the generated color difference map using our code.

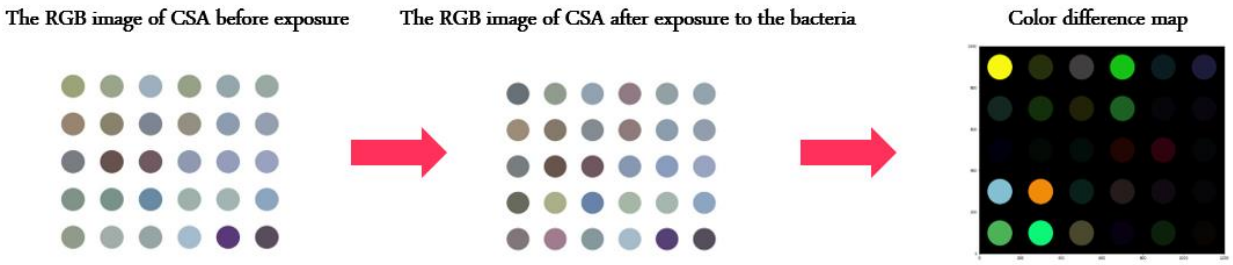

Figure 20: the images of a CSA before and after exposure to the bacteria along with the generated color difference map using our code.

5.7 Preliminary results

We have started testing the ability of 30 different indicator compounds spotted on PVDF membrane to detect volatile metabolites released by different pathogens including *E. coli*, *S. aureus*, *P. aeruginosa*, and *Candida albicans* (*C. albicans*) grown on tryptic soy agar (TSA) plates and wounded pig skins for 24h incubation (Figure 21). These preliminary tests have revealed that arrays of color changing dyes produce unique signatures associated with each microbe which can be used to diagnose their presence *diagnose their presence on both TSA plates and pig skins.*

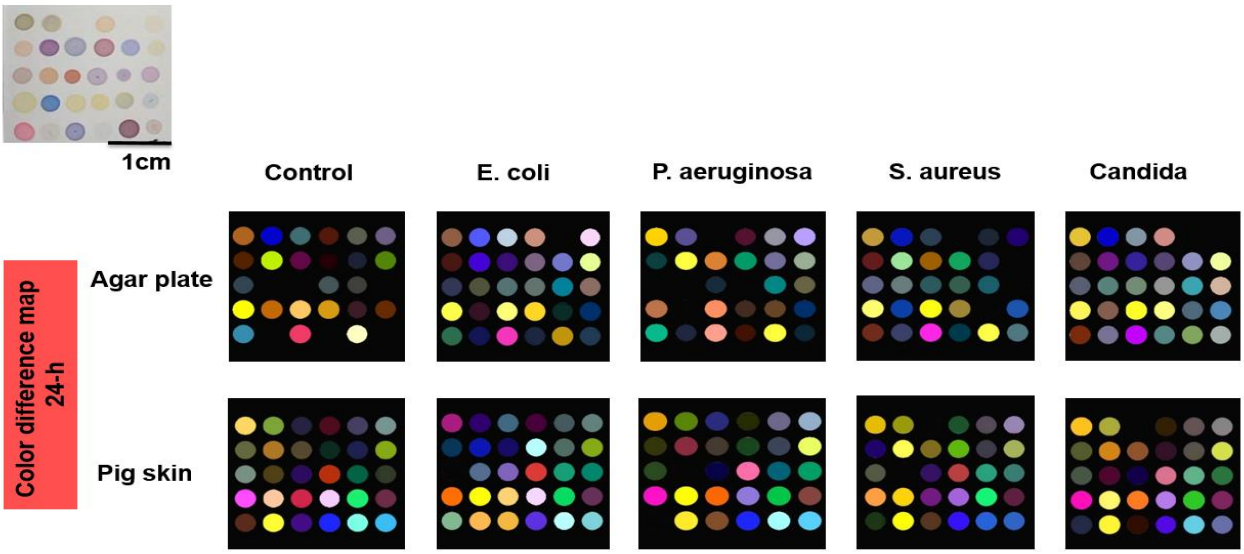

Figure 21: Colorimetric sensor arrays to detect volatile metabolites from common wound microbes. Color maps of sensor array after 24 hours' exposure to TSA plates and infected pig skins with E. coli, S. aureus, P aeruginosa, S. aureus and C. albicans (Note: the top left image shows the picture of developed CSA before exposing to the bacterial environment).

Furthermore, the stability of developed CSAs in different temperature and 100% humidity has been evaluated. In this regard, the CSAs were digitally imaged with a smart phone using LED box before and after exposure to different temperature and humidity. Color difference maps for the arrays were generated using our code by subtraction of the image before exposure from the image after exposure. As can be seen from the Figure 22, we find that there is no change in the color response for arrays stored at -4, 25, 37 °C and 100% humidity for more than two weeks. However, CSAs incubated at 45°C showed some color change.

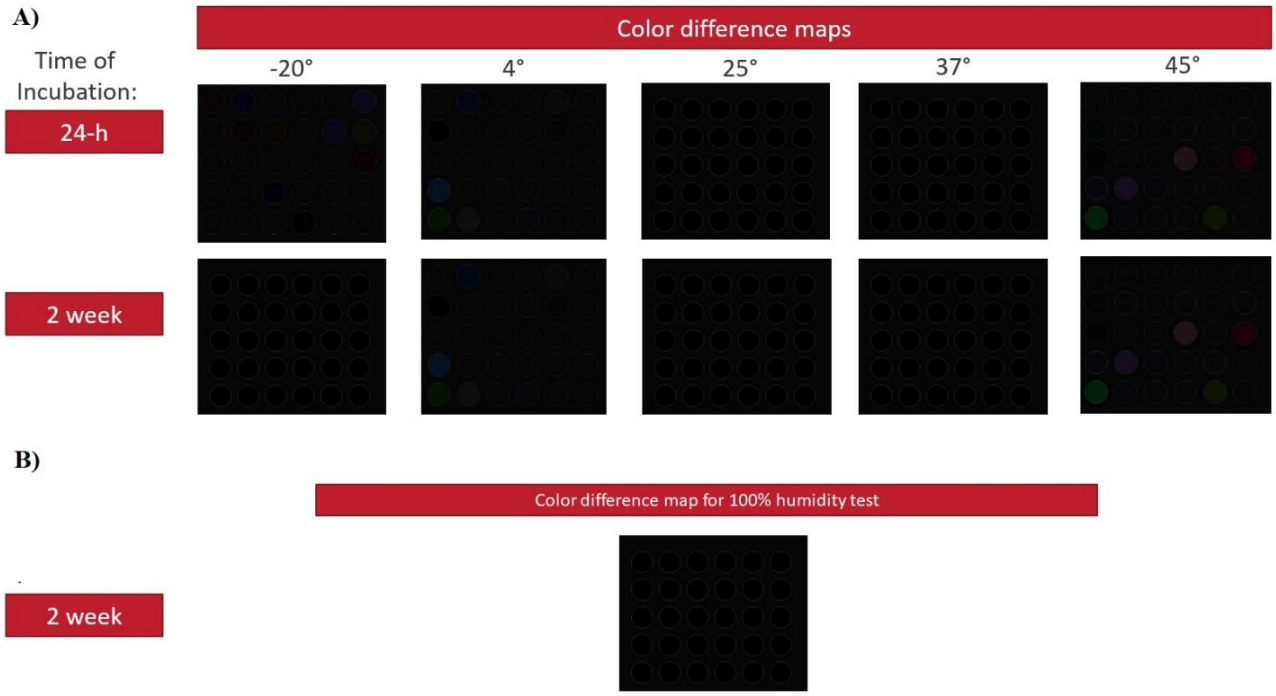

Figure 22: the stability of CSAs in different A) Temperatures and B) 100% humidity

Classification of specific bacterial strains based on the colorimetric sensor array data was successfully accomplished using an independent technique (k-nearest neighbors (k-NN) algorithm). For quantitative analysis, the color change values for each experiment were analyzed as "time stacked" vectors in order to capture the temporal behavior of the response profiles[128]. The k-nearest neighbors (k-NN) algorithm classifies the results with 94.4% accuracy (Figure 23).

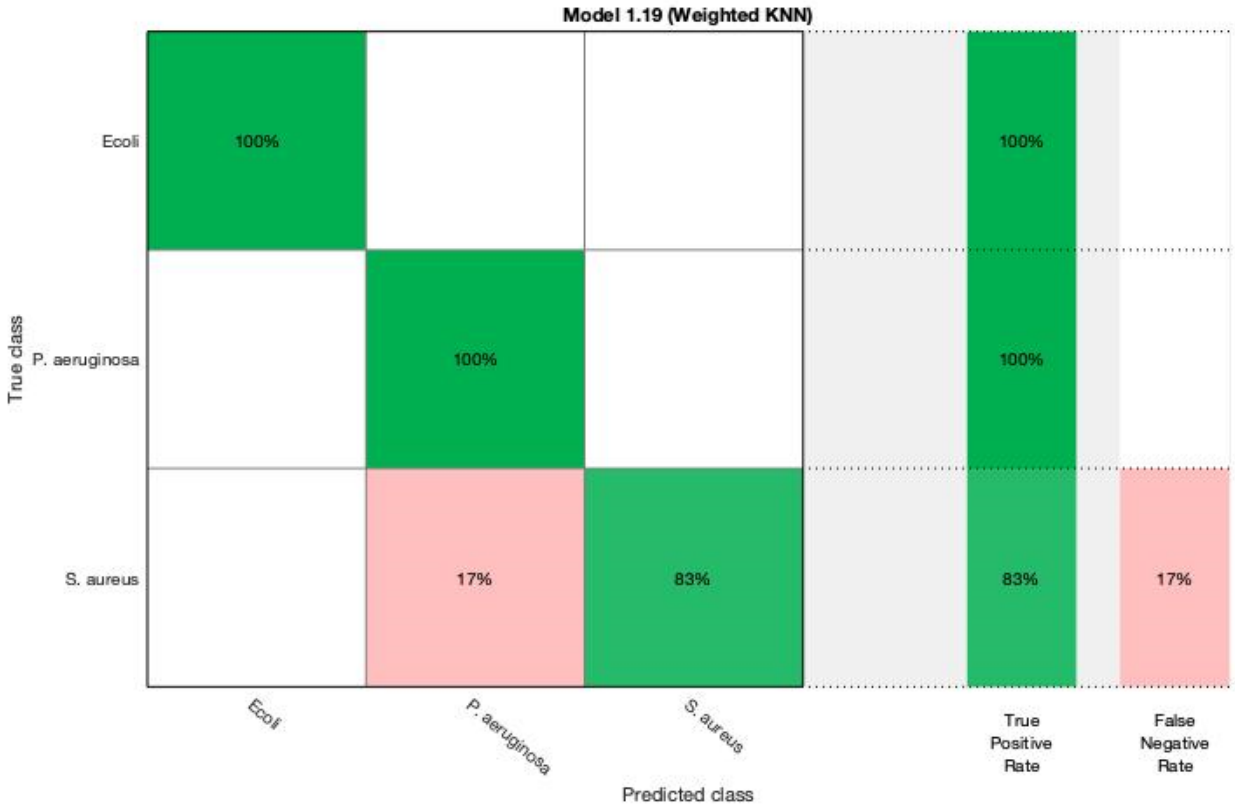

Figure 23: the classification accuracy data for 3 different type of bacteria

Conclusion

In this study we fabricated a new HA-SF/ZO wound dressing that consisted of a core-shell structure, was biocompatible, and possesses highly effective antibacterial properties for burn wound treatment. The core-shell structure of HA-SF nanofiber was examined through TEM observation. The different concentrations of ZO were successfully incorporated into HA-SF nanofibers using co-electrospinning technique. The compositions of fabricated nanofibers and presence of ZO were measured with FTIR. The antibacterial investigations showed that the antibacterial activities of the wound dressings were enhanced with increment of ZO content against both E. coli and S. aureus. The cell culture using HaCat cells demonstrated that the HA-SF nanofibers exhibited good cell attachment, cell proliferation, and viability in culture for up to 3% ZO doping. Similar trend was observed in the scratch assay since HA-SF/3ZO induced the migration of HaCat cells. This combination was also efficient in in vitro wound healing. Based on the in vitro experimentations HA-SF/3ZO was chosen to validate the results to carry out in vivo investigation. Histopathological analysis proved that the HA-SF/3ZO wound dressing material enhanced burn wound healing and skin regeneration. This combination stimulated epidermis, hair follicles, and sebaceous glands formation, and promoted collagen deposition. Furthermore, immunohistopathological staining showed that the treated burn site with HA-SF/3ZO nanofiber matrix decreased the inflammatory response compared to the gauze and HA-SF groups. Being multifunctional dressing, the HA-SF/3ZO composite nanofibers indicated a great potential in burn treatment and wound healing.

Furthermore, in another study we fabricated CSAs for detection and identification of bacteria using different dyes on PVDF membrane. Our next goal is electrospinning PVDF dressing to print Chemoresponsive dyes on it since in our first study electrospun dressing has showed good properties.

Future work

Engineered electrospun nanofibers can be adopted for a wide range of applications as wound dressings. In future, we are planning to incorporate a sensing element (Chemoresponsive dyes) in our electrospun nanofiber dressing in order to manage wound healing plus monitoring wound infection.

Supplementary information

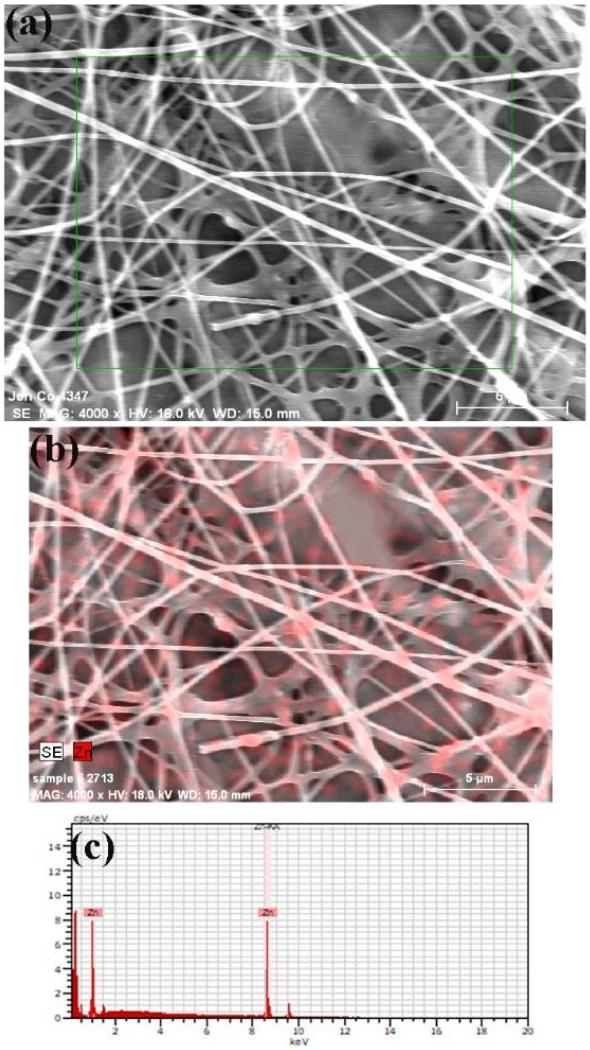

Figure S1: (a) The SEM image of HA-SF/5ZO, (b) EDX elemental mapping of Zinc within the electrospun fibers and (c) EDX elemental spectrum.

References

1. Norlén, L., Molecular structure and function of the skin barrier. In *Percutaneous Absorption*, CRC Press: 2021; pp 1-8.
2. Wysocki, A. B., Skin anatomy, physiology, and pathophysiology. *The Nursing Clinics of North America* **1999,** *34* (4), 777-97, v.
3. Ng, W. L.; Yeong, W. Y.; Naing, M. W., Cellular approaches to tissue-engineering of skin: A review. *Journal of Tissue Science & Engineering* **2015,** *6* (2), 1.
4. Dehdashtian, A.; Stringer, T. P.; Warren, A. J.; Mu, E. W.; Amirlak, B.; Shahabi, L., Anatomy and Physiology of the Skin. In *Melanoma*, Springer: 2018; pp 15-26.
5. McGrath, J.; Eady, R.; Pope, F., Anatomy and organization of human skin. *Rook's textbook of dermatology* **2004,** *1*, 3.2-3.80.
6. Kabashima, K.; Honda, T.; Ginhoux, F.; Egawa, G., The immunological anatomy of the skin. *Nature Reviews Immunology* **2019,** *19* (1), 19-30.
7. Honari, G., Skin structure and function. In *Sensitive Skin Syndrome*, CRC Press: 2017; pp 16-22.
8. Coppa, A.; Guha, S.; Fourcade, S.; Parameswaran, J.; Ruiz, M.; Moser, A. B.; Schlüter, A.; Murphy, M. P.; Lizcano, J. M.; Miranda-Vizuete, A., The peroxisomal fatty acid transporter ABCD1/PMP-4 is required in the C. elegans hypodermis for axonal maintenance: A worm model for adrenoleukodystrophy. *Free Radical Biology and Medicine* **2020,** *152*, 797-809.
9. George Broughton, I.; Janis, J. E.; Attinger, C. E., Wound healing: an overview. *Plastic and reconstructive surgery* **2006,** *117* (7S), 1e-S-32e-S.
10. Nunan, R.; Harding, K. G.; Martin, P., Clinical challenges of chronic wounds: searching for an optimal animal model to recapitulate their complexity. *Dis Model Mech* **2014,** *7* (11), 1205-13.
11. Sen, C. K.; Gordillo, G. M., Sashwati Roy, Robert Kirsner, Lynn Lambert, Thomas K Hunt, Finn Gottrup, Geoffrey C Gurtner, and Michael T Longaker. Human skin wounds: a major and snowballing threat to public health and the economy. *Wound repair and regeneration* **2009,** *17* (6), 763-771.
12. Sen, C. K., Human wounds and its burden: an updated compendium of estimates. Mary Ann Liebert, Inc., publishers 140 Huguenot Street, 3rd Floor New …: 2019.

13. Demidova-Rice, T. N.; Hamblin, M. R.; Herman, I. M., Acute and impaired wound healing: pathophysiology and current methods for drug delivery, part 1: normal and chronic wounds: biology, causes, and approaches to care. *Advances in skin & wound care* **2012,** *25* (7), 304.

14. Frykberg, R. G.; Banks, J., Challenges in the Treatment of Chronic Wounds. *Adv Wound Care (New Rochelle)* **2015,** *4* (9), 560-582.

15. Sen, C. K.; Gordillo, G. M.; Roy, S.; Kirsner, R.; Lambert, L.; Hunt, T. K.; Gottrup, F.; Gurtner, G. C.; Longaker, M. T., Human skin wounds: a major and snowballing threat to public health and the economy. *Wound Repair Regen* **2009,** *17* (6), 763-71.

16. Phillips, P.; Sampson, E.; Yang, Q.; Antonelli, P.; Progulske-Fox, A.; Schultz, G., Bacterial biofilms in wounds: Chronic wounds. *Wound Healing Southern Africa* **2008,** *1* (2), 10-12.

17. Remoué, N.; Bonod, C.; Fromy, B.; Sigaudo-Roussel, D., Animal models in chronic wound healing research: for innovations and emerging technologies in wound care. In *Innovations and Emerging Technologies in Wound Care*, Elsevier: 2020; pp 197-224.

18. Ansell, D. M.; Holden, K. A.; Hardman, M. J., Animal models of wound repair: Are they cutting it? *Experimental dermatology* **2012,** *21* (8), 581-585.

19. Andreu, V.; Mendoza, G.; Arruebo, M.; Irusta, S., Smart dressings based on nanostructured fibers containing natural origin antimicrobial, anti-inflammatory, and regenerative compounds. *Materials* **2015,** *8* (8), 5154-5193.

20. Shin, J. Y.; Yi, H. S., Diagnostic accuracy of laser Doppler imaging in burn depth assessment: Systematic review and meta-analysis. *Burns* **2016,** *42* (7), 1369-1376.

21. Gholipourmalekabadi, M.; Seifalian, A. M.; Urbanska, A. M.; Omrani, M. D.; Hardy, J. G.; Madjd, Z.; Hashemi, S. M.; Ghanbarian, H.; Brouki Milan, P.; Mozafari, M., 3D protein-based bilayer artificial skin for the guided scarless healing of third-degree burn wounds in vivo. *Biomacromolecules* **2018,** *19* (7), 2409-2422.

22. Kirsner, R. S.; Eaglstein, W. H., The wound healing process. *Dermatologic clinics* **1993,** *11* (4), 629-640.

23. Tiwari, V., Burn wound: How it differs from other wounds? *Indian journal of plastic surgery* **2012,** *45* (02), 364-373.

24. IMUNOMODULADORA, I. D. D., MARIA CECÍLIA CLOSS ONO.

25. Hanks, J. B.; Thyroid, Q.; Townsend, C.; Beauchamp, R.; Evers, B.; Mattox, K., Sabiston Textbook of Surgery. Philadelphia: Saunders: 2004.

26. Jeschke, M. G.; van Baar, M. E.; Choudhry, M. A.; Chung, K. K.; Gibran, N. S.; Logsetty, S., Burn injury. *Nature Reviews Disease Primers* **2020,** *6* (1), 1-25.

27. O'Callaghan, S.; Galvin, P.; O'Mahony, C.; Moore, Z.; Derwin, R., 'Smart'wound dressings for advanced wound care: a review. *Journal of Wound Care* **2020,** *29* (7), 394-406.

28. Negut, I.; Grumezescu, V.; Grumezescu, A. M., Treatment Strategies for Infected Wounds. *Molecules* **2018,** *23* (9).

29. Vuerstaek, J. D.; Vainas, T.; Wuite, J.; Nelemans, P.; Neumann, M. H.; Veraart, J. C., State-of-the-art treatment of chronic leg ulcers: a randomized controlled trial comparing vacuum-assisted closure (VAC) with modern wound dressings. *Journal of vascular surgery* **2006,** *44* (5), 1029-1037.

30. Dhivya, S.; Padma, V. V.; Santhini, E., Wound dressings–a review. *BioMedicine* **2015,** *5* (4).

31. Mostafalu, P.; Kiaee, G.; Giatsidis, G.; Khalilpour, A.; Nabavinia, M.; Dokmeci, M. R.; Sonkusale, S.; Orgill, D. P.; Tamayol, A.; Khademhosseini, A., A textile dressing for temporal and dosage controlled drug delivery. *Advanced Functional Materials* **2017,** *27* (41), 1702399.

32. Walczak, M.; Michalska-Sionkowska, M.; Kaczmarek, B.; Sionkowska, A., Surface and antibacterial properties of thin films based on collagen and thymol. *Materials Today Communications* **2020,** *22*, 100949.

33. Namviriyachote, N.; Lipipun, V.; Akkhawattanangkul, Y.; Charoonrut, P.; Ritthidej, G. C., Development of polyurethane foam dressing containing silver and asiaticoside for healing of dermal wound. *Asian J Pharm Sci* **2019,** *14* (1), 63-77.

34. Chuysinuan, P.; Chimnoi, N.; Reuk-Ngam, N.; Khlaychan, P.; Makarasen, A.; Wetprasit, N.; Dechtrirat, D.; Supaphol, P.; Techasakul, S., Development of gelatin hydrogel pads incorporated with Eupatorium adenophorum essential oil as antibacterial wound dressing. *Polymer Bulletin* **2019,** *76* (2), 701-724.

35. Kamble, A.; Shetty, V.; Shendokar, S.; Chavan, S.; Kaul-Ghanekar, R., Synthesis, Characterization and Antibacterial Activity of Ciprofloxacin Loaded Electrospun Gelatin Nanofibers. *Journal of Bionanoscience* **2018,** *12* (5), 715-720.

36. Yang, X.; Fan, L.; Ma, L.; Wang, Y.; Lin, S.; Yu, F.; Pan, X.; Luo, G.; Zhang, D.; Wang, H., Green electrospun Manuka honey/silk fibroin fibrous matrices as potential wound dressing. *Materials & Design* **2017,** *119*, 76-84.

37. Mirani, B.; Pagan, E.; Currie, B.; Siddiqui, M. A.; Hosseinzadeh, R.; Mostafalu, P.; Zhang, Y. S.; Ghahary, A.; Akbari, M., An advanced multifunctional hydrogel-based dressing for wound monitoring and drug delivery. *Advanced healthcare materials* **2017,** *6* (19), 1700718.

38. Akbari, M.; Mirani, B.; Ghahary, A.; Siddiqui, M. A. Wound covering for wound monitoring and therapeutic agent delivery. 2018.

39. Zarghami, A.; Irani, M.; Mostafazadeh, A.; Golpour, M.; Heidarinasab, A.; Haririan, I., Fabrication of PEO/chitosan/PCL/olive oil nanofibrous scaffolds for wound dressing applications. *Fibers and Polymers* **2015,** *16* (6), 1201-1212.

40. Saghazadeh, S.; Rinoldi, C.; Schot, M.; Kashaf, S. S.; Sharifi, F.; Jalilian, E.; Nuutila, K.; Giatsidis, G.; Mostafalu, P.; Derakhshandeh, H., Drug delivery systems and materials for wound healing applications. *Advanced drug delivery reviews* **2018,** *127*, 138-166.

41. Derakhshandeh, H.; Kashaf, S. S.; Aghabaglou, F.; Ghanavati, I. O.; Tamayol, A., Smart bandages: the future of wound care. *Trends in biotechnology* **2018,** *36* (12), 1259-1274.

42. Simões, D.; Miguel, S. P.; Ribeiro, M. P.; Coutinho, P.; Mendonça, A. G.; Correia, I. J., Recent advances on antimicrobial wound dressing: A review. *European journal of pharmaceutics and biopharmaceutics* **2018,** *127*, 130-141.

43. Păunica-Panea, G.; Ficai, A.; Marin, M. M.; Marin, Ș.; Albu, M. G.; Constantin, V. D.; Dinu-Pîrvu, C.; Vuluga, Z.; Corobea, M. C.; Ghica, M. V., New collagen-dextran-zinc oxide composites for wound dressing. *Journal of Nanomaterials* **2016,** *2016*.

44. Pawar, H.; Tetteh, J.; Boateng, J., Preparation, optimisation and characterisation of novel wound healing film dressings loaded with streptomycin and diclofenac. *Colloids and Surfaces B: Biointerfaces* **2013,** *102*, 102-110.

45. Cerchiara, T.; Abruzzo, A.; Palomino, R. A. Ñ.; Vitali, B.; De Rose, R.; Chidichimo, G.; Ceseracciu, L.; Athanassiou, A.; Saladini, B.; Dalena, F., Spanish Broom (Spartium junceum L.) fibers impregnated with vancomycin-loaded chitosan nanoparticles as new antibacterial wound dressing: Preparation, characterization and antibacterial activity. *European Journal of Pharmaceutical Sciences* **2017,** *99*, 105-112.

46. Shao, W.; Liu, H.; Wang, S.; Wu, J.; Huang, M.; Min, H.; Liu, X., Controlled release and antibacterial activity of tetracycline hydrochloride-loaded bacterial cellulose composite membranes. *Carbohydrate polymers* **2016,** *145*, 114-120.

47. Pásztor, N.; Rédai, E.; Szabó, Z.-I.; Sipos, E., Preparation and characterization of levofloxacin-loaded nanofibers as potential wound dressings. *Acta Medica Marisiensis* **2017,** *63* (2), 66-69.

48. Rios, A. C.; Moutinho, C. G.; Pinto, F. C.; Del Fiol, F. S.; Jozala, A.; Chaud, M. V.; Vila, M. M.; Teixeira, J. A.; Balcao, V. M., Alternatives to overcoming bacterial resistances: State-of-the-art. *Microbiol Res* **2016,** *191*, 51-80.

49. Williamson, R.; Collatz, E.; Gutmann, L., Mechanisms of action of beta-lactam antibiotics and mechanisms of non-enzymatic resistance. *Presse medicale (Paris, France: 1983)* **1986,** *15* (46), 2282-2289.

50. Zeng, D.; Debabov, D.; Hartsell, T. L.; Cano, R. J.; Adams, S.; Schuyler, J. A.; McMillan, R.; Pace, J. L., Approved glycopeptide antibacterial drugs: mechanism of action and resistance. *Cold Spring Harbor perspectives in medicine* **2016,** *6* (12), a026989.

51. Kumar, S. Synthesis and antimicrobial study of some Schiff bases of sulfonamides. Rajiv Gandhi University of Health Sciences, 2010.

52. Udumula, V.; Ham, Y. W.; Fosso, M. Y.; Chan, K. Y.; Rai, R.; Zhang, J.; Li, J.; Chang, C.-W. T., Investigation of antibacterial mode of action for traditional and amphiphilic aminoglycosides. *Bioorganic & medicinal chemistry letters* **2013,** *23* (6), 1671-1675.

53. Chopra, I.; Roberts, M., Tetracycline antibiotics: mode of action, applications, molecular biology, and epidemiology of bacterial resistance. *Microbiol. Mol. Biol. Rev.* **2001,** *65* (2), 232-260.

54. Aldred, K. J.; Kerns, R. J.; Osheroff, N., Mechanism of quinolone action and resistance. *Biochemistry* **2014,** *53* (10), 1565-1574.

55. Kurczewska, J.; Pecyna, P.; Ratajczak, M.; Gajęcka, M.; Schroeder, G., Halloysite nanotubes as carriers of vancomycin in alginate-based wound dressing. *Saudi pharmaceutical journal* **2017,** *25* (6), 911-920.

56. Altoé, L. S.; Alves, R. S.; Sarandy, M. M.; Morais-Santos, M.; Novaes, R. D.; Gonçalves, R. V., Does antibiotic use accelerate or retard cutaneous repair? A systematic review in animal models. *PloS one* **2019,** *14* (10).

57. He, J.; Shi, M.; Liang, Y.; Guo, B., Conductive adhesive self-healing nanocomposite hydrogel wound dressing for photothermal therapy of infected full-thickness skin wounds. *Chemical Engineering Journal* **2020**, 124888.

58. Roy, D. C.; Tomblyn, S.; Isaac, K. M.; Kowalczewski, C. J.; Burmeister, D. M.; Burnett, L. R.; Christy, R. J., Ciprofloxacin-loaded keratin hydrogels reduce infection and support healing in a porcine partial-thickness thermal burn. *Wound Repair and Regeneration* **2016,** *24* (4), 657-668.

59. Elsner, J. J.; Egozi, D.; Ullmann, Y.; Berdicevsky, I.; Shefy-Peleg, A.; Zilberman, M., Novel biodegradable composite wound dressings with controlled release of antibiotics: Results in a guinea pig burn model. *Burns* **2011,** *37* (5), 896-904.

60. Green, B. N.; Johnson, C. D.; Egan, J. T.; Rosenthal, M.; Griffith, E. A.; Evans, M. W., Methicillin-resistant Staphylococcus aureus: an overview for manual therapists. *Journal of chiropractic medicine* **2012,** *11* (1), 64-76.

61. Ventola, C. L., The antibiotic resistance crisis: part 1: causes and threats. *P T* **2015,** *40* (4), 277-83.

62. Luepke, K. H.; Suda, K. J.; Boucher, H.; Russo, R. L.; Bonney, M. W.; Hunt, T. D.; Mohr III, J. F., Past, present, and future of antibacterial economics: increasing bacterial resistance, limited antibiotic pipeline, and societal implications. *Pharmacotherapy: The Journal of Human Pharmacology and Drug Therapy* **2017,** *37* (1), 71-84.

63. Cui, B.; Zhang, C.; Gan, B.; Liu, W.; Liang, J.; Fan, Z.; Wen, Y.; Yang, Y.; Peng, X.; Zhou, Y., Collagen-tussah silk fibroin hybrid scaffolds loaded with bone mesenchymal stem cells promote skin wound repair in rats. *Materials Science and Engineering: C* **2020,** *109*, 110611.

64. Tao, G.; Wang, Y.; Cai, R.; Chang, H.; Song, K.; Zuo, H.; Zhao, P.; Xia, Q.; He, H., Design and performance of sericin/poly (vinyl alcohol) hydrogel as a drug delivery carrier for potential wound dressing application. *Materials Science and Engineering: C* **2019,** *101*, 341-351.

65. Bakhsheshi-Rad, H.; Hadisi, Z.; Ismail, A.; Aziz, M.; Akbari, M.; Berto, F.; Chen, X., In vitro and in vivo evaluation of chitosan-alginate/gentamicin wound dressing nanofibrous with high antibacterial performance. *Polymer Testing* **2020,** *82*, 106298.

66. Brianezi, S. F. S.; Castro, K. C.; Piazza, R. D.; Melo, M. d. S. F.; Pereira, R. M.; Marques, R. F. C.; Campos, M. G. N., Preparation and Characterization of Chitosan/mPEG-PCL Blended Membranes for Wound Dressing and Controlled Gentamicin Release. *Materials Research* **2018,** *21* (6).

67. Dhand, C.; Venkatesh, M.; Barathi, V. A.; Harini, S.; Bairagi, S.; Leng, E. G. T.; Muruganandham, N.; Low, K. Z. W.; Fazil, M. H. U. T.; Loh, X. J., Bio-inspired crosslinking and matrix-drug interactions for advanced wound dressings with long-term antimicrobial activity. *Biomaterials* **2017,** *138*, 153-168.

68. Cui, S.; Sun, X.; Li, K.; Gou, D.; Zhou, Y.; Hu, J.; Liu, Y., Polylactide nanofibers delivering doxycycline for chronic wound treatment. *Materials Science and Engineering: C* **2019,** *104*, 109745.

69. Anbazhagan, S.; Thangavelu, K. P., Application of tetracycline hydrochloride loaded-fungal chitosan and Aloe vera extract based composite sponges for wound dressing. *Journal of advanced research* **2018,** *14*, 63-71.

70. Li, H.; Williams, G. R.; Wu, J.; Lv, Y.; Sun, X.; Wu, H.; Zhu, L.-M., Thermosensitive nanofibers loaded with ciprofloxacin as antibacterial wound dressing materials. *International journal of pharmaceutics* **2017,** *517* (1-2), 135-147.

71. Evranos, B.; Aycan, D.; Alemdar, N., Production of ciprofloxacin loaded chitosan/gelatin/bone ash wound dressing with improved mechanical properties. *Carbohydrate polymers* **2019,** *222*, 115007.

72. Siafaka, P. I.; Zisi, A. P.; Exindari, M. K.; Karantas, I. D.; Bikiaris, D. N., Porous dressings of modified chitosan with poly (2-hydroxyethyl acrylate) for topical wound delivery of levofloxacin. *Carbohydrate polymers* **2016,** *143*, 90-99.

73. Barrientos, I. J. H.; Paladino, E.; Brozio, S.; Passarelli, M. K.; Moug, S.; Black, R. A.; Wilson, C. G.; Lamprou, D. A., Fabrication and characterisation of drug-loaded electrospun polymeric nanofibers for controlled release in hernia repair. *International journal of pharmaceutics* **2017,** *517* (1-2), 329-337.

74. Ma, R.; Wang, Y.; Qi, H.; Shi, C.; Wei, G.; Xiao, L.; Huang, Z.; Liu, S.; Yu, H.; Teng, C., Nanocomposite sponges of sodium alginate/graphene oxide/polyvinyl alcohol as potential wound dressing: In vitro and in vivo evaluation. *Composites Part B: Engineering* **2019,** *167*, 396-405.

75. Pandit, A. P.; Koyate, K. R.; Kedar, A. S.; Mute, V. M., Spongy wound dressing of pectin/carboxymethyl tamarind seed polysaccharide loaded with moxifloxacin beads for effective wound heal. *International journal of biological macromolecules* **2019,** *140*, 1106-1115.

76. Safdari, M.; Shakiba, E.; Kiaie, S. H.; Fattahi, A., Preparation and characterization of Ceftazidime loaded electrospun silk fibroin/gelatin mat for wound dressing. *Fibers and Polymers* **2016,** *17* (5), 744-750.

77. Ye, S.; Jiang, L.; Su, C.; Zhu, Z.; Wen, Y.; Shao, W., Development of gelatin/bacterial cellulose composite sponges as potential natural wound dressings. *International journal of biological macromolecules* **2019,** *133*, 148-155.

78. Tamahkar, E.; Özkahraman, B.; Süloğlu, A. K.; İdil, N.; Perçin, I., A novel multilayer hydrogel wound dressing for antibiotic release. *Journal of Drug Delivery Science and Technology* **2020**, 101536.

79. Ullah, S.; Hashmi, M.; Khan, M. Q.; Kharaghani, D.; Saito, Y.; Yamamoto, T.; Kim, I. S., Silver sulfadiazine loaded zein nanofiber mats as a novel wound dressing. *RSC advances* **2019,** *9* (1), 268-277.

80. Ma, C.; Liu, L.; Hua, W.; Cai, Y.; Yao, J., Fabrication and characterization of absorbent and antibacterial alginate fibers loaded with sulfanilamide. *Fibers and Polymers* **2015,** *16* (6), 1255-1261.

81. Li, C.; Fu, R.; Yu, C.; Li, Z.; Guan, H.; Hu, D.; Zhao, D.; Lu, L., Silver nanoparticle/chitosan oligosaccharide/poly (vinyl alcohol) nanofibers as wound dressings: a preclinical study. *International journal of nanomedicine* **2013,** *8*, 4131.

82. Cai, N.; Li, C.; Han, C.; Luo, X.; Shen, L.; Xue, Y.; Yu, F., Tailoring mechanical and antibacterial properties of chitosan/gelatin nanofiber membranes with Fe3O4 nanoparticles for potential wound dressing application. *Applied Surface Science* **2016,** *369*, 492-500.

83. Archana, D.; Singh, B. K.; Dutta, J.; Dutta, P., In vivo evaluation of chitosan–PVP–titanium dioxide nanocomposite as wound dressing material. *Carbohydrate polymers* **2013,** *95* (1), 530-539.

84. Chaturvedi, A.; Bajpai, A. K.; Bajpai, J.; Singh, S. K., Evaluation of poly (vinyl alcohol) based cryogel–zinc oxide nanocomposites for possible applications as wound dressing materials. *Materials Science and Engineering: C* **2016,** *65*, 408-418.

85. Shaikh, S.; Nazam, N.; Rizvi, S. M. D.; Ahmad, K.; Baig, M. H.; Lee, E. J.; Choi, I., Mechanistic Insights into the Antimicrobial Actions of Metallic Nanoparticles and Their Implications for Multidrug Resistance. *Int J Mol Sci* **2019,** *20* (10), 2468.

86. Weir, E.; Lawlor, A.; Whelan, A.; Regan, F., The use of nanoparticles in anti-microbial materials and their characterization. *Analyst* **20008,** *133* (7), 835-845.

87. Slavin, Y. N.; Asnis, J.; Hafeli, U. O.; Bach, H., Metal nanoparticles: understanding the mechanisms behind antibacterial activity. *J Nanobiotechnology* **2017,** *15* (1), 65.

88. Abdal Dayem, A.; Hossain, M. K.; Lee, S. B.; Kim, K.; Saha, S. K.; Yang, G. M.; Choi, H. Y.; Cho, S. G., The Role of Reactive Oxygen Species (ROS) in the Biological Activities of Metallic Nanoparticles. *Int J Mol Sci* **2017,** *18* (1).

89. Sirelkhatim, A.; Mahmud, S.; Seeni, A.; Kaus, N. H. M.; Ann, L. C.; Bakhori, S. K. M.; Hasan, H.; Mohamad, D., Review on zinc oxide nanoparticles: antibacterial activity and toxicity mechanism. *Nano-Micro Letters* **2015,** *7* (3), 219-242.

90. Rajeshkumar, S.; Bharath, L., Mechanism of plant-mediated synthesis of silver nanoparticles–a review on biomolecules involved, characterisation and antibacterial activity. *Chemico-biological interactions* **2017,** *273*, 219-227.

91. Behera, S. S.; Patra, J. K.; Pramanik, K.; Panda, N.; Thatoi, H., Characterization and evaluation of antibacterial activities of chemically synthesized iron oxide nanoparticles. *World J Nano Sci Eng* **2012,** *2* (4), 196-200.

92. Foster, H. A.; Ditta, I. B.; Varghese, S.; Steele, A., Photocatalytic disinfection using titanium dioxide: spectrum and mechanism of antimicrobial activity. *Applied microbiology and biotechnology* **2011,** *90* (6), 1847-1868.

93. Tang, S.; Zheng, J., Antibacterial activity of silver nanoparticles: structural effects. *Advanced healthcare materials* **2018,** *7* (13), 1701503.

94. Singla, R.; Soni, S.; Patial, V.; Kulurkar, P. M.; Kumari, A.; Mahesh, S.; Padwad, Y. S.; Yadav, S. K., In vivo diabetic wound healing potential of nanobiocomposites containing bamboo cellulose nanocrystals impregnated with silver nanoparticles. *International journal of biological macromolecules* **2017,** *105*, 45-55.

95. Abdel-Mohsen, A.; Jancar, J.; Abdel-Rahman, R.; Vojtek, L.; Hyršl, P.; Dušková, M.; Nejezchlebová, H., A novel in situ silver/hyaluronan bio-nanocomposite fabrics for wound and chronic ulcer dressing: in vitro and in vivo evaluations. *International journal of pharmaceutics* **2017,** *520* (1-2), 241-253.

96. Masood, N.; Ahmed, R.; Tariq, M.; Ahmed, Z.; Masoud, M. S.; Ali, I.; Asghar, R.; Andleeb, A.; Hasan, A., Silver nanoparticle impregnated chitosan-PEG hydrogel enhances wound healing in diabetes induced rabbits. *International journal of pharmaceutics* **2019,** *559*, 23-36.

97. Wright, J. B.; Lam, K.; Buret, A. G.; Olson, M. E.; Burrell, R. E., Early healing events in a porcine model of contaminated wounds: effects of nanocrystalline silver on matrix metalloproteinases, cell apoptosis, and healing. *Wound Repair and Regeneration* **2002,** *10* (3), 141-151.

98. Silva, M. M. P.; de Aguiar, M. I. F.; Rodrigues, A. B.; Miranda, M. D. C.; Araújo, M. Â. M.; Rolim, I. L. T. P.; Alves, A. M., The use of nanoparticles in wound treatment: a systematic review. *Revista da Escola de Enfermagem da USP* **2017,** *51*, 1-9.

99. Sankar, R.; Dhivya, R.; Shivashangari, K. S.; Ravikumar, V., Wound healing activity of Origanum vulgare engineered titanium dioxide nanoparticles in Wistar Albino rats. *Journal of Materials Science: Materials in Medicine* **2014,** *25* (7), 1701-1708.

100. Ahmed, R.; Tariq, M.; Ali, I.; Asghar, R.; Khanam, P. N.; Augustine, R.; Hasan, A., Novel electrospun chitosan/polyvinyl alcohol/zinc oxide nanofibrous mats with antibacterial and antioxidant properties for diabetic wound healing. *International journal of biological macromolecules* **2018,** *120*, 385-393.

101. Das, M.; Goswami, U.; Kandimalla, R.; Kalita, S.; Ghosh, S. S.; Chattopadhyay, A., Iron–Copper Bimetallic Nanocomposite Reinforced Dressing Materials for Infection Control and Healing of Diabetic Wound. *ACS Applied Bio Materials* **2019,** *2* (12), 5434-5445.

102. Nam, G.; Rangasamy, S.; Purushothaman, B.; Song, J. M., The application of bactericidal silver nanoparticles in wound treatment. *Nanomaterials and Nanotechnology* **2015,** *5* (Godište 2015), 5-23.

103. AshaRani, P.; Sethu, S.; Lim, H. K.; Balaji, G.; Valiyaveettil, S.; Hande, M. P., Differential regulation of intracellular factors mediating cell cycle, DNA repair and inflammation following exposure to silver nanoparticles in human cells. *Genome integrity* **2012,** *3* (1), 2.

104. Ahamed, M.; Karns, M.; Goodson, M.; Rowe, J.; Hussain, S. M.; Schlager, J. J.; Hong, Y., DNA damage response to different surface chemistry of silver nanoparticles in mammalian cells. *Toxicology and applied pharmacology* **2008,** *233* (3), 404-410.

105. Chen, X.; Schluesener, H. J., Nanosilver: a nanoproduct in medical application. *Toxicology letters* **2008,** *176* (1), 1-12.

106. GhavamiNejad, A.; Rajan Unnithan, A.; Ramachandra Kurup Sasikala, A.; Samarikhalaj, M.; Thomas, R. G.; Jeong, Y. Y.; Nasseri, S.; Murugesan, P.; Wu, D.; Hee Park, C., Mussel-inspired electrospun nanofibers functionalized with size-controlled silver nanoparticles for wound dressing application. *ACS applied materials & interfaces* **2015,** *7* (22), 12176-12183.

107. Wu, C.-N.; Fuh, S.-C.; Lin, S.-P.; Lin, Y.-Y.; Chen, H.-Y.; Liu, J.-M.; Cheng, K.-C., TEMPO-oxidized bacterial cellulose pellicle with silver nanoparticles for wound dressing. *Biomacromolecules* **2018,** *19* (2), 544-554.

108. Khampieng, T.; Brikshavana, P.; Supaphol, P., Silver nanoparticle-embedded poly (vinyl pyrrolidone) hydrogel dressing: gamma-ray synthesis and biological evaluation. *Journal of Biomaterials Science, Polymer Edition* **2014,** *25* (8), 826-842.

109. Ismail, N. A.; Amin, K. A. M.; Majid, F. A. A.; Razali, M. H., Gellan gum incorporating titanium dioxide nanoparticles biofilm as wound dressing: Physicochemical, mechanical, antibacterial properties and wound healing studies. *Materials Science and Engineering: C* **2019,** *103*, 109770.

110. Khalid, A.; Ullah, H.; Ul-Islam, M.; Khan, R.; Khan, S.; Ahmad, F.; Khan, T.; Wahid, F., Bacterial cellulose–TiO 2 nanocomposites promote healing and tissue regeneration in burn mice model. *RSC advances* **2017,** *7* (75), 47662-47668.

111. El-Aassar, M.; El-Deeb, N. M.; Hassan, H. S.; Mo, X., Electrospun polyvinyl alcohol/pluronic F127 blended nanofibers containing titanium dioxide for antibacterial wound dressing. *Applied biochemistry and biotechnology* **2016,** *178* (8), 1488-1502.

112. Khorasani, M. T.; Joorabloo, A.; Adeli, H.; Mansoori-Moghadam, Z.; Moghaddam, A., Design and optimization of process parameters of polyvinyl (alcohol)/chitosan/nano zinc oxide hydrogels as wound healing materials. *Carbohydrate polymers* **2019,** *207*, 542-554.

113. Khalid, A.; Khan, R.; Ul-Islam, M.; Khan, T.; Wahid, F., Bacterial cellulose-zinc oxide nanocomposites as a novel dressing system for burn wounds. *Carbohydrate polymers* **2017,** *164*, 214-221.

114. Moreno-Eutimio, M. A.; Espinosa-Monroy, L.; Orozco-Amaro, T.; Torres-Ramos, Y.; Montoya-Estrada, A.; Hicks, J. J.; Rodríguez-Ayala, E.; Del Moral, P.; Moreno, J.; Cueto-García, J., Enhanced healing and anti-inflammatory effects of a carbohydrate polymer with zinc oxide in patients with chronic venous leg ulcers: preliminary results. *Archives of Medical Science: AMS* **2018,** *14* (2), 336.

115. Lin, P.-H.; Sermersheim, M.; Li, H.; Lee, P. H.; Steinberg, S. M.; Ma, J., Zinc in wound healing modulation. *Nutrients* **2018,** *10* (1), 16.

116. PT, S. K.; Lakshmanan, V.-K.; Raj, M.; Biswas, R.; Hiroshi, T.; Nair, S. V.; Jayakumar, R., Evaluation of wound healing potential of β-chitin hydrogel/nano zinc oxide composite bandage. *Pharmaceutical research* **2013,** *30* (2), 523-537.

117. Chhabra, H.; Deshpande, R.; Kanitkar, M.; Jaiswal, A.; Kale, V. P.; Bellare, J. R., A nano zinc oxide doped electrospun scaffold improves wound healing in a rodent model. *RSC advances* **2016,** *6* (2), 1428-1439.

118. Vasile, B. S.; Oprea, O.; Voicu, G.; Ficai, A.; Andronescu, E.; Teodorescu, A.; Holban, A., Synthesis and characterization of a novel controlled release zinc oxide/gentamicin–chitosan

composite with potential applications in wounds care. *International Journal of Pharmaceutics* **2014,** *463* (2), 161-169.

119. Pati, R.; Mehta, R. K.; Mohanty, S.; Padhi, A.; Sengupta, M.; Vaseeharan, B.; Goswami, C.; Sonawane, A., Topical application of zinc oxide nanoparticles reduces bacterial skin infection in mice and exhibits antibacterial activity by inducing oxidative stress response and cell membrane disintegration in macrophages. *Nanomedicine: Nanotechnology, Biology and Medicine* **2014,** *10* (6), 1195-1208.

120. Homaeigohar, S.; Boccaccini, A. R., Antibacterial biohybrid nanofibers for wound dressings. *Acta Biomater* **2020,** *107*, 25-49.

121. Aya, K. L.; Stern, R., Hyaluronan in wound healing: rediscovering a major player. *Wound repair and regeneration* **2014,** *22* (5), 579-593.

122. Jeon, O.; Song, S. J.; Lee, K.-J.; Park, M. H.; Lee, S.-H.; Hahn, S. K.; Kim, S.; Kim, B.-S., Mechanical properties and degradation behaviors of hyaluronic acid hydrogels cross-linked at various cross-linking densities. *Carbohydrate polymers* **2007,** *70* (3), 251-257.

123. Lewandowska, K.; Alina, S.; Grabska, S.; Michalska, M., Characterisation of chitosan/hyaluronic acid blend films modified by collagen. *Progress on Chemistry and Application of Chitin and its Derivatives* **2017,** *22*, 125-134.

124. Hadisi, Z.; Nourmohammadi, J.; Nassiri, S. M., The antibacterial and anti-inflammatory investigation of Lawsonia Inermis-gelatin-starch nano-fibrous dressing in burn wound. *International journal of biological macromolecules* **2018,** *107*, 2008-2019.

125. Dhandayuthapani, B.; Krishnan, U. M.; Sethuraman, S., Fabrication and characterization of chitosan-gelatin blend nanofibers for skin tissue engineering. *Journal of Biomedical Materials Research Part B: Applied Biomaterials* **2010,** *94* (1), 264-272.

126. Zhang, W.; Li, Y.; Jiang, D.; Xie, S.; Zeng, M.; Chen, J.; Chen, L.; Ouyang, H.; Zou, X., Promotion of hernia repair with high-strength, flexible, and bioresorbable silk fibroin mesh in a large abdominal hernia model. *ACS Biomaterials Science & Engineering* **2017,** *4* (6), 2067-2080.

127. Woodford, N.; Livermore, D. M., Infections caused by Gram-positive bacteria: a review of the global challenge. *Journal of Infection* **2009,** *59*, S4-S16.

128. Carey, J. R.; Suslick, K. S.; Hulkower, K. I.; Imlay, J. A.; Imlay, K. R.; Ingison, C. K.; Ponder, J. B.; Sen, A.; Wittrig, A. E., Rapid identification of bacteria with a disposable colorimetric sensing array. *Journal of the American Chemical Society* **2011,** *133* (19), 7571-7576.

129. Borisov, S. M.; Wolfbeis, O. S., Optical biosensors. *Chemical reviews* **2008,** *108* (2), 423-461.

130. Suslick, K. S., Synesthesia in science and technology: more than making the unseen visible. *Current opinion in chemical biology* **2012,** *16* (5-6), 557-563.

131. Li, Z.; Askim, J. R.; Suslick, K. S., The optoelectronic nose: colorimetric and fluorometric sensor arrays. *Chemical reviews* **2018,** *119* (1), 231-292.

132. Suslick, K. S.; Rakow, N. A.; Sen, A., Colorimetric sensor arrays for molecular recognition. *Tetrahedron* **2004,** *60* (49), 11133-11138.

133. Rakow, N. A.; Sen, A.; Janzen, M. C.; Ponder, J. B.; Suslick, K. S., Molecular recognition and discrimination of amines with a colorimetric array. *Angewandte Chemie* **2005,** *117* (29), 4604-4608.

134. Soga, T.; Jimbo, Y.; Suzuki, K.; Citterio, D., Inkjet-printed paper-based colorimetric sensor array for the discrimination of volatile primary amines. *Analytical chemistry* **2013,** *85* (19), 8973-8978.

135. Janzen, M. C.; Ponder, J. B.; Bailey, D. P.; Ingison, C. K.; Suslick, K. S., Colorimetric sensor arrays for volatile organic compounds. *Analytical chemistry* **2006,** *78* (11), 3591-3600.

136. Bie, X.; Khan, M. Q.; Ullah, A.; Ullah, S.; Kharaghani, D.; Phan, D.-N.; Tamada, Y.; Kim, I. S., Fabrication and characterization of wound dressings containing gentamicin/silver for wounds in diabetes mellitus patients. *Materials Research Express* **2020,** *7* (4), 045004.

137. Heunis, T. d. J. Development of an antimicrobial wound dressing by co-electrospinning bacteriocins of lactic acid bacteria into polymeric nanofibers. Stellenbosch: Stellenbosch University, 2012.

138. Mohammadi, S.; Ramakrishna, S.; Laurent, S.; Shokrgozar, M. A.; Semnani, D.; Sadeghi, D.; Bonakdar, S.; Akbari, M., Fabrication of Nanofibrous PVA/Alginate-Sulfate Substrates for Growth Factor Delivery. *Journal of Biomedical Materials Research Part A* **2019,** *107* (2), 403-413.

139. Mirani, B.; Pagan, E.; Shojaei, S.; Dabiri, S. M. H.; Savoji, H.; Mehrali, M.; Sam, M.; Alsaif, J.; Bhiladvala, R. B.; Dolatshahi-Pirouz, A., Facile method for fabrication of meter-long multifunctional hydrogel fibers with controllable biophysical and biochemical features. *ACS Applied Materials & Interfaces* **2020,** *12* (8), 9080-9089.

140. Wang, F.; Sun, Y.; Li, D.; Zhong, B.; Wu, Z.; Zuo, S.; Yan, D.; Zhuo, R.; Feng, J.; Yan, P., Microwave absorption properties of 3D cross-linked Fe/C porous nanofibers prepared by electrospinning. *Carbon* **2018,** *134*, 264-273.

141. Chen, L.-F.; Lu, Y.; Yu, L.; Lou, X. W. D., Designed formation of hollow particle-based nitrogen-doped carbon nanofibers for high-performance supercapacitors. *Energy & Environmental Science* **2017,** *10* (8), 1777-1783.

142. Niu, Q.; Zeng, L.; Mu, X.; Nie, J.; Ma, G., Preparation and characterization of core-shell nanofibers by electrospinning combined with in situ UV photopolymerization. *Journal of industrial and engineering chemistry* **2016,** *34*, 337-343.

143. Naeimirad, M.; Zadhoush, A.; Kotek, R.; Esmaeely Neisiany, R.; Nouri Khorasani, S.; Ramakrishna, S., Recent advances in core/shell bicomponent fibers and nanofibers: A review. *Journal of Applied Polymer Science* **2018,** *135* (21), 46265.

144. Elahi, M. F.; Lu, W.; Guoping, G.; Khan, F., Core-shell fibers for biomedical applications-a review. *J. Bioeng. Biomed. Sci* **2013,** *3* (1), 1-14.

145. Ono, S.; Imai, R.; Ida, Y.; Shibata, D.; Komiya, T.; Matsumura, H., Increased wound pH as an indicator of local wound infection in second degree burns. *Burns* **2015,** *41* (4), 820-824.

146. Lambers, H.; Piessens, S.; Bloem, A.; Pronk, H.; Finkel, P., Natural skin surface pH is on average below 5, which is beneficial for its resident flora. *International journal of cosmetic science* **2006,** *28* (5), 359-370.

147. Gethin, G., The significance of surface pH in chronic wounds. *Wounds uk* **2007,** *3* (3), 52.

148. Pakolpakçıl, A.; Osman, B.; Göktalay, G.; Özer, E. T.; Şahan, Y.; Becerir, B.; Karaca, E., Design and in vivo evaluation of alginate-based pH-sensing electrospun wound dressing containing anthocyanins. *Journal of Polymer Research* **2021,** *28* (2), 1-13.

149. Maftoonazad, N.; Ramaswamy, H., Design and testing of an electrospun nanofiber mat as a pH biosensor and monitor the pH associated quality in fresh date fruit (Rutab). *Polymer Testing* **2019,** *75*, 76-84.

150. Branski, L. K.; Al-Mousawi, A.; Rivero, H.; Jeschke, M. G.; Sanford, A. P.; Herndon, D. N., Emerging infections in burns. *Surgical infections* **2009,** *10* (5), 389-397.

151. Păunica-Panea, G.; Ficai, A.; Marin, M. M.; Marin, Ş.; Albu, M. G.; Constantin, V. D.; Dinu-Pîrvu, C.; Vuluga, Z.; Corobea, M. C.; Ghica, M. V., New collagen-dextran-zinc oxide composites for wound dressing. *Journal of Nanomaterials* **2016,** *2016*, 34.

152. Akturk, O.; Kismet, K.; Yasti, A. C.; Kuru, S.; Duymus, M. E.; Kaya, F.; Caydere, M.; Hucumenoglu, S.; Keskin, D., Collagen/gold nanoparticle nanocomposites: a potential skin wound healing biomaterial. *Journal of biomaterials applications* **2016,** *31* (2), 283-301.

153. Rath, G.; Hussain, T.; Chauhan, G.; Garg, T.; Goyal, A. K., Collagen nanofiber containing silver nanoparticles for improved wound-healing applications. *Journal of drug targeting* **2016,** *24* (6), 520-529.

154. Bidgoli, S. A.; Mahdavi, M.; Rezayat, S. M.; Korani, M.; Amani, A.; Ziarati, P., Toxicity assessment of nanosilver wound dressing in Wistar rat. *Acta Medica Iranica* **2013,** *51* (4), 203-208.

155. Lin, P.-H.; Sermersheim, M.; Li, H.; Lee, P.; Steinberg, S.; Ma, J., Zinc in wound healing modulation. *Nutrients* **2018,** *10* (1), 16.

156. Zhang, W.; Chen, L.; Chen, J.; Wang, L.; Gui, X.; Ran, J.; Xu, G.; Zhao, H.; Zeng, M.; Ji, J., Silk fibroin biomaterial shows safe and effective wound healing in animal models and a randomized controlled clinical trial. *Advanced healthcare materials* **2017,** *6* (10), 1700121.

157. Farokhi, M.; Mottaghitalab, F.; Fatahi, Y.; Khademhosseini, A.; Kaplan, D. L., Overview of Silk Fibroin Use in Wound Dressings. *Trends in biotechnology* **2018**.

158. Gholipourmalekabadi, M.; Khosravimelal, S.; Nokhbedehghan, Z.; Sameni, M.; Jajarmi, V.; Urbanska, A. M.; Mirzaei, H.; Salimi, M.; Chauhan, N. P. S.; Mobaraki, M., Modulation of hypertrophic scar formation using amniotic membrane/electrospun silk fibroin bilayer membrane in a rabbit ear model. *ACS Biomaterials Science & Engineering* **2019**.

159. Dovedytis, M.; Liu, Z. J.; Bartlett, S., Hyaluronic acid and its biomedical applications: A review. *Engineered Regeneration* **2020,** *1*, 102-113.

160. Castro, K. C.; Campos, M. G. N.; Mei, L. H. I., Hyaluronic acid electrospinning: Challenges, applications in wound dressings and new perspectives. *International Journal of Biological Macromolecules* **2021,** *173*, 251-266.

161. Zhou, Z.; Yang, Z.; Kong, L.; Liu, L.; Liu, Q.; Zhao, Y.; Zeng, W.; Yi, Q.; Cao, D., Preparation and characterization of hyaluronic acid hydrogel blends with gelatin. *Journal of Macromolecular Science, Part B* **2012,** *51* (12), 2392-2400.

162. Qi, Y.; Wang, H.; Wei, K.; Yang, Y.; Zheng, R.-Y.; Kim, I.; Zhang, K.-Q., A review of structure construction of silk fibroin biomaterials from single structures to multi-level structures. *International journal of molecular sciences* **2017,** *18* (3), 237.

163. Rockwood, D.; Preda, R., TYU cel, X. Wang, ML Lovett and DL Kaplan. *Nat. Protoc* **2011,** *6*, 1612-1631.

164. Hadisi, Z.; Nourmohammadi, J.; Mohammadi, J., Composite of porous starch-silk fibroin nanofiber-calcium phosphate for bone regeneration. *Ceramics International* **2015,** *41* (9), 10745-10754.

165. Brenner, E. K.; Schiffman, J. D.; Thompson, E. A.; Toth, L. J.; Schauer, C. L., Electrospinning of hyaluronic acid nanofibers from aqueous ammonium solutions. *Carbohydrate Polymers* **2012,** *87* (1), 926-929.

166. Fathollahipour, S.; Abouei Mehrizi, A.; Ghaee, A.; Koosha, M., Electrospinning of PVA/chitosan nanocomposite nanofibers containing gelatin nanoparticles as a dual drug delivery system. *Journal of Biomedical Materials Research Part A* **2015,** *103* (12), 3852-3862.

167. Bakhsheshi-Rad, H. R.; Akbari, M.; Ismail, A. F.; Aziz, M.; Hadisi, Z.; Pagan, E.; Daroonparvar, M.; Chen, X., Coating biodegradable magnesium alloys with electrospun poly-L-lactic acid-åkermanite-doxycycline nanofibers for enhanced biocompatibility, antibacterial activity, and corrosion resistance. *Surface and Coatings Technology* **2019,** *377*, 124898.

168. Zak, A. K.; Razali, R.; Majid, W. A.; Darroudi, M., Synthesis and characterization of a narrow size distribution of zinc oxide nanoparticles. *International journal of nanomedicine* **2011,** *6*, 1399.

169. Matharu, R. K.; Porwal, H.; Ciric, L.; Edirisinghe, M., The effect of graphene–poly (methyl methacrylate) fibres on microbial growth. *Interface focus* **2018,** *8* (3), 20170058.

170. Weir, M.; Johnson, D.; Boothroyd, S.; Savage, R.; Thompson, R.; King, S.; Rogers, S.; Coleman, K.; Clarke, N., Distortion of chain conformation and reduced entanglement in polymer–graphene oxide nanocomposites. *ACS Macro Letters* **2016,** *5* (4), 430-434.

171. Liao, Y.; Fukuda, T.; Kamata, N.; Tokunaga, M., Diameter control of ultrathin zinc oxide nanofibers synthesized by electrospinning. *Nanoscale research letters* **2014,** *9* (1), 267.

172. Lu, Q.; Wang, X.; Lu, S.; Li, M.; Kaplan, D. L.; Zhu, H., Nanofibrous architecture of silk fibroin scaffolds prepared with a mild self-assembly process. *Biomaterials* **2011,** *32* (4), 1059-1067.

173. Jiang, B.-P.; Zhang, L.; Zhu, Y.; Shen, X.-C.; Ji, S.-C.; Tan, X.-Y.; Cheng, L.; Liang, H., Water-soluble hyaluronic acid–hybridized polyaniline nanoparticles for effectively targeted photothermal therapy. *Journal of Materials Chemistry B* **2015,** *3* (18), 3767-3776.

174. de Oliveira, S. A.; da Silva, B. C.; Riegel-Vidotti, I. C.; Urbano, A.; de Sousa Faria-Tischer, P. C.; Tischer, C. A., Production and characterization of bacterial cellulose membranes with hyaluronic acid from chicken comb. *International journal of biological macromolecules* **2017,** *97*, 642-653.

175. Zhang, Q.; Chen, S.; You, R.; Tariq, Z.; Huang, J.; Li, M.; Yan, S., Silk fibroin/hyaluronic acid porous scaffold for dermal wound healing. *Fibers and Polymers* **2017,** *18* (6), 1056-1063.

176. Zahedi, P.; Rezaeian, I.; Ranaei-Siadat, S. O.; Jafari, S. H.; Supaphol, P., A review on wound dressings with an emphasis on electrospun nanofibrous polymeric bandages. *Polymers for Advanced Technologies* **2010,** *21* (2), 77-95.

177. Bian, S.; He, M.; Sui, J.; Cai, H.; Sun, Y.; Liang, J.; Fan, Y.; Zhang, X., The self-crosslinking smart hyaluronic acid hydrogels as injectable three-dimensional scaffolds for cells culture. *Colloids and Surfaces B: Biointerfaces* **2016,** *140*, 392-402.

178. Anderson, K.; Hamm, R. L., Factors that impair wound healing. *Journal of the American College of Clinical Wound Specialists* **2012,** *4* (4), 84-91.

179. Burke, S. E.; Barrett, C. J., Swelling behavior of hyaluronic acid/polyallylamine hydrochloride multilayer films. *Biomacromolecules* **2005,** *6* (3), 1419-1428.

180. Gianak, O.; Pavlidou, E.; Sarafidis, C.; Karageorgiou, V.; Deliyanni, E., Silk Fibroin Nanoparticles for Drug Delivery: Effect of Bovine Serum Albumin and Magnetic Nanoparticles Addition on Drug Encapsulation and Release. *Separations* **2018,** *5* (2), 25.

181. Hu, X.; Lu, Q.; Sun, L.; Cebe, P.; Wang, X.; Zhang, X.; Kaplan, D. L., Biomaterials from ultrasonication-induced silk fibroin− hyaluronic acid hydrogels. *Biomacromolecules* **2010,** *11* (11), 3178-3188.

182. Wu, Y.-B.; Yu, S.-H.; Mi, F.-L.; Wu, C.-W.; Shyu, S.-S.; Peng, C.-K.; Chao, A.-C., Preparation and characterization on mechanical and antibacterial properties of chitsoan/cellulose blends. *Carbohydrate Polymers* **2004,** *57* (4), 435-440.

183. Dowling, D. P.; Miller, I. S.; Ardhaoui, M.; Gallagher, W. M., Effect of surface wettability and topography on the adhesion of osteosarcoma cells on plasma-modified polystyrene. *Journal of biomaterials applications* **2011,** *26* (3), 327-347.

184. Groth, T.; Altankov, G., Studies on cell-biomaterial interaction: role of tyrosine phosphorylation during fibroblast spreading on surfaces varying in wettability. *Biomaterials* **1996,** *17* (12), 1227-1234.

185. Stewart, S. A.; Domínguez-Robles, J.; Donnelly, R. F.; Larrañeta, E., Implantable polymeric drug delivery devices: Classification, manufacture, materials, and clinical applications. *Polymers* **2018,** *10* (12), 1379.

186. Allison, S. D., Analysis of initial burst in PLGA microparticles. *Expert opinion on drug delivery* **2008,** *5* (6), 615-628.

187. Chen, G.; Sato, T.; Ohgushi, H.; Ushida, T.; Tateishi, T.; Tanaka, J., Culturing of skin fibroblasts in a thin PLGA–collagen hybrid mesh. *Biomaterials* **2005,** *26* (15), 2559-2566.

188. Raia, N. R.; Partlow, B. P.; McGill, M.; Kimmerling, E. P.; Ghezzi, C. E.; Kaplan, D. L., Enzymatically crosslinked silk-hyaluronic acid hydrogels. *Biomaterials* **2017,** *131*, 58-67.

189. Chernousova, S.; Epple, M., Silver as antibacterial agent: ion, nanoparticle, and metal. *Angewandte Chemie International Edition* **2013,** *52* (6), 1636-1653.

190. Liu, J.; Detrembleur, C.; Mornet, S.; Jérôme, C.; Duguet, E., Design of hybrid nanovehicles for remotely triggered drug release: an overview. *Journal of Materials Chemistry B* **2015,** *3* (30), 6117-6147.

191. Yucel, T.; Lovett, M. L.; Kaplan, D. L., Silk-based biomaterials for sustained drug delivery. *Journal of Controlled Release* **2014,** *190*, 381-397.

192. Heo, M.; Lee, S. J.; Heo, D. N.; Lee, D.; Lim, H.-N.; Moon, J.-H.; Kwon, I. K., Multilayered co-electrospun scaffold containing silver sulfadiazine as a prophylactic against osteomyelitis: Characterization and biological in vitro evaluations. *Applied Surface Science* **2018,** *432*, 308-316.

193. Sood, A.; Granick, M. S.; Tomaselli, N. L., Wound dressings and comparative effectiveness data. *Advances in wound care* **2014,** *3* (8), 511-529.

194. Cui, W.; Zhu, X.; Yang, Y.; Li, X.; Jin, Y., Evaluation of electrospun fibrous scaffolds of poly (dl-lactide) and poly (ethylene glycol) for skin tissue engineering. *Materials Science and Engineering: C* **2009,** *29* (6), 1869-1876.

195. Tsuchiya, K.; Masunaga, H.; Numata, K., Tensile reinforcement of silk films by the addition of telechelic-type polyalanine. *Biomacromolecules* **2017,** *18* (3), 1002-1009.

196. Luangbudnark, W.; Viyoch, J.; Laupattarakasem, W.; Surakunprapha, P.; Laupattarakasem, P., Properties and biocompatibility of chitosan and silk fibroin blend films for application in skin tissue engineering. *The Scientific World Journal* **2012,** *2012*.

197. Baimark, Y.; Srihanam, P.; Srisuwan, Y., Preparation of flexible silk fibroin films plasticized with glucose. *Asian J. Mater. Sci* **2009,** *1*, 29-35.

198. Gomes, S.; Rodrigues, G.; Martins, G.; Roberto, M.; Mafra, M.; Henriques, C.; Silva, J., In vitro and in vivo evaluation of electrospun nanofibers of PCL, chitosan and gelatin: A comparative study. *Materials Science and Engineering: C* **2015,** *46*, 348-358.

199. Xi, Y.; Ge, J.; Guo, Y.; Lei, B.; Ma, P. X., Biomimetic elastomeric polypeptide-based nanofibrous matrix for overcoming multidrug-resistant bacteria and enhancing full-thickness wound healing/skin regeneration. *ACS nano* **2018,** *12* (11), 10772-10784.

200. Datta, P.; Ray, A., Cellular behavior of L929 and MG-63 cells cultured on electrospun nanofibers of chitosan with different degrees of phosphorylation. *Progress in biomaterials* **2016,** *5* (2), 93-100.

201. Chen, C.-Y.; Ke, C.-J.; Yen, K.-C.; Hsieh, H.-C.; Sun, J.-S.; Lin, F.-H., 3D porous calcium-alginate scaffolds cell culture system improved human osteoblast cell clusters for cell therapy. *Theranostics* **2015,** *5* (6), 643.

202. Hadisi, Z.; Nourmohammadi, J.; Haghighipour, N.; Heidari, S., How direct electrospinning in methanol bath affects the physico-chemical and biological properties of silk fibroin nanofibrous scaffolds. *Micro & Nano Letters* **2016,** *11* (9), 514-517.

203. Mostafalu, P.; Tamayol, A.; Rahimi, R.; Ochoa, M.; Khalilpour, A.; Kiaee, G.; Yazdi, I. K.; Bagherifard, S.; Dokmeci, M. R.; Ziaie, B., Smart bandage for monitoring and treatment of chronic wounds. *Small* **2018,** *14* (33), 1703509.

204. Wang, S.; Zheng, F.; Huang, Y.; Fang, Y.; Shen, M.; Zhu, M.; Shi, X., Encapsulation of amoxicillin within laponite-doped poly (lactic-co-glycolic acid) nanofibers: preparation, characterization, and antibacterial activity. *ACS applied materials & interfaces* **2012,** *4* (11), 6393-6401.

205. Lansdown, A. B.; Mirastschijski, U.; Stubbs, N.; Scanlon, E.; Ågren, M. S., Zinc in wound healing: theoretical, experimental, and clinical aspects. *Wound repair and regeneration* **2007,** *15* (1), 2-16.

206. O'Dell, B. L., Zinc plays both structural and catalytic roles in metalloproteins. *Nutrition reviews* **1992,** *50* (2), 48-50.

207. Tenaud, I.; Sainte-Marie, I.; Jumbou, O.; Litoux, P.; Dreno, B., In vitro modulation of keratinocyte wound healing integrins by zinc, copper and manganese. *The British journal of dermatology* **1999,** *140* (1), 26-34.

208. Feng, P.; Wei, P.; Shuai, C.; Peng, S., Characterization of mechanical and biological properties of 3-D scaffolds reinforced with zinc oxide for bone tissue engineering. *PloS one* **2014,** *9* (1), e87755.

209. Bandyopadhyay, A.; Withey, E. A.; Moore, J.; Bose, S., Influence of ZnO doping in calcium phosphate ceramics. *Materials Science and Engineering: C* **2007,** *27* (1), 14-17.

210. Cherumannil Karumuthil, S.; Prabha Rajeev, S.; Valiyaneerilakkal, U.; Athiyanathil, S.; Varghese, S., Electrospun Poly (vinylidene fluoride-trifluoroethylene)-Based Polymer Nanocomposite Fibers for Piezoelectric Nanogenerators. *ACS applied materials & interfaces* **2019,** *11* (43), 40180-40188.

211. Barui, A. K.; Veeriah, V.; Mukherjee, S.; Manna, J.; Patel, A. K.; Patra, S.; Pal, K.; Murali, S.; Rana, R. K.; Chatterjee, S., Zinc oxide nanoflowers make new blood vessels. *Nanoscale* **2012,** *4* (24), 7861-7869.

212. Sharir, H.; Zinger, A.; Nevo, A.; Sekler, I.; Hershfinkel, M., Zinc released from injured cells is acting via the Zn2+-sensing receptor, ZnR, to trigger signaling leading to epithelial repair. *Journal of Biological Chemistry* **2010,** *285* (34), 26097-26106.

213. Averbeck, M.; Gebhardt, C. A.; Voigt, S.; Beilharz, S.; Anderegg, U.; Termeer, C. C.; Sleeman, J. P.; Simon, J. C., Differential regulation of hyaluronan metabolism in the epidermal and dermal compartments of human skin by UVB irradiation. *Journal of Investigative Dermatology* **2007,** *127* (3), 687-697.

214. Ewins, B.; Vassiliadou, M.; Minihane, A.; Rimbach, G.; Weinberg, P., Techniques for quantifying effects of dietary antioxidants on transcription factor translocation and nitric oxide production in cultured cells. *Genes & nutrition* **2006,** *1* (2), 125-131.

215. Choi, J.-H.; Jun, J. H.; Kim, J. H.; Sung, H. J.; Lee, J. H., Synergistic effect of interleukin-6 and hyaluronic acid on cell migration and ERK activation in human keratinocytes. *Journal of Korean medical science* **2014,** *29* (Suppl 3), S210-S216.

216. Xie, Y.; He, Y.; Irwin, P. L.; Jin, T.; Shi, X., Antibacterial activity and mechanism of action of zinc oxide nanoparticles against Campylobacter jejuni. *Applied and environmental microbiology* **2011,** *77* (7), 2325-2331.

217. Mostafa, A. A., Antibacterial Activity of Zinc Oxide Nanoparticles Against Toxigenic Bacillus cereus and Staphylococcus aureus Isolated from Some Egyptian Food. *Intl. J* **2015,** *6* (2), 145-154.

218. Kadiyala, U.; Turali-Emre, E. S.; Bahng, J. H.; Kotov, N. A.; VanEpps, J. S., Unexpected insights into antibacterial activity of zinc oxide nanoparticles against methicillin resistant Staphylococcus aureus (MRSA). *Nanoscale* **2018,** *10* (10), 4927-4939.

219. Ohira, T.; Kawamura, M.; Fukuda, M.; Alvarez, K.; Özkal, B.; Yamamoto, O., Extension of the optical absorption range in Zn-Doped MgO powders and its effect on antibacterial activity. *Journal of materials engineering and performance* **2010,** *19* (3), 374-379.

220. Bakhsheshi-Rad, H. R.; Hamzah, E.; Ismail, A. F.; Aziz, M.; Kasiri-Asgarani, M.; Ghayour, H.; Razzaghi, M.; Hadisi, Z., In vitro corrosion behavior, bioactivity, and antibacterial performance of the silver-doped zinc oxide coating on magnesium alloy. *Materials and Corrosion* **2017,** *68* (11), 1228-1236.

221. Becheri, A.; Dürr, M.; Nostro, P. L.; Baglioni, P., Synthesis and characterization of zinc oxide nanoparticles: application to textiles as UV-absorbers. *Journal of Nanoparticle Research* **2008,** *10* (4), 679-689.

222. Perez, R.; Davis, S. C., Relevance of animal models for wound healing. *Wounds: a compendium of clinical research and practice* **2008,** *20* (1), 3-8.

223. Friedrich, E. E.; Washburn, N. R., Transport patterns of anti-TNF-α in burn wounds: Therapeutic implications of hyaluronic acid conjugation. *Biomaterials* **2017,** *114*, 10-22.

224. Liu, X.; Wang, Z.; Wang, R.; Zhao, F.; Shi, P.; Jiang, Y.; Pang, X., Direct comparison of the potency of human mesenchymal stem cells derived from amnion tissue, bone marrow and adipose tissue at inducing dermal fibroblast responses to cutaneous wounds. *International journal of molecular medicine* **2013,** *31* (2), 407-415.

225. Loeffelbein, D. J.; Rohleder, N. H.; Eddicks, M.; Baumann, C. M.; Stoeckelhuber, M.; Wolff, K.-D.; Drecoll, E.; Steinstraesser, L.; Hennerbichler, S.; Kesting, M. R., Evaluation of human amniotic membrane as a wound dressing for split-thickness skin-graft donor sites. *BioMed research international* **2014,** *2014*.

226. Sun, L. T.; Friedrich, E.; Heuslein, J. L.; Pferdehirt, R. E.; Dangelo, N. M.; Natesan, S.; Christy, R. J.; Washburn, N. R., Reduction of burn progression with topical delivery of (antitumor necrosis factor-α)-hyaluronic acid conjugates. *Wound Repair and Regeneration* **2012,** *20* (4), 563-572.

227. Hadisi, Z.; Nourmohammadi, J.; Nassiri, S. M., The antibacterial and anti-inflammatory investigation of Lawsonia Inermis-gelatin-starch nano-fibrous dressing in burn wound. *International Journal of Biological Macromolecules* **2017**.

228. Hakkarainen, T.; Koivuniemi, R.; Kosonen, M.; Escobedo-Lucea, C.; Sanz-Garcia, A.; Vuola, J.; Valtonen, J.; Tammela, P.; Mäkitie, A.; Luukko, K., Nanofibrillar cellulose wound dressing in skin graft donor site treatment. *Journal of Controlled Release* **2016,** *244*, 292-301.

229. Litwiniuk, M.; Krejner, A.; Speyrer, M.; Gauto, A.; Grzela, T., Hyaluronic acid in inflammation and tissue regeneration. *Wounds* **2016,** *28* (3), 78-88.

230. Aruffo, A.; Stamenkovic, I.; Melnick, M.; Underhill, C. B.; Seed, B., CD44 is the principal cell surface receptor for hyaluronate. *Cell* **1990,** *61* (7), 1303-1313.

231. Price, R. D.; Myers, S.; Leigh, I. M.; Navsaria, H. A., The role of hyaluronic acid in wound healing. *American journal of clinical dermatology* **2005,** *6* (6), 393-402.

232. Misra, S.; Hascall, V. C.; Markwald, R. R.; Ghatak, S., Interactions between hyaluronan and its receptors (CD44, RHAMM) regulate the activities of inflammation and cancer. *Frontiers in immunology* **2015,** *6*, 201.

233. Zaman, A.; Cui, Z.; Foley, J. P.; Zhao, H.; Grimm, P. C.; DeLisser, H. M.; Savani, R. C., Expression and role of the hyaluronan receptor RHAMM in inflammation after bleomycin injury. *American journal of respiratory cell and molecular biology* **2005,** *33* (5), 447-454.

234. Meizarini, A.; Aryati, W. R.; Puteri, A., Anti-inflammatory properties of a wound dressing combination of zinc oxide and turmeric extract. *Veterinary world* **2018,** *11* (1), 25.

235. Agarwal, H.; Nakara, A.; Shanmugam, V. K., Anti-inflammatory mechanism of various metal and metal oxide nanoparticles synthesized using plant extracts: A review. *Biomedicine & Pharmacotherapy* **2019,** *109*, 2561-2572.

236. Gottrup, F., A specialized wound-healing center concept: importance of a multidisciplinary department structure and surgical treatment facilities in the treatment of chronic wounds. *The American journal of surgery* **2004,** *187* (5), S38-S43.

237. Kallstrom, G., Are quantitative bacterial wound cultures useful? *Journal of clinical microbiology* **2014,** *52* (8), 2753-2756.

238. Clerc, O.; Greub, G., Routine use of point-of-care tests: usefulness and application in clinical microbiology. *Clinical Microbiology and Infection* **2010,** *16* (8), 1054-1061.

239. Peters, R. P.; Savelkoul, P. H.; Vandenbroucke-Grauls, C. M., Future diagnosis of sepsis. *The Lancet* **2010,** *375* (9728), 1779-1780.

240. Martin, G. S.; Mannino, D. M.; Eaton, S.; Moss, M., The epidemiology of sepsis in the United States from 1979 through 2000. *New England Journal of Medicine* **2003,** *348* (16), 1546-1554.

241. Smith, M. E.; Robinowitz, N.; Chaulk, P.; Johnson, K., Comparison of chronic wound culture techniques: swab versus curetted tissue for microbial recovery. *British journal of community nursing* **2014,** *19* (Sup9), S22-S26.

242. Rhoads, D. D.; Cox, S. B.; Rees, E. J.; Sun, Y.; Wolcott, R. D., Clinical identification of bacteria in human chronic wound infections: culturing vs. 16S ribosomal DNA sequencing. *BMC infectious diseases* **2012,** *12* (1), 1-8.

243. Kangas, M. J.; Burks, R. M.; Atwater, J.; Lukowicz, R. M.; Williams, P.; Holmes, A. E., Colorimetric sensor arrays for the detection and identification of chemical weapons and explosives. *Critical reviews in analytical chemistry* **2017,** *47* (2), 138-153.

244. Puchtler, H.; Meloan, S.; Spencer, M., Current chemical concepts of acids and bases and their application to anionic ("acid") and cationic ("basic") dyes. *Histochemistry* **1985,** *82* (4), 301-306.

245. Barrow, S. J.; Kasera, S.; Rowland, M. J.; Del Barrio, J.; Scherman, O. A., Cucurbituril-based molecular recognition. *Chemical reviews* **2015,** *115* (22), 12320-12406.

246. Sessler, J. L.; Kim, S. K.; Gross, D. E.; Lee, C.-H.; Kim, J. S.; Lynch, V. M., Crown-6-calix [4] arene-capped calix [4] pyrrole: an ion-pair receptor for solvent-separated CsF ions. *Journal of the American Chemical Society* **2008,** *130* (39), 13162-13166.

247. Reichardt, C.; Welton, T., *Solvents and solvent effects in organic chemistry*. John Wiley & Sons: 2011.

248. Jungreis, E.; Ben-Dor, L., Organic spot test analysis. In *Comprehensive Analytical Chemistry*, Elsevier: 1980; Vol. 10, pp 1-60.

249. Lim, S. H.; Feng, L.; Kemling, J. W.; Musto, C. J.; Suslick, K. S., An optoelectronic nose for the detection of toxic gases. *Nature chemistry* **2009,** *1* (7), 562-567.

250. Capitán-Vallvey, L. F.; Lopez-Ruiz, N.; Martinez-Olmos, A.; Erenas, M. M.; Palma, A. J., Recent developments in computer vision-based analytical chemistry: A tutorial review. *Analytica Chimica Acta* **2015,** *899*, 23-56.

251. Askim, J. R.; Mahmoudi, M.; Suslick, K. S., Optical sensor arrays for chemical sensing: the optoelectronic nose. *Chemical Society Reviews* **2013,** *42* (22), 8649-8682.